University of Alberta

Evaluation of Phosphatidylserine-Binding Peptides Radiolabeled with Fluorine 18 for *in vivo* Imaging of Apoptosis

by

Janice Sarah Kapty

A thesis submitted to the Faculty of Graduate Studies and Research
in partial fulfillment of the requirements for the degree of

Doctor of Philosophy

Oncology

©Janice Sarah Kapty

Spring 2012
Edmonton, Alberta

Permission is hereby granted to the University of Alberta Libraries to reproduce single copies of this thesis and to lend or sell such copies for private, scholarly or scientific research purposes only. Where the thesis is converted to, or otherwise made available in digital form, the University of Alberta will advise potential users of the thesis of these terms.

The author reserves all other publication and other rights in association with the copyright in the thesis and, except as herein before provided, neither the thesis nor any substantial portion thereof may be printed or otherwise reproduced in any material form whatsoever without the author's prior written permission.

Abstract

We currently do not have a clinical method to directly assess apoptosis induced by cancer therapies. Phosphatidylserine (PS) is an attractive target for imaging apoptosis since it is on the exterior of the apoptotic cells and PS externalization is an early marker of apoptosis. PS-binding peptides are an attractive option for developing an imaging probe to detect apoptosis using positron emission tomography. In this study we evaluated binding characteristics of PS-binding peptides for ability to bind to PS, radiolabeled PS-binding peptides with fluorine-18, and performed *in vitro* and *in vivo* analysis of ^{18}F radiolabeled PS-binding peptides including biodistribution analysis and dynamic PET imaging in a murine tumor model of apoptosis. Four peptides were evaluated for PS binding characteristics using a plate based assay system, a liposome mimic of cell membrane PS presentation, and a cell assay of apoptosis. The results indicate that all four peptides bind to PS and are specific to apoptotic cells. The widely used ^{18}F prosthetic group *N*-succinimidyl-4-[^{18}F]fluorobenzoate ([^{18}F]SFB) and the recently developed *N*-[6-(4-[^{18}F]fluorobenzylidene) aminooxyhexyl]maleimide ([^{18}F]FBAM) were investigated for radiolabeling of two representative phosphatidylserine-binding peptides. The prosthetic groups were compared with respect to required reaction conditions for optimum labeling, radiolabeling yield and chemoselectivity. The N-terminus labeled product produced by reaction of [^{18}F]SFB with binding peptide LIKKPF was produced in 18% radiochemical yield while no N-terminus labeled product could be isolated following [^{18}F]SFB

reaction with PDGLSR. When the peptides were modified by addition of a cysteine residue at the N-terminus they provided almost quantitative radiochemical yields with [^{18}F]FBAM. Results indicate that for the peptides in this study, [^{18}F]FBAM is a more useful prosthetic group compared to [^{18}F]SFB due to its excellent chemo-selectivity and high radiochemical yield. We report the first experiments where PS-binding peptides were radiolabeled with ^{18}F and evaluated as possible radiotracers for imaging apoptosis. We investigated two radio-peptides ([^{18}F]FBAM-CLIKKPF and [^{18}F]FBAM-CPGDLSR) *in vitro* and *in vivo* as possible radiotracers able to bind to apoptotic cells and to image chemotherapy induced apoptosis.

Acknowledgements

There are several people that deserve thanks for their help during my doctoral studies. First of all I would like to thank my husband for listening to me talk about my research every day and for helping with day to day life in order to make things go easier during my thesis.

Thank you to Dr. Mercer, my supervisor, who has allowed me some freedom during my PhD to work on my own schedule and to pursue a research project on peptides rather than DNA. He was supportive of my interest in teaching and encouraged me to participate in teaching opportunities. In addition he helped to provide opportunities during my thesis that have helped me to learn many new things including but not limited to: participation in the CARS PET course, sending me to various research conferences, applying for research patents and helping to prepare the DAAD (German Academic Exchange Service) scholarship application.

To my supervisory committee I would like to thank you for your guidance and feedback on my research project that has helped to shape the work in this thesis. Thank you for helping to point me in the right direction. To Dr. Murray thank you for initiating the review article on radiotracers and getting me to begin writing as an academic. I really appreciate the effort you made to edit the many versions of the manuscript before publication.

To Dr. Frank Wuest thank you for mentoring me and assisting with the peptide research project. You encouraged my research on the peptide project and

this fueled my interest in this approach. I am also thankful that you began to work at the Cross Cancer Institute in 2007, since I had opportunity to work with such an excellent peptide chemist. You have a great passion for science and always many new ideas for future research. I also very much appreciate your help to prepare the DAAD scholarship application for research at your old institution Forschungszentrum Dresden-Rossendorf (FZD) in Germany. Without your assistance and contacts at FZD the application would have been much more difficult.

During my research project in Dresden, Germany I was hosted by FZD and my supervisor Dr. Torsten Kniess. I would like to thank Dr. Kniess for arranging everything for my stay and ensuring that I had all the required equipment in order to complete my research project. As a result, I was very productive and able to complete many experiments during my six week visit. I really enjoyed my time working at FZD and I am very grateful to Dr. Kniess for his assistance. During my research project at FZD I received technical assistance from Peggy Wecke and Uta Lenkeit and I would like to thank them for showing me around the laboratory and training me on various pieces of equipment.

Susan Richter, deserves special mention since she kept me company every weekend during my stay in Dresden and helped to teach me more German words since my language skills were terrible. We had a lot of fun and I will always remember the time we spent together. In addition, while Susan did her first research exchange to Edmonton she helped to perfect the [^{18}F]SFB automated radio-synthesis which helped with future research with [^{18}F]SFB.

I am also grateful to my good friend Cynthia Stretch for discussing research with me and for helping to keep me motivated. I am glad that we worked on dissertation research at the same time and your friendship made the journey more enjoyable.

For the fluorescence studies there were several people that helped to ensure this research was completed. I gratefully acknowledge the technical help of Gerry Baron from Imaging Facility, Department of Oncology. For the cell testing of the fluorescent peptides I am very grateful to Shanna Banman who did confocal microscopy analysis of the peptides binding to apoptotic and healthy Jurkat cells. Shanna is patient and yet motivated to get the results of the experiment and I am glad that we got to work together during my thesis. I need to also thank Dr. Ing-Swie Goping who allowed Shanna and I to work together and do the peptide testing in her laboratory.

For the animal experiments there are many people to thank since these were quite long research days that could not have been completed by me alone. I am grateful to John Wilson and David Clendeling for radio-isotope production. I am grateful to Soraya Shahhosseini for technical assistance with the GE Tracerlab FX FDG hardware and for training me how to use this equipment so that I could do the radio-synthesis of [^{18}F]SFB on my own. The authors are grateful to Jenilee Way for assistance with [^{18}F]FBAM production. Your help with the synthesis of [^{18}F]FBAM made my research possible and I am very grateful to your detailed work and dedication to the unit in order to ensure that each synthesis is

successful. I also need to thank you for arriving at work very early for some of the animal experiments. I am grateful to Monica Wang for assistance with cell culture and animal dissections. Thank you for taking the time to teach me new techniques including cell culture and the TUNEL assay. For the PET imaging experiments on mice I am grateful to Dr. Melinda Wuest for her assistance and for teaching me about animal experimentation.

Finally I have several organizations to thank regarding financial assistance for this research and for my doctoral studies. I would like to thank the Alberta Cancer Research Institute (ACRI) for financial support for this research. I would like to thank the Department of Oncology for various forms of support (financial, professional development programs, research space, and administrative support). I have been very fortunate to receive several scholarships during my doctoral studies. I have received the ACRI Graduate Studentship, Killam Scholarship, DAAD research grant, and several travel awards. Sincere thanks to all of the organizations that provided the scholarships and promoted the research in this dissertation.

TABLE OF CONTENTS

LIST OF TABLES

LIST OF FIGURES

List of Abbreviations

*as*ODNs	antisense oligonucleotide probes
BTAP	bisthioacetamido-pentanoyl
Bq	Becquerel
°C	degrees Celsius
$CaCl_2$	calcium chloride
cc	cubic centimeter
CT	computed tomography
DAPI	4',6-diamidino-2-phenylindole
DFNSH	5-(dimethylamino)-N'-(4-fluorobenzylidene)naphthalene-1-sulfonohydrazide
DNA	deoxyribonucleic acid
DPPC	1,2-dipalmitoyl-*sn*-glycero-3-phosphocholine
DPPS	1,2-dipalmitoyl-*sn*-glycero-3-[phospho-L-serine] (sodium salt)
DTPA	diethylenetriaminepentaaceticacid
5-FAM	5-carboxy fluorescein amidite
[^{18}F]FBAM)	N-[6-(4-[^{18}F]fluorobenzylidene)aminooxyhexyl]maleimide
^{18}F-FDG	^{18}F-Fluorodeoxyglucose
^{18}F-FLT	3′-deoxy-3′-[^{18}F]-fluorothymidine
FITC	fluorescein isothiocyanate
[^{18}F]SFB	*N*-succinimidyl 4-[^{18}F]fluorobenzoate
Gd	gadolinium
Gd-DTPA	gadolinium-diethylenetriaminepentaacetic acid

h	hour
HEPES	(4-(2-hydroxyethyl)-1-piperazineethanesulfonic acid)
H&NSCC	head and neck squamous cell carcinoma
HPLC	high performance liquid chromatography
HYNIC	hydrazinonicotinamide
%ID/g	percent of injected dose per gram
K_d	dissociation constant
kDa	kilodalton
LC3	microtubule-associated protein light chain 3
M	molar
MBq	megaBecquerel
µL	microlitre
mL	mililitre
ML-9	butyl-2-methyl-malonic acid
ML-10	2-(5-fluoro-pentyl)-2-methyl-malonic acid
MRI	magnetic resonance imaging
mRNA	messenger ribonucleic acid
mTOR	mammalian target of rapamycin
NaCl	sodium chloride
NSCLC	non-small cell lung cancer
NST-732	(5-dimethylamino)-1-napththalene-sulfonyl-α-ethyl-fluoroalanine
PBS	phosphate buffered saline
PEG	poly(ethylene glycol)

PET	positron emission tomography
p.i.	post injection
PS	phosphatidylserine
PC	phosphatidylcholine
Radio-TLC	radio-thin layer chromatography
R_f	retention factor
RFU	relative fluorescence units
R_t	retention time
ROI	regions of interest
SA-β-gal	senescence-associated β-galactosidase
SD	standard deviation
SEM	standard error of the mean
SPET	single photon emission tomography
SUV	standardized uptake value
TAC	time-activity curve
TUNEL	terminal deoxynucleotidyl transferase-mediated deoxyuridine triphosphate nick-end labeling
XRT	radiation therapy

Chapter 1

Radiotracers for Non-Invasive Molecular Imaging of Tumor Cell Death

A version of this chapter has been published. **Kapty, J.,** Murray, D., Mercer, J. *Cancer Biotherapy and Radiopharmaceuticals*, (Dec 2010) 25(6): 615-628.

1.1 Introduction.

Effective radiation therapy (XRT) or chemotherapy will inactivate cancer cells either through programmed (apoptosis, autophagy) or uncontrolled (necrosis) cell death or through the induction of cellular premature senescence. Apoptosis is a well studied tumor response to therapy; however, other mechanisms of tumor cell death are also induced following treatment. For instance, it is known that necrosis occurs in some tumor types and, while necrotic cell death is usually characterized as “uncontrolled”, there is now accumulating evidence that in some cases cellular events and cascades in necrosis represent a more programmed course of events (Golstein and Kroemer, 2007). Research has also highlighted the importance of cell senescence and autophagy after treatment with cytotoxic agents. Cells are able to use these various mechanisms to respond to cell stress. The interplay between modes of cell death and how they are connected is complex (Kondo et al., 2005; Steeves et al., 2010; Young and Narita, 2009). The type of cell death executed in a particular system depends on factors such as the cell type, genotype, microenvironment, whether cells are adherent, and the dose and nature of the cytotoxic agent. A detailed account of the biology of cell death mechanisms is beyond the scope of this review, but the general characteristics of each mechanism are outlined in Table 1-1 and an excellent review on cell death mechanisms in tumors has been presented by Okada and Mak (Okada and Mak, 2004). Our understanding of these processes is predominantly derived from studies on cells in culture and at present there are very limited options to probe these processes in solid tumors before and following therapy.

Radiopharmaceutical-based nuclear medicine techniques have the potential to image cell death mechanisms at the cellular level due to their very high sensitivity. The science of radiopharmaceutical design is such that it is often possible to rationally design an appropriate ligand once a suitable target has been identified. Imaging of the various modes of cell death relies on (i) the identification of cellular targets that are unique to that process and (ii) the development of radiolabeled probes that will bind with high selectivity and specificity to that target. Unfortunately, no single generic radiotracer is capable of imaging the above-mentioned four very different and complex mechanisms that result in tumor cell death. This is because there is no single cellular target that is common to all cell death mechanisms and yet sufficiently unique to identify cell death from other biological processes. The induction of cell death by the mechanism of apoptosis is a desired effect of chemotherapy and radiotherapy. If the treatment does not induce apoptosis it may be inducing necrosis, which could lead to undesirable inflammatory effects, or it may invoke a senescence response. At a preclinical level, probing the individual mechanisms of cell death will provide details of cellular response to novel therapies, while at the clinical level the physician will be better positioned to use this information to make informed decisions about patient care, such as changing a course of therapy which is not inducing a desired cell death response. Multiple probes will be required to effectively determine the mechanisms of cell death, and this realization has resulted in both preclinical and clinical investigations with imaging radiotracers.

In a clinical context, imaging cell death *in vivo* has great significance in evaluating therapeutic response and has the potential to assist in the design of appropriate individualized and optimized therapy. Conventional imaging modalities (e.g., computed tomography and magnetic resonance imaging) typically provide anatomical information which may not indicate tumor response to therapy until 6-12 weeks after treatment initiation. Using conventional imaging modalities, ineffective therapies may be used for long periods of time before the treatment's ineffectiveness becomes evident. Evaluation of tumor response to chemotherapy and XRT after the earliest cycles of therapy would allow optimization of dosing and therapies, thereby improving patient outcomes and quality of life. Advantages of imaging with radiotracers include: (i) non-invasiveness; (ii) the ability to detect lesions earlier than X-ray-based or MRI imaging modalities; and (iii) the fact that various parameters can be imaged with different probes. There are a number of tracers at various stages of development as possible probes for imaging cell death which will be discussed in this paper (Table 1-2).

1.2 Imaging tumors and tumor reponse to therapy with conventional radiotracers.

We are able to measure metabolic activity of tumors using the positron emission tomography (PET) radiopharmaceutical [^{18}F]-fluorodeoxyglucose (^{18}F-FDG) where the uptake of this agent is tied to glucose transport and utilization. [^{18}F]-FDG is an excellent probe for many tumors with its primary applications

being in the detection of metastatic disease, the staging of primary tumors and in the follow-up to assess residual or recurrent disease. Some cancers such as prostate, thyroid, testicular, renal and bladder cancers have variable or low uptake of [^{18}F]-FDG which limits the use of [^{18}F]-FDG PET in staging of these diseases and makes [^{18}F]-FDG a poor candidate for assessing early tumor response (Juweid and Cheson, 2006). Furthermore, since inflammatory cells, which are often present following therapy, have a high uptake of [^{18}F]-FDG, this tracer is generally not used for the early assessment of tumor viability. The ability of [^{18}F]-FDG to predict treatment outcome may be dependent on tumor type or on the measured parameter (i.e., standardized uptake value (SUV) or metabolic tumor volume (MTV)) (Chung et al., 2009; Suzuki et al., 2009). [^{18}F]-FDG PET does not provide direct information on cell death and only provides an indirect measurement of tumor response. Since biochemical responses of cells to chemotherapy and XRT occur within the first few days there has been a vigorous research effort to develop molecular imaging tracers that will be able to assess specific features of cell death within 1-3 days.

^{18}F-FDG PET is approved for monitoring response to treatment in breast cancer (Juweid and Cheson, 2006). After one cycle of chemotherapy, responding tumors indicated a decline in SUV of [^{18}F]-FDG (Juweid and Cheson, 2006). Tumor cells are also capable of changing their energy source in order to survive (De Saint-Hubert et al., 2009). For example, some breast tumors can use fructose as an energy source, which decreases the usefulness of [^{18}F]-FDG PET as an

imaging tool and minimizing its value for assessing tumor response to therapy (Godoy et al., 2006).

Apoptosis is an energy dependent process, and it may logically be considered that successful treatment will induce apoptosis and a subsequent increase in glucose (or [^{18}F]-FDG) uptake. This is known as a "flare" effect of tumor uptake (Wahl et al., 2009). The flare effect is not well studied and may not be a universal effect in all tumors. However, it is advised that breast cancer patients wait after chemotherapy for a minimum of 10 days before a ^{18}F-FDG PET scan (Wahl et al., 2009) in order to avoid this flaring effect and to avoid increased uptake due to inflammatory response. The wait time indicated for other tumor types is even longer. Guidelines for lymphoma recommend three weeks between the last chemotherapy treatment and [^{18}F]-FDG PET, and after XRT it is recommended waiting for 8-12 weeks before [^{18}F]-FDG PET (Wahl et al., 2009). It is clear that [^{18}F]-FDG has serious limitations in timely and effective imaging of cell death and tumor response to therapy.

1.3 Apoptosis molecular imaging.

Apoptosis is a genetically controlled process (i.e., a form of programmed cell death) that is characterized by distinct biochemical and morphological changes including nuclear condensation, phosphatidylserine (PS) externalization, cytoplasm shrinkage, non-random DNA degradation, plasma membrane blebbing and fragmentation of the cell into small "apoptotic bodies"(Vangestel et al., 2009). It is mediated by both *intrinsic* (Kolesnick and Fuks, 2003) and *extrinsic*

(Shankar et al., 2004) pathways that result in activation of a biochemical cascade in which cysteine-aspartic proteases (caspases) function as either initiators (caspases 2, 8, 9, 10) or executioners (caspases 3, 6, 7). The deregulation and suppression of apoptosis in tumors results in increased proliferative capacity and resistance to therapy. Tumor response to XRT is poorly understood and the role of apoptosis as a cell death mechanism after XRT is not well defined (Meyn et al., 2009; Okada and Mak, 2004). Therefore, the *in vivo* imaging of apoptosis with a radiopharmaceutical would be of great value in understanding the role and prevalence of apoptosis after XRT and chemotherapy. The changes in cell structure and biochemical processes during apoptosis provide attractive targets for molecular imaging. PS externalization and caspase activation have been the main cellular processes investigated as targets for molecular imaging. PS, which is ordinarily restricted to the inner layer of the phospholipid membrane, is externalized early in the apoptotic process (Devaux, 1991; Vance and Steenbergen, 2005). This has led to the development of imaging probes for apoptosis which bind to externalized PS, as discussed below, and probes targeting activated caspases.

1.3.1 Caspase targeted probes.

A target for imaging apoptosis is the presence of activated executioner caspases 3, 6, and 7 (Zhou et al., 2006). Most caspase-directed probes bind directly to activated caspases and act as inhibitors. Current challenges of caspase-directed probes include efficient cell entry and cellular accumulation. The caspase

inhibitor WC-II-89 has been radiolabeled with ^{18}F and the inhibitor WC98 has been radiolabelled with ^{11}C and both of these probes have been used with PET to image caspase-3 activation in tissues undergoing apoptosis (Chen et al., 2011; Zhou et al., 2009; Zhou et al., 2006). WC-II-89 is a non-peptide-based isatin sulfonamide analog and has been shown to inhibit human recombinant caspase 3 and caspase 7 using *in vitro* models (Zhou et al., 2006). WC-II-89 was radiolabeled with ^{18}F and evaluated in a rat liver model of apoptosis induced by cycloheximide treatment (Zhou et al., 2006). Small-animal PET images indicate higher uptake of ^{18}F-WC-II-89 in the liver of rats treated with cycloheximide compared to healthy rats (Zhou et al., 2006). This suggests that the probe is able to bind to apoptotic cells; however, it does not indicate the sensitivity of this probe since there is a high level of apoptosis induced in the liver model. Recent research on ^{18}F-WC-II-89 and ^{11}C-WC98 indicates that they are able to bind to caspase 3 *in vivo*; however, their sensitivity is limited (Chen et al., 2011). Further development of this probe requires apoptosis evaluation using a tumor model to determine if it is able to detect the lower levels of apoptosis that would be expected after treatment in tumors. Other isatin analogs which inhibit caspase 3 and 7 have been radiolabeled with ^{18}F for development into radiotracers (Smith et al., 2008). Recently a caspase 3/7 specific isatin sulfonamide (ICMT11) has been radiolabeled with ^{18}F and evaluated for imaging apoptosis in a murine lymphoma model treated with cyclophosphamide (Glaser et al., 2011; Nguyen et al., 2009). Overall uptake of ^{18}F-ICMT11 into the tumors was low (Glaser et al., 2011). This tracer was able to detect tumor apoptosis 24 hours after treatment; however, the

PET images indicate high retention of the tracer in liver and intestines which may limit its value, especially in the abdominal region (Nguyen et al., 2009). This tracer is likely metabolized in the liver and eliminated via hepatobiliary excretion and therefore does not have optimal biodistribution for development into a clinical tracer for imaging apoptosis. Caspase probes have not been tested in humans and this class of probes warrants further development and preclinical testing.

1.3.2 Small molecule probes.

The compounds under development are membrane permeable and respond to alterations in the membrane potential and phospholipid scrambling allowing accumulation inside cells undergoing apoptosis (Reshef et al., 2008). The compound NST-732 (5-dimethylamino)-1-napththalene-sulfonyl-α-ethyl-fluoroalanine, MW = 368) contains a fluorophore and binds to apoptotic cells early in the biochemical process; however, it is not known where this compound is binding in the cell (Aloya et al., 2006). NST-732 was tested in three cell lines: human adult T-cell leukemia Jurkat cells; mouse lymphoma Ly-S cells; and CT26 colon adenocarcinoma cells; after treatment of cells with either anti-Fas antibody or with the anticancer drug carmustine, NST-732 bound to apoptotic cells (Aloya et al., 2006). NST-732 was also evaluated in three *ex vivo* animal studies: radiation-induced cell death in lymphoma; renal ischemia and reperfusion; and cerebral stroke. Uptake of NST-732 was correlated with cell death based on histology analysis for the three animal studies (Aloya et al., 2006). The authors of this study suggest that since NST-732 contains a fluorine atom it could be radiolabeled with ^{18}F and used as a PET tracer (Aloya et al., 2006). A different

group prepared the compound 5-(dimethylamino)-N'-(4-fluorobenzylidene)naphthalene-1-sulfonohydrazide (DFNSH) which binds to cells undergoing apoptosis (Zeng et al., 2008) and subsequently radiolabeled it with ^{18}F. The ^{18}F-DFNSH was evaluated as a PET tracer in a ketamine-induced model of neuronal apoptosis in rats (Zhang et al., 2011). The uptake of ^{18}F-DFNSH was significantly increased in the frontal cortex of rats treated with ketamine compared to healthy rats (Zhang et al., 2011).

Other low molecular weight compounds such as butyl-2-methyl-malonic acid (ML-9) and 2-(5-fluoro-pentyl)-2-methyl-malonic acid (ML-10) are able to bind to cells undergoing apoptosis; however, the biological binding site should be determined if such compounds are to be optimized for clinical use (Cohen et al., 2009; Grimberg et al., 2009). ^{3}H-ML-9 was evaluated by autoradiography using a mouse colon carcinoma model after chemotherapy (Grimberg et al., 2009). ^{3}H-ML-9 indicated increased uptake in tumors after therapy compared to before therapy (Grimberg et al., 2009). This compound could be developed into a radiotracer by radiolabeling with ^{99m}Tc or ^{18}F and re-evaluated in an animal model of apoptosis. ML-10 was radiolabeled with ^{18}F and successfully used as a microPET probe to assess neurovascular apoptosis in a mouse model of ischemic cerebral stroke *in vivo* (Reshef et al., 2008). ^{18}F-ML10 has proceeded into Phase I/II clinical trials for imaging of apoptosis (De Saint-Hubert et al., 2009). The Phase I study was successful in that ^{18}F-ML10 was safe when administered to healthy human volunteers (Hoglund et al., 2011). ^{18}F-ML10 selectively accumulated in the testes where defective germ cells undergo apoptosis (Hoglund

et al., 2011). The human studies indicate that ^{18}F-ML10 has high stability *in vivo*, rapid distribution, and is eliminated through the urine (Hoglund et al., 2011).

There are two Phase-II clinical trials evaluating ^{18}F-ML10 as a PET radiotracer for early detection of response of brain metastases after XRT (2008a; 2008b). Recently it was reported that ^{18}F-ML10 is able to detect cell death induced by XRT in patients with brain metastases (Shirvan, 2009). PET images from ten patients were obtained before initiation of treatment and on day 9 or 10 after initiation of XRT (Shirvan, 2009). Results of this initial study indicate that the signal in tumors increased after irradiation (Shirvan, 2009). The use of ^{18}F-ML10 in the clinic may be feasible since it has shown some success in Phase I clinical trials, has financial support for future clinical trials, and is able to detect tumor response after XRT. Future research should include evaluation of tumor response to chemotherapy and testing of ^{18}F-ML10 in other tumor models.

1.3.3 Annexin V-based probes for imaging apoptosis.

Annexin V is a naturally occurring 36 kDa human phosphatidyl binding protein which binds with high affinity to externalized PS on apoptotic cells (Andree et al., 1990). Annexin V has been widely investigated as a probe for the detection and molecular imaging of apoptosis. Fluorescently labeled annexin V analogs are frequently used for the assessment of *in vitro* apoptosis with techniques such as flow cytometry and confocal microscopy (Koopman et al., 1994; van Engeland et al., 1998; Vermes et al., 1995). The use of annexin V as a potential radiopharmaceutical has some limitations including the requirement of (i) its production as an expensive human recombinant protein, and (ii) calcium for

binding to PS (Belhocine et al., 2004). Despite these challenges, annexin V is the most established probe for imaging apoptosis and the *in vivo* and clinical evaluation of this probe will be discussed in turn. As a cautionary note, *in vitro* analysis indicates that radiolabeled annexin V can also bind to necrotic cells; therefore, studies with annexin V need to be initially validated using a second molecular imaging probe to detect and confirm apoptosis (Blankenberg et al., 1999).

1.3.3.1 Annexin V for imaging apoptosis *in vivo*. Radiolabeling annexin V with various radionuclides results in the production of imaging agents for use with single photon emission tomography (SPET) and PET. SPET is an imaging modality that can image non-invasively by making use of radioisotopes (such as ^{99m}Tc) that emit gamma photons which are detected by a gamma camera. The development of annexin V into a SPET tracer has been studied in depth, mostly focusing on the use of ^{99m}Tc and ^{125}I labeling. Annexin V was derivatized with hydrazinonicotinamide (HYNIC) and coupled to ^{99m}Tc and subsequently evaluated in three animal models of apoptosis: hepatic apoptosis induced by anti-Fas antibody in mice; acute rejection in rats with transplanted cardiac allografts; and cyclophosphamide treatment of transplanted murine B cell lymphomas (Blankenberg et al., 1998). Imaging in these animal models indicated a promising two to six fold increase in uptake of annexin V at sites of apoptosis (Blankenberg et al., 1998). Hepatoma tumors in rats showed significantly increased uptake of ^{99m}Tc-HYNIC-annexin V after a single dose of cyclophosphamide compared to untreated rats (Mochizuki et al., 2003). Terminal deoxynucleotidyl transferase-

mediated deoxyuridine triphosphate nick-end labeling (TUNEL), an established assay for apoptosis, was used to analyze tumor tissue samples and the results indicated that TUNEL-positive cells in the tumor sample correlated well with the uptake of ^{99m}Tc-annexin V (Mochizuki et al., 2003). The feasibility of using ^{99m}Tc-annexin V for repetitive detection of apoptosis was evaluated in a rat model of hepatoma treated with cyclophosphamide and the results indicated that annexin V can be useful in this context, which is critical for the clinical use of this tracer (Kuge et al., 2004). Longitudinal monitoring is especially important since the baseline detection of apoptosis before treatment will be required for correct analysis of apoptotic response to therapy. Annexin V labeled with ^{125}I was evaluated in ependymoblastoma tumor xenografts in mice after irradiation with 2, 5 or 10 Gray of X-rays (Watanabe et al., 2006). Three hours after ^{125}I-annexin V injection the animals were sacrificed and autoradiographic analysis on tissue slices suggested that annexin V was significantly bound to irradiated tumors (Watanabe et al., 2006). The use of XRT to induce apoptosis in tumor models was recently evaluated in murine models of lymphoma and sarcoma by obtaining SPET images 24 hours after XRT using the tracer ^{99m}Tc-HYNIC-annexin V (Guo et al., 2009). Tracer uptake in lymphoma increased as the XRT dose escalated from 0 to 8 Gray (Guo et al., 2009). Annexin V uptake in lymphomas also correlated with apoptosis from the histology analysis (Guo et al., 2009). However, when xenograft sarcoma tumors were treated to 8 Gray, the uptake of ^{99m}Tc-HYNIC-annexin V was similar to the background and the tumor was not clearly defined in the images (Guo et al., 2009). ^{99m}Tc-HYNIC-annexin V may therefore

be useful in some cases to detect radiation-induced apoptosis *in vivo* (or lack thereof) and may be predictive of radiation response of different tumors; however, caution would be required since imaging with ^{99m}Tc-HYNIC-annexin V may not be useful for some tumor types, such as sarcoma tumors, and this imaging technique should be validated for specific tumor types. The absence of apoptosis in these sarcoma xenografts after treatment with XRT using the tracer ^{99m}Tc-HYNIC-annexin V clearly warrants further investigation to determine which mechanism of cell death occurs in this tumor after XRT. Other tracers may be more useful for this type of tumor, and we will discuss tracers for imaging other cell death mechanisms below.

The development of annexin V into a PET tracer is still underway. Keen *et al* directly labeled annexin V with ^{124}I and evaluated this compound in a mouse liver model of apoptosis induced by anti-Fas antibody (Keen et al., 2005). The PET images indicate that ^{124}I-annexin V localized in apoptotic liver (Keen et al., 2005). However, this group did not compare with other tracers such as annexin V labeled with ^{99m}Tc or ^{18}F; therefore, it is not clear if ^{124}I imparts any advantages as a radionuclide. The half life of ^{124}I is 4.2 days, and this and other unfavorable radionuclide properties will cause patients to be exposed to a high dose of radiation if used in the clinic; furthermore, labeling with ^{124}I is laborious, making it unfavorable for imaging purposes (Boersma et al., 2005). Annexin V has recently been radiolabeled with ^{68}Ga and evaluated *in vivo* (Bauwens et al., 2011; Wangler et al., 2011). Bauwens *et al* radiolabeled annexin V with ^{68}Ga and evaluated in a mouse model of hepatic apoptosis and a lymphoma tumor model of

apoptosis (Bauwens et al., 2011). They found the radiotracer to be quite stable in plasma; however, they were not able to image tumor apoptosis using microPET, despite the high level of treatment to induce apoptosis (cyclophosphamide 125 mg/kg and 10 Gy XRT)(Bauwens et al., 2011). Wangler *et al* radiolabeled annexin V with ^{68}Ga and evaluated in a model of myocardial infarction(Wangler et al., 2011). They were able to successfully image apoptosis in the infarct area; however, the usefulness of ^{68}Ga radiolabeling of annexin V may be limited by its physical half life of 68 minutes. Since annexin V is a large protein, distribution is not immediate and requires time. For mice a waiting period of 1-2 hours is typical after injection of annexin V. In this case we are waiting approximately one to two half lives of ^{68}Ga simply to allow the ^{68}Ga-annexin V to distribute throughout the body. In humans, it is recommended to wait 24 hours after administration of annexin V to allow for bioistribution. This time frame is much too long for imaging with ^{68}Ga-annexin V to be successful. Murakami *et al* labeled annexin V with ^{18}F and analyzed biodistribution in healthy rats and in an ischemia model of apoptosis (Murakami et al., 2004). Annexin V labeled with ^{99m}Tc and ^{18}F were compared to determine which radionuclide enhanced the capabilities of the tracer (Murakami et al., 2004). Results indicate that ^{18}F-annexin V had lower liver, spleen and kidney uptake compared to the ^{99m}Tc-annexin V (Murakami et al., 2004). An advantage of the ^{18}F-annexin V as a radiotracer therefore is better images due to lower background and use of PET for data acquisition, which is quantitative and has superior image resolution to SPET. When ^{18}F-annexin V was evaluated in a liver model of apoptosis in rats induced by treatment with

cycloheximide, PET images displayed a 3-9 fold increased uptake of ^{18}F-annexin V in apoptotic liver (Yagle et al., 2005). The biodistribution of ^{18}F-annexin V in normal rats showed highest uptake in kidneys and bladder (Yagle et al., 2005). In addition, ^{18}F-annexin V allows the use of PET imaging modality which, as noted above, produces better images due to the sensitivity of this modality. However, there is limited research published on the use of ^{18}F-annexin V as a PET radiotracer.

Of the eight papers discussed that used animals to test annexin V, the models employed were: hepatic apoptosis (Blankenberg et al., 1998; Keen et al., 2005; Yagle et al., 2005); ischemia (Murakami et al., 2004); allograft rejection (Blankenberg et al., 1998); lymphoma treated with cyclophosphamide (Blankenberg et al., 1998); lymphoma and sarcoma treated with XRT (Guo et al., 2009); ependymoblastoma xenograft tumors treated with XRT (Watanabe et al., 2006); and liver tumor models treated with cyclophosphamide (Kuge et al., 2004; Mochizuki et al., 2003); and ketamine-induced neurodegeneration (Zhang et al., 2009). The authors suggest that these models are all providing an apoptosis target and are therefore capable of evaluating annexin V binding to apoptotic cells *in vivo*. However, some models will invoke large amounts of apoptosis which is readily detected by the probe. For example, the hepatic apoptosis models cause massive amounts of cell death in the liver, which may not reflect the levels of apoptosis that will be present in animal or human tumors following anti-cancer treatment. There is, therefore, a critical need to be able to detect the apoptotic signal compared to the background and to develop a tracer that will be specific

enough to detect lower signal levels. The hepatoma model may be less than ideal since there is liver uptake of annexin V in healthy animals and therefore a high background. One consideration for xenograft tumor models is that the tumor micro-environment is usually different depending on where the tumor is located in the body, and this may influence the tumor uptake of tracer and the corresponding images that are produced. Nonetheless, annexin V has proceeded into clinical trials and has been used to evaluate response to therapy in various tumor models.

1.3.3.2 Annexin V for imaging apoptosis in clinical trials. Annexin V has to date only been evaluated as a SPET tracer in humans. A Phase-I study of the radiotracer ^{99m}Tc-annexin V determined the safety and feasibility of this probe for imaging of apoptosis in tumors after the first course of chemotherapy (Belhocine et al., 2002). In this study, annexin V was conjugated to bisthioacetamido-pentanoyl (BTAP) using the N_2S_2 method for labeling (Belhocine and Blankenberg, 2005). Fifteen patients with lymphoma, lung cancer or breast cancer were included in the study and underwent ^{99m}Tc-annexin V SPET scans before and within three days after the first round of chemotherapy (Belhocine et al., 2002). There was no tracer uptake before therapy; however, after therapy, seven patients indicated significant ^{99m}Tc-annexin V tumor uptake (an example of a patient with ^{99m}Tc-annexin V tumor uptake is shown in Figure 1-1) (Belhocine et al., 2002). These patients had a complete or partial response after the full course of therapy (Belhocine et al., 2002). Of the other eight patients with no ^{99m}Tc-annexin V tumor uptake, six had progressive disease (Belhocine et al., 2002). The two patients with no ^{99m}Tc-annexin V tumor uptake and no

progressive disease were breast cancer patients (Belhocine et al., 2002). The use of ^{99m}Tc-annexin V in this small scale analysis was therefore useful for predicting response of lymphoma and lung cancer but was not predictive of breast cancer response. Since only two breast cancer patients were included in this study, the effectiveness of ^{99m}Tc-annexin V should be evaluated in a clinical trial with a larger cohort of breast cancer patients. ^{99m}Tc-Annexin V is safe for clinical use and biodistribution of the tracer includes uptake in salivary glands, liver, spleen, bone marrow, colon, kidneys and bladder (Belhocine et al., 2002). The BTAP form of Annexin V used by Belhocine *et al* has a major disadvantage of hepatic uptake and excretion into the digestive system which prevents imaging of the abdomen (Figure 1-1B) (Belhocine et al., 2002).

"Contrast level" is defined as the signal (apoptosis) to background (no apoptosis) ratio (Belhocine and Blankenberg, 2005). The better the contrast level for a radiotracer the better the quality of images. ^{99m}Tc-HYNIC-annexin V accumulates in kidneys and is taken up by liver, red marrow, and the spleen and is excreted in the urine (Boersma et al., 2005). However, compared to the BTAP Annexin V form, the HYNIC form has a more favorable biodistribution since there is less uptake in the intestines and bowel (Belhocine and Blankenberg, 2005). Labeling of annexin V-HYNIC with ^{99m}Tc is well established in a premade kit (Boersma et al., 2005) and the majority of human studies have used ^{99m}Tc-HYNIC-annexin V.

Evaluation of ^{99m}Tc-HYNIC-annexin V in healthy male volunteers indicated that it has a better biodistribution than the radiotracer used by Belhocine

et al (Belhocine et al., 2002) (BTAP form) since there is less uptake in the abdomen (Kemerink et al., 2003). This form of radiolabeled annexin V has been studied the most in human patients for the purpose of imaging apoptosis. Unfortunately, 50% of this tracer's injected dose accumulated in the kidneys three hours after injection (Kemerink et al., 2003). Other organs that indicated significant accumulation were the liver, red marrow and spleen (Kemerink et al., 2003). Future apoptosis-indicating probes should be designed to have less uptake in these organs and hence a more favorable biodistribution.

^{99m}Tc-HYNIC-annexin V SPET was evaluated in eleven lymphoma patients after XRT, and this was the first study to image radiation-induced apoptosis in lymphoma patients at early stages of treatment (Haas et al., 2004). Follicular lymphoma was chosen since it is highly sensitive to XRT and undergoes rapid onset of response (Haas et al., 2004). Tumor ^{99m}Tc-HYNIC-annexin V uptake was increased after 2 fractions of 2 Gray XRT and the increased uptake correlated with the appearance of apoptotic morphology as determined by cytology and subsequent clinical outcome (Haas et al., 2004).

^{99m}Tc-HYNIC-annexin V SPET was used in another study by Kartachova *et al* (Kartachova et al., 2004) to evaluate tumor response to therapy in 33 patients with malignant lymphoma, leukemia, non-small cell lung cancer (NSCLC), and head and neck squamous cell carcinoma (H&NSCC). XRT was used to treat 27 patients, chemotherapy for 5 patients and one patient received both. Complete or partial response was associated with an increase in annexin V uptake soon after treatment initiation compared to baseline (before treatment) (Kartachova et al.,

2004). Apoptosis could be detected after treatment with either XRT or chemotherapy. The tumors in the study were considered both apoptosis sensitive (lymphoma) and apoptosis resistant (NSCLC and H&NSCC). The results suggest that annexin V may be used as a predictive assay for early treatment response. Unfortunately there is a need for a larger patient cohort and awareness that annexin V will not discriminate between apoptotic cells versus necrotic cells (Kartachova et al., 2004).

NSCLC is a malignancy where early knowledge of potential response to therapy could significantly help clinicians and improve patient outcomes. Chemotherapy results in a modest improvement in advanced lung cancer patients; however, it is also associated with significant toxicity (Kartachova et al., 2007). Sixteen patients with NSCLC scheduled for platinum-based chemotherapy were evaluated with ^{99m}Tc-HYNIC-annexin V SPET before and 48 hours after start of therapy (Kartachova et al., 2007). In this study, SPET scans at 48 hours showing an increase in annexin V tumor uptake correlated with patient response (complete or partial response) (Kartachova et al., 2007). Progressive disease was associated with a *decrease* in annexin V tumor uptake (Kartachova et al., 2007). Compared to small cell lung cancer, NSCLC is relatively insensitive to chemotherapy. This may be due to the frequent alteration of p53 and development of resistance to apoptosis. In one study of 118 NSCLC specimens, p53 alterations were detected in 63% of the tumors (Mori et al., 2004).

H&NSCC is treated with a course of chemoradiation therapy that can be effective yet accompanied by toxic side effects (Hoebers et al., 2008). ^{99m}Tc-HYNIC-annexin V SPET was performed in 13 H&NSCC patients before and 48 hours after the start of chemoradiation; however, there was no correlation between annexin V tumor uptake and patient outcome (Hoebers et al., 2008). This may be partly due to baseline necrosis in these tumors (before treatment) that confounds the use of ^{99m}Tc-HYNIC-annexin V SPET as a predictive tool. A previous study found that imaging of apoptosis can be quantitative even if using a SPET radiotracer; however, this result is only apparent when there is an absence of necrosis in the tumor (van de Wiele et al., 2003). Van de Wiele *et al* (van de Wiele et al., 2003) found that the uptake of ^{99m}Tc-HYNIC-annexin V in tumors of head and neck cancer patients correlated well with the number of apoptotic cells derived from TUNEL assays of the tumor from surgical resection, supporting the validity of the imaging approach.

There is some concern about the optimal time for imaging cell death after treatment of breast cancer (Green and Steinmetz, 2002). Baseline uptake of ^{99m}Tc-annexin V has been identified in some tumors (Green and Steinmetz, 2002). This highlights the requirement to obtain baseline images in order to determine whether treatment is in fact inducing new cell death (Green and Steinmetz, 2002). Experience with ^{99m}Tc-annexin V indicates that the optimal time for imaging apoptosis due to chemotherapy treatment is 24-72 hours after the first dose of chemotherapy (Belhocine and Blankenberg, 2005). Timing is also important

because apoptotic cells will be removed by macrophages and the rate of apoptosis may be specific to tumor type.

Due to the variation of kinetics of cell death, the optimal imaging time for acquiring images with annexin V may vary with the type of therapy and possibly also with tumor type (Belhocine and Blankenberg, 2005). It remains unclear if multiple annexin V scans will improve assessment of response (Belhocine and Blankenberg, 2005). Conventional SPET imaging may miss some of the apoptotic cells within a tumor due to poor contrast level (Belhocine and Blankenberg, 2005). ^{99m}Tc-annexin V studies with human patients have shown that it can sometimes be a useful predictive assay for treatment response early in therapy (Verheij, 2008). Despite the development of annexin V into a SPET tracer it is not particularly promising because the chemistry possibilities for enhancing this tracer are almost exhausted and because the funding for the commercialization of this probe is lacking. Future research should focus on the development of annexin V into a PET tracer in order to obtain better quality images.

1.3.4 Phosphatidylserine-binding peptides.

PS-binding peptides may provide advantages as imaging agents because they are smaller than the PS-binding annexin V and this may contribute to a more favorable biodistribution for imaging purposes. Recently, research has been published by various groups using phage display to isolate peptides that bind to PS and cells undergoing apoptosis (Burtea et al., 2009; Caberoy et al., 2009; Hong et al., 2008; Laumonier et al., 2006; Shao et al., 2007; Thapa et al., 2008). Other

groups which did not use phage display technology, have identified fluorescently labeled peptides which are able to bind to apoptotic cells (DiVittorio et al., 2006; Lee et al., 2011). These peptides are candidates to be radiolabeled with radionuclides and evaluated as radiotracers to image apoptosis. Some groups have focused on developing MRI constrast agents based on PS-binding peptides; however, they have had limited success with this imaging modality (Burtea et al., 2009; Radermacher et al., 2010). A PS-binding peptide isolated by Laumonier *et al* has been evaluated in PS-binding assays but has not yet been evaluated in cell models of apoptosis (Laumonier et al., 2006). A fluorescently-labeled peptide isolated by Hong *et al* was shown to bind to ischemic tissue from a rat model without binding healthy tissues (Hong et al., 2008). A fluorescently labeled peptide described by DiVittorio *et al* was shown to bind to Jurkat cells and Hela cells undergoing apoptosis(DiVittorio et al., 2006). Thapa *et al* evaluated a PS-binding peptide in H460 and H157 human lung cancer cells and U937 leukemia cells undergoing apoptosis after etoposide treatment (Thapa et al., 2008). An optical imaging technique was also used *ex vivo* to evaluate the fluorescently-labeled peptide in tumor-bearing mice (H460 lung cancer xenograft model) treated with a single dose of camptothecin (Thapa et al., 2008). The results of optical imaging indicate that the peptide specifically bound to apoptotic cells and surprisingly to tumor vasculature (Thapa et al., 2008). Previous research has found that vascular endothelial cells in tumors, but not in normal vasculature, externalize PS which may be caused by oxidative stress and activating cytokines associated with the tumor (Ran and Thorpe, 2002). PS externalization in tumor

vasculature would explain the optical imaging results using a fluorescently-labeled peptide; however, this finding reinforces the importance of imaging before and after treatment in order to analyze changes in PS externalization due to treatment of the tumor.

Recently three PS-binding peptides were isolated by phage display technology and shown to bind to apoptotic cells with high affinity (Burtea et al., 2009). One selective and high affinity peptide (LIKKPF, $K_d = 2 \times 10^{-9}$ M) was selected for development into a magnetic resonance imaging (MRI) contrast agent by conjugating to diethylenetriaminepentaaceticacid (DTPA)-isothiocyanate and complexing with gadolinium chloride (Burtea et al., 2009). This contrast agent was tested with apoptotic Jurkat cells treated with camptothecin and in a mouse model of liver apoptosis in wild type mice induced by anti-Fas antibody (Burtea et al., 2009). This research group is interested in the contribution of apoptosis to the instability of atherosclerotic lesions and aimed to image apoptosis in plaques in order to diagnose plaques vulnerable to rupture (Burtea et al., 2009). Apoptosis of macrophages and smooth muscle cells contributes to the expansion of the necrotic core and thinning of the fibrous cap which could possibly play a role in the plaque rupture (Burtea et al., 2009). Atherosclerotic lesions were successfully imaged with MRI in $ApoE^{-/-}$ transgenic mice, indicating that this agent could potentially be used to image apoptosis in various disease states (Burtea et al., 2009). However, a major limitation of this MRI contrast agent is the low sensitivity which limits detection of apoptosis in regions with low PS concentration (Burtea

et al., 2009). This challenge might be overcome by preparing radiolabeled analogs of the peptides and by using SPET or PET imaging techniques.

Various PS-binding peptides have displayed high affinity binding to apoptotic cells, suggesting that these peptides should be radiolabeled with various radionuclides for development into novel PET and SPET probes. Currently only two studies evaluated radiolabeled PS-binding peptides for molecular imaging purposes. The peptide from Hong *et al* was radiolabeled with ^{131}I and autoradiography images indicate that the peptide bound to ischemic lesions in a rat model of apoptosis (Hong et al., 2008). A recent report by Xiong *et al* evaluated a peptide with high affinity for PS (K_d= 100 nM) (Xiong et al., 2011). The peptide was radiolabeled with ^{99m}Tc and evaluated in a melanoma model of apoptosis in mice treated with poly(L-glutamic acid)-paclitaxel. There was a significant different between the %ID/g in treated versus untreated tumor using the ^{99m}Tc radiolabeled peptide (Xiong et al., 2011). This is a very promising approach to develop a peptide based tracer for imaging of apoptosis. It would be very interesting to see the potential SPET images generated from this radiotracer, unfortunately no SPET images were acquired in this report. Future work could focus on radiolabeling PS-binding peptides with ^{18}F to promote the development of novel probes for PET. PS-binding peptides have not been tested in humans and require further development and pre-clinical evaluation.

The research in this thesis is on imaging apoptosis; however, for completeness we discuss several modes of cell death including senescence, necrosis, and autophagy.

1.4 Imaging premature senescence.

Premature senescence (also referred to as accelerated senescence or stress-induced premature senescence) is a genetically-programmed response to DNA damage that is regulated by the $p21^{WAF1}$ protein (hereafter simply called p21) (Roninson, 2003; Shay and Roninson, 2004). p21 is encoded by the $p21^{WAF}$ gene that is transcriptionally transactivated by the p53 tumor-suppressor protein in response to genotoxic stress caused by DNA-damaging agents such as ionizing radiation and various anticancer chemotherapeutic drugs. Premature senescence was originally described in fibroblasts, where exposure to ionizing radiation was seen to trigger a permanently growth-arrested phenotype with a striking resemblance to telomere-based "replicative" senescence (Di Leonardo et al., 1994; Linke et al., 1996). This mode of cell death has also been observed in many human tumor cell lines that express wild-type (WT) p53 following exposure to ionizing radiation and chemotherapeutic drugs(Chen et al., 1998; Mirzayans et al., 2005; Wang et al., 1999). Irradiation of some p53-deficient tumor cells also appears to activate at least some aspects of the premature senescence program, albeit to a much lesser extent than in p53-WT cells (R Mirzayans and D Murray, unpublished).

Current *in-vitro* markers for cells undergoing premature senescence in response to genotoxic stress include: (i) marked alterations in cell morphology, including enlargement and flattening, although the cells do retain cell membrane integrity (viability) and continue to function metabolically; (ii) acquisition of senescence-associated β-galactosidase (SA-β-gal) activity(Chang et al., 1999; Mirzayans et al., 2005; Wang et al., 1999); and (iii) sustained up-regulation of the *p21* gene/p21 protein in the nucleus(Chen et al., 1995; Di Leonardo et al., 1994; Dulic et al., 1994; el-Deiry et al., 1994; Kang et al., 2004; Mirzayans and Murray, 2007; Mirzayans et al., 2005). The role of p21 in activating premature senescence appears to involve multiple mechanisms, including the inhibition of various cyclin-dependent kinases, thereby preventing cell-cycle progression(Rousseau et al., 1999), suppression of DNA synthesis via an interaction with proliferating cell nuclear antigen (PCNA) (Rousseau et al., 1999), and modulation of gene expression (Baylin, 1997; Chang et al., 2000; Roninson et al., 2001). The loss of cellular clonogenic potential associated with premature senescence may be an important contributor to tumor control following both chemotherapy (Schmitt et al., 2002) and XRT (Suzuki and Boothman, 2008).

1.4.1 Potential for imaging *p21* transcripts by PET using ^{18}F-labeled antisense oligonucleotide probes. Currently there are no validated probes for the *in vivo* imaging of senescence. Although SA-β-gal staining has been performed with murine tumors treated with cyclophosphamide *in vivo*, this necessitated invasive sectioning of cryopreserved tissue (Schmitt et al., 2002). One approach that could prove useful for the non-invasive *in-vivo* monitoring of premature

senescence in tumor cells post-therapy using PET involves imaging *p21* gene expression using ^{18}F-labeled antisense oligonucleotide probes (*as*ODNs) (Koslowsky et al., 2007). *as*ODNs are small synthetic molecules that can bind to their complementary 'target' mRNA in cells, and thus they have the potential for use as probes for the *in vivo* molecular imaging of specific gene transcripts (Dewanjee et al., 1994; Roivainen et al., 2004; Wang et al., 2003). Given the above-mentioned key role of sustained *p21* gene activation in driving the premature senescence response to DNA damage *in vitro*, the ability to non-invasively monitor changes in the levels of this transcript *in situ* could provide an important marker for premature senescence *in vivo*. An elegant proof-of-principle study for this approach used a breast cancer xenograft model in which tumor *p21* mRNA levels were stimulated using epidermal growth factor (EGF); the tumors were successfully imaged with a gamma camera using ^{111}In-labeled anti-*p21* *as*ODNs (Wang et al., 2003). As noted in previous sections of this review, the extension of this technology to PET imaging should provide a significant increase in sensitivity and utility and is currently being evaluated by our group. Based on previously-described sequences (Tian et al., 2000; Wang et al., 2003), we have synthesized a fully phosphorothioated 18-nucleotide *as*ODN targeted to the 3′-untranslated region of the human *p21* mRNA. We have validated this *as*ODN for targeting *p21* mRNA *in vitro* in HCT116 human colon cancer cells (Koslowsky et al., 2009; von Guggenberg et al., 2009) and have seen no loss of activity following radiofluorination (with ^{18}F) of these ODNs using an established protocol

(Kuhnast, 2003). To date, this probe has not been tested in *in vivo* models but it is a promising approach that warrants further investigation.

1.4.2 Other approaches. It may be possible to use standard PET imaging techniques to monitor cells undergoing premature senescence *in vivo* by focusing on the unique biology of these cells. Proliferating tumor cells are typically positive for ^{18}F-FDG which, as noted in section 2, is believed to reflect their increased glycolytic rate and glucose avidity (Quon and Gambhir, 2005), and they are also positive for 3′-deoxy-3′-[^{18}F]-fluorothymidine (^{18}F-FLT) which measures cell proliferation independent of cellular metabolism (Weissleder, 2006). As noted above, a hallmark of tumor cells that have undergone premature senescence is that they maintain a significant level of metabolic activity despite being permanently growth-arrested (Roninson, 2003). It is therefore possible that whereas proliferating tumor cells will be both FDG^{+} and FLT^{+}, those tumor cells that activate the premature senescence program following therapy will cease to proliferate (and thus exhibit minimal FLT uptake) but will maintain significant metabolic activity (and thus will continue to take up FDG).

Although this hypothesis has not been tested directly, there are anecdotal examples in the literature where tumors were irradiated and monitored at early times using both FDG and FLT. For example, Yang and colleagues exposed SCCVI murine squamous cell carcinoma tumors to X-rays and monitored their response using PET imaging; these tumors were initially ^{18}F-FDG^{+}/^{18}F-FLT^{+} by PET imaging, but became dramatically ^{18}F-FLT^{-} at 24 and 48 h after a single exposure to 10 or 20 Gy of X-rays while retaining full ^{18}F-FDG-avidity (Figure 1-

2)(Yang et al., 2006). The authors suggested that this effect might be caused by an anticipated suppression of the enzyme thymidine kinase by X-rays (Yang et al., 2006); although this may indeed be the explanation in whole or in part, it is interesting that this is also the behavior that might be expected of a tumor in which the premature senescence phenotype was playing a significant role following XRT. The creative use of ^{18}F-FDG and other recently introduced clinical PET tracers such as ^{18}F-FLT may have some value in determining the specific tissue response to therapy. However, these measurements will always be non-specific and therefore do not directly measure cell death.

1.5 Imaging necrosis

Necrosis is generally regarded as a non-specific (i.e., not genetically regulated) mode of cell death characterized by cell swelling, denaturation/coagulation of cytoplasmic proteins, random fragmentation of DNA, and disintegration of sub-cellular organelles and of the cell membrane with release of cytotoxic cell components (Okada and Mak, 2004). Necrosis is usually determined *in vitro* using microscopy analysis (Verheij, 2008). There has been some development of necrosis probes based on the synaptic vesicle membrane protein synaptotagmin. This protein does not specifically bind to PS; however, it does bind to anionic phospholipids (such as PS and phophatidylethanolamine) which are exposed when the cell membrane is disrupted and which might be used to indicate necrosis (Davletov and Sudhof, 1993; Zhao et al., 2006). The C2A domain of synaptotagmin has been radiolabeled with ^{99m}Tc and used as a molecular probe for non-invasive imaging of acute myocardial infarction and

ischemia (Audi et al., 2007; Liu et al., 2007; Zhao et al., 2006). Synaptotagmin-^{99m}Tc has been evaluated in a healthy rat model and in a rat model of acute myocardial infarction (Zhao et al., 2006). Myocardial infarct and ischemia is clearly visible in the SPET images obtained with this tracer (Zhao et al., 2006). Synaptotagmin-^{99m}Tc has been evaluated in a mouse model of NSCLC and found to bind to tumors after chemotherapy; however, this tracer also indicated uptake in kidneys and liver (Wang et al., 2008). Synaptotagmin has not been evaluated in humans, and its clinical use is uncertain. It may have some applications that warrant use in clinical practice; however, due to its lack of specificity it may not be as powerful as other tracers under development. Other probes for imaging necrosis take advantage of the characteristic loss of cell membrane integrity, and these have been recently reviewed (De Saint-Hubert et al., 2009). Other compounds that can bind to cells with loss of membrane potential could potentially be developed into radiotracers. Future work should focus on developing new potential probes for *in vivo* imaging of necrosis in order to generate a specific probe for necrosis (i.e., that do not overlap with phosphatidylserine/apoptosis) which will help to differentiate cell death response(s) after treatment.

1.6 Imaging autophagy

Autophagy is a conserved stress response in which cells exit the cell cycle, autodigest proteins and damaged organelles, shrink, and recycle amino acids and fatty acids (Hait et al., 2006). It is controlled by pathways that signal through the

mTOR (mammalian target of rapamycin) protein and occurs in some tumor cell lines following exposure to XRT or chemotherapeutic agents (Ito et al., 2005; Paglin and Yahalom, 2006). It is unclear if autophagy provides cancer cells with an escape mechanism or if autophagy is used to eliminate tumor cells in the body (Kondo et al., 2005). It is also not clear whether autophagy is a separate form of cell death or if failure of autophagy to rescue cells from stress can lead to cell death by either apoptosis or necrosis. Currently, transmission electron microscopy is the standard method for *in vitro* detection of autophagy (Verheij, 2008). Microtubule-associated protein light chain 3 (LC3) is now widely used for *in vitro* detection of autophagy (Mizushima and Yoshimori, 2007). Endogenous LC3 is detected as two bands following sodium dodecyl sulfate polyacrylamide gel electrophoresis and immunoblotting. One band is LC3-I which is cytosolic and the other is LC3-II which is bound to phosphatidylethanolamine and is present on autophagosomes (Mizushima and Yoshimori, 2007). The amount of LC3-II is correlated with the number of autophagosomes and experiments can detect the LC3 conversion of LC3-I to LC3-II (Mizushima and Yoshimori, 2007). The development of a radiotracer specific for autophagy is a possibility if a compound could be isolated which binds specifically to LC3-II with high affinity. Autophagy may be an important mode of tumor cell death after treatment but, at present, we do not have a specific method to image it *in vivo* (de Bruin and Medema, 2008). A basic research initiative is required to firstly identify a target which is unique to autophagy and secondly to develop an imaging probe based on this target.

1.7 Summary and future directions.

Our present understanding of cell death is mainly derived from observations on cells *in vitro* and *ex vivo* tissues. There is now an increasingly clear picture of the distinct modes of cell death in terms of their morphological changes and the genomic and proteomic changes that are characteristic of each mode. This remains an area of vigorous research activity including applying the observations made in cells and isolated tissues to the investigation of cell death *in vivo*. In this context, and as outlined in this review, we are starting to see the development and preclinical and clinical exploitation of radionuclide-based molecular imaging probes with the capacity to selectively and non-invasively image the different modes of cell death.

Apoptosis has been the most intensively studied mode of cell death and the majority of tracer development has focused on this pathway. The four classes of imaging agents for apoptosis described in this review are: (i) caspase binding probes in pre-clinical development, (ii) low molecular weight probes in Phase-II clinical trials for PET imaging, (iii) annexin V in Phase-II/III clinical trials for SPET imaging, and (iv) PS-binding peptides in pre-clinical development. Imaging of premature senescence is being approached using ^{18}F-labeled antisense oligonucleotide probes to image *p21* transcripts with PET. Necrosis has one main tracer, synaptotagmin, in preclinical development as a SPET radiopharmaceutical. The role of autophagy in tumor response to therapy is not completely understood; however, the development of probes to image autophagy would help to explore the prevalence and define the importance of this pathway.

Interestingly, a number of the radiotracers in use or under development for imaging cell death are analogs of targeting agents first applied as fluorescent probes for *in vitro* cell studies or for probing tissues from animal studies or human biopsy. This is the case for annexin V, where the radionuclide probes labeled with ^{99m}Tc or ^{18}F have exploited the known PS targeting of fluorescent probes such as annexin V fluorescein isothiocyanate (van Engeland et al., 1996). Thus other fluorophore-based probes should be considered as lead compounds for potential radionuclide probes. For example, a recently developed fluorogenic substrate, 5-dodecanoylaminofluorescein di-β-D-galactopyranoside (C_{12}FDG), is the basis for fluorescence imaging of senescent cell-associated β galactosidase activity (Debacq-Chainiaux et al., 2009). As a substrate for β galactosidase, this agent is trapped following cleavage of galactose from the fluorescent core of the molecule. This raises the possibility of radiolabeling the sugar portion of the probe which would be trapped following phosphorylation, thereby providing a radionuclide imaging probe specific for senescent cells.

In spite of recent developments in identifying targets and probes for cell death and the progression of several of the radiolabeled probes into preclinical and clinical development, there are a number of significant challenges to effectively imaging the various modes of cell death *in vivo*. Imaging needs to be performed before and after treatment and the protocol needs to be consistent in how the images are obtained. Other factors to consider include the injection dose, type of SPET or PET camera used to obtain images, acquisition protocol, software for

analysis, and interpretation criteria (Belhocine and Blankenberg, 2005). These factors need to be consistent in multi-center clinical trial evaluation of radiotracers and the same factors also need to be consistent in patients when obtaining pre- and post-therapy images. As noted above, tumor cells may also die at varying rates, and the time course also depends on the type of treatment. This is important to consider when evaluating a radiotracer in various cancers and associated therapies. *In vivo*, this may be due to many factors including the tumor micro-environment and accessibility of the tumor to vasculature. Thus any effective imaging protocol will need to explore these features to provide appropriate guidelines for the timing of imaging following treatment.

The overall message of this review is that early tumor response to therapy is very complex. This review discusses four possible cell death mechanisms, each of which represents unique and complex pathways. The use of radiotracers to image individual cell death mechanisms would provide valuable information on tumor response in a rapid and non-invasive manner, and this information could be used to make subsequent decisions about patient treatment. Ideally these imaging agents would be specific for one mode of cell death and would be properly validated and capable for use with PET. Currently the mechanism of cell death is unknown for most solid tumors, and tumor regression may actually be due to a combination of cell death mechanisms resulting in overall tumor size reduction (Okada and Mak, 2004; Schmitt et al., 2002). Responses at the cellular level can have profound clinical implications in selecting and applying effective therapy.

Given that tumor cells can lose their clonogenic potential through several different pathways, it will be critical to better understand and monitor modes of cell death in tumors from individual patients in order to better exploit inter-individual differences when combining conventional genotoxic therapeutics with modifying agents. Thus there would appear to be a clinical role for imaging agents that could identify the specific cellular response to therapy. Imaging agents would also have an important role to play in preclinical investigations in animal models in helping to understand the induction and progression of the various cell death mechanisms and in drug development studies. While this review has concentrated on cancer, it must be remembered that cell death is a factor in many diseases both as an acute event (stroke, heart attack) or chronic progression (arthritis, neurodegeneration). Consequently we can expect that the research efforts will continue as we attempt to fully understand the cell death mechanisms and to develop probes for *in vitro* and *in vivo* imaging.

1.8 Research question

We currently do not have an established clinical method to assess apoptosis induced by cancer therapies. Currently the effectiveness of cancer treatment is ascertained by a change in tumor size which requires weeks to months. Detection of apoptosis would give an almost immediate indication of effective cancer treatment before the tumor changes in size and could be evaluated 1-3 days after the patient receives treatment. We aim to address the above problem by specifically imaging the apoptotic response after therapy as a way to

non-invasively assess tumor response to therapy. Our goal is to assess tumor response to chemotherapy and radiation therapy by developing a suitable radiopharmaceutical to monitor the apoptotic response using PET imaging.

One approach is to develop a molecular imaging probe based on radiolabeled peptides which bind to externalized PS. Peptides may provide advantages as imaging agents because they are smaller than the PS-binding annexin V and this may contribute to a more favorable biodistribution for imaging purposes. Peptides have a number of potential advantages as radiotracers including small size, good tissue diffusion, rapid targeting, low antigenicity, easy synthesis, well developed radiolabeling, fast blood clearance, and inexpensive production (Langer and Beck-Sickinger, 2001; Reubi and Maecke, 2008; Weiner and Thakur, 2002, 2005). We propose that PS-binding peptides radiolabeled with ^{18}F could be effective radiotracers for imaging apoptosis *in vivo*. Recently, Burtea et al. (2009) isolated two phages displaying the peptides LIKKPF and PGDLSR, which have high affinity and specificity for PS. The preliminary report of these peptides prompted us to investigate their application as possible molecular imaging probes for use with PET.

1.9 Hypothesis

We hypothesize that a peptide radiopharmaceutical binding to apoptotic cells can be developed and can be used to image cell death *in vivo* using PET.

1.10 Objectives:

The objectives of this thesis are:

- 1) Evaluate binding characteristics of four peptides for ability to bind to PS.

- 2) Radiolabel PS-binding peptides with ^{18}F.

- 3) Perform *in vitro* and *in vivo* analysis of ^{18}F radiolabeled PS-binding peptides including biodistribution analysis and dynamic PET imaging in a murine tumor model of apoptosis.

1.11 Experimental overview

In this body of research we characterized four peptides for their ability to bind to PS and apoptotic cells, we radiolabeled PS-binding peptides with ^{18}F using two prosthetic groups, and we evaluated two radiolabeled PS-binding peptides *in vitro* and *in vivo* using dynamic PET imaging and biodistribution analysis. We determined the dissociation constant of four peptides binding to PS using a plate assay, determined binding of peptides to PS using a liposome assay, and confirmed binding of the peptides to apoptotic Jurkat cells. We radiolabeled the PS-binding peptides with ^{18}F using the prosthetic groups N-succinimidyl-4-[^{18}F]fluorobenzoate ([^{18}F]SFB) and N-[6-(4-[^{18}F]fluorobenzylidene)aminooxyhexyl]maleimide ([^{18}F]FBAM) and we

compared the scope and limitations of both of these prosthetic groups. We then evaluated two radiolabeled PS-binding peptides *in vitro* to determine ability of the radiolabeled peptides to bind to apoptotic Jurkat cells. Finally, we evaluated two radiolabeled peptides *in vivo* to determine metabolic stability, biodistribution, and ability to image apoptosis using dynamic PET.

Table 1-1. Characteristics of different types of cell death.

Type of Cell Death	**Morphological Changes**			**Biochemical features**	**Examples of common *in vitro* detection methods**
	Nucleus	**Cell membrane**	**Cytoplasm**		
Apoptosis	Chromatin condensation; nuclear fragmentation; DNA laddering	Blebbing	Fragmentation (formation of apoptotic bodies)	Caspase-dependent; phosphatidylserine externalization	Electron microscopy; TUNEL staining; annexin staining; caspase-activity assays; DNA-fragmentation assays
Premature Senescence	Distinct heterochromatic foci; upregulation of p21 gene/p21 protein in nucleus	-	Flattening and increased granularity	senescence-associated β-galactosidase activity	Electron microscopy; SA-β-gal staining; growth-arrest assays
Necrosis	Clumping and random degradation of nuclear DNA	Swelling; rupture	Increased vacuolation; organelle degeneration; mitochondrial swelling	-	Electron microscopy; nuclear staining (usually negative); detection of inflammation and damage in surrounding tissues
Autophagy	Partial chromatin condensation; no DNA laddering	Blebbing	Increased number of autophagic vesicles	Caspase-independent; increased lysosomal activity; increased LC3-II	Electron microscopy; protein-degradation assays;

LC3-II, microtubule-associated protein light chain 3-II; TUNEL, Terminal deoxynucleotidyl transferase dUTP nick end labeling. **Modified from: Okada and Mak, 2004.**

Table 1-2. Agents for Imaging cell death mechanisms.

Cell Death Mechanism	**Molecular Target**	**Imaging Agent**	**Status of Agent**
Apoptosis	Caspases	Caspase inhibitors (WC-II-98 and other isatin analogs)	Animal studies
	Unknown (Accumulates in apoptotic cells)	Small molecule probes (NST-732, ^{18}F-ML10)	Animal studies
		^{18}F-ML10	Clinical trials
	PS externalization	^{99m}Tc-Annexin V	Animal studies
		^{99m}Tc-Annexin V	Clinical trials
		^{125}I-Annexin V	Animal studies
		^{124}I-Annexin V	Animal studies
		^{18}F-Annexin V	Animal studies
		^{68}Ga-Annexin V	Animal studies
		PS-binding peptides	Animal studies
Premature Senescence	*p21* gene	^{18}F-labeled antisense-ODN probes	*In vitro*
	Metabolism signature	^{18}F-FLT/^{18}F-FDG	N/A
	β-galactosidase activity	Suggested as a target for development.	*In vitro*
Necrosis	Anionic phospholipids	C2A domain of ^{99m}Tc-synaptotagmin	Animal studies
Autophagy	LC3	Suggested as a target for development.	

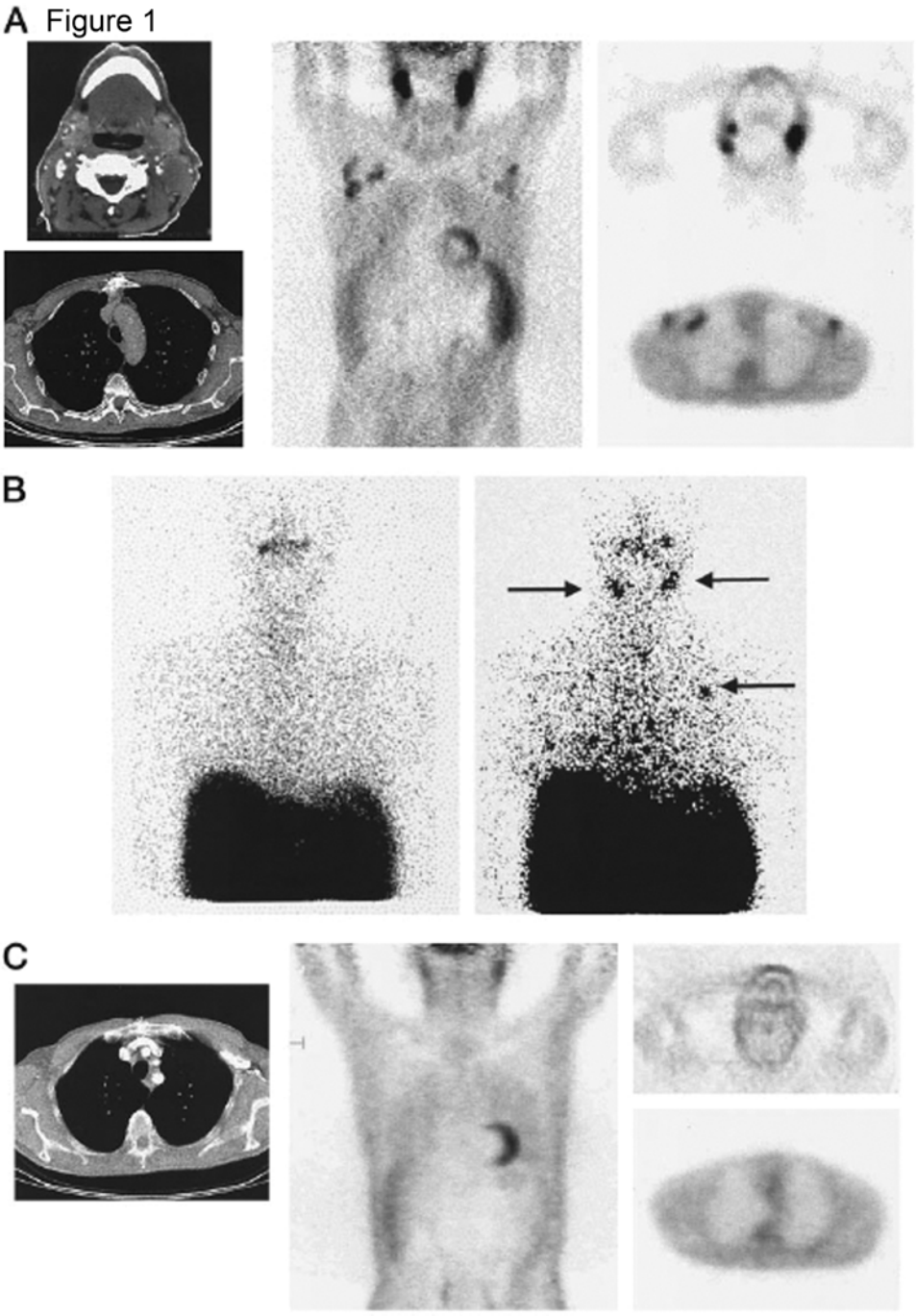

Figure 1-1. A case of non-Hodgkins lymphoma (stage IV) treated by cyclophosphamide-doxorubicine-vincristine-prednisone protocol with a positive ^{99m}Tc-annexin V study. *A*, the CTs of the neck and of the thorax (*left*) and the ^{18}FDG PET scan (*middle* and *right*) performed before treatment showed a lymph

node dissemination at the cervical and axillary levels. *B*, the annexin V imaging performed immediately before (*left*) and 48 h after chemotherapy (*right*) demonstrated an increased uptake of the apoptosis agent at the tumor sites (*arrows*). *C*, the posttreatment evaluation by the CT and PET scans showed complete disappearance of disease. From: (Belhocine et al., 2002) Figure 2.

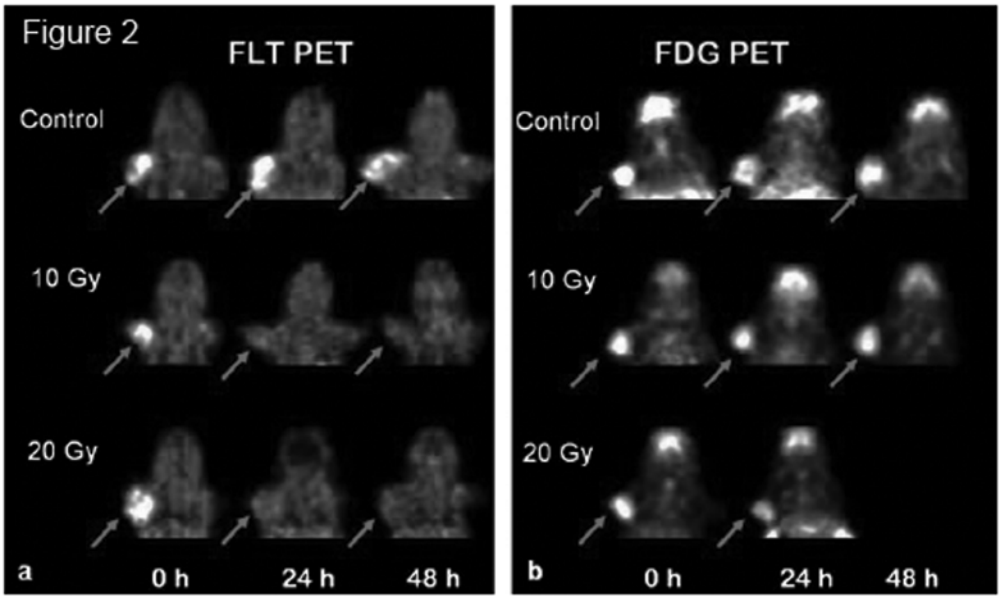

Figure 1-2. Serial PET images of murine small cell carcinoma VII tumors after radiation treatment. (A) FLT PET images showing that the tumor uptake of FLT (arrows) was markedly reduced 24 h and 48 h after irradiation. (B) FDG PET images showing that tumor uptake was not affected by radiation treatment (one FDG image at 48 h is missing). From: (Yang et al., 2006) Figure 4.

1.12 References:

2008a. Evaluation of [18F]-ML-10 as a PET imaging radiotracer for early detection of response of brain metastases to whole brain radiation therapy., Clinical Trials.gov: A service of the US National Institutes of Health.

2008b. Evaluation of the efficacy and safety of [18F]-ML-10, as a PET imaging radiotracer, in early detection of response of brain metastases of solid tumors to radiation therapy., Clinical Trials.gov: A service of the US National Institutes of Health. .

Andree, H.A., Reutelingsperger, C.P., Hauptmann, R., Hemker, H.C., Hermens, W.T., Willems, G.M., 1990. Binding of vascular anticoagulant alpha (VAC alpha) to planar phospholipid bilayers. J Biol Chem 265, 4923-4928.

Baylin, S.B., 1997. Tying it all together: epigenetics, genetics, cell cycle, and cancer. Science 277, 1948-1949.

Belhocine, T.Z., Blankenberg, F.G., 2005. 99mTc-Annexin A5 uptake and imaging to monitor chemosensitivity. Methods Mol Med 111, 363-380.

Belhocine, T.Z., Tait, J.F., Vanderheyden, J.L., Li, C., Blankenberg, F.G., 2004. Nuclear medicine in the era of genomics and proteomics: lessons from annexin V. J Proteome Res 3, 345-349.

Burtea, C., Laurent, S., Lancelot, E., Ballet, S., Murariu, O., Rousseaux, O., Port, M., Vander Elst, L., Corot, C., Muller, R.N., 2009. Peptidic targeting of phosphatidylserine for the MRI detection of apoptosis in atherosclerotic plaques. Mol Pharm 6, 1903-1919.

Caberoy, N.B., Zhou, Y., Alvarado, G., Fan, X., Li, W., 2009. Efficient identification of phosphatidylserine-binding proteins by ORF phage display. Biochem Biophys Res Commun 386, 197-201.

Chang, B.D., Broude, E.V., Dokmanovic, M., Zhu, H., Ruth, A., Xuan, Y., Kandel, E.S., Lausch, E., Christov, K., Roninson, I.B., 1999. A senescence-like phenotype distinguishes tumor cells that undergo terminal proliferation arrest after exposure to anticancer agents. Cancer Res 59, 3761-3767.

Chang, B.D., Watanabe, K., Broude, E.V., Fang, J., Poole, J.C., Kalinichenko, T.V., Roninson, I.B., 2000. Effects of p21Waf1/Cip1/Sdi1 on cellular gene expression: implications for carcinogenesis, senescence, and age-related diseases. Proc Natl Acad Sci U S A 97, 4291-4296.

Chen, D.L., Zhou, D., Chu, W., Herrbrich, P., Engle, J.T., Griffin, E., Jones, L.A., Rothfuss, J.M., Geraci, M., Hotchkiss, R.S., Mach, R.H., 2011. Radiolabeled isatin binding to caspase-3 activation induced by anti-Fas antibody. Nucl Med Biol.

Chen, Q., Fischer, A., Reagan, J.D., Yan, L.J., Ames, B.N., 1995. Oxidative DNA damage and senescence of human diploid fibroblast cells. Proc Natl Acad Sci U S A 92, 4337-4341.

Chen, Q.M., Bartholomew, J.C., Campisi, J., Acosta, M., Reagan, J.D., Ames, B.N., 1998. Molecular analysis of H2O2-induced senescent-like growth arrest in normal human fibroblasts: p53 and Rb control G1 arrest but not cell replication. Biochem J 332 (Pt 1), 43-50.

Debacq-Chainiaux, F., Erusalimsky, J.D., Campisi, J., Toussaint, O., 2009. Protocols to detect senescence-associated beta-galactosidase (SA-betagal) activity, a biomarker of senescent cells in culture and in vivo. Nat Protoc 4, 1798-1806.

Di Leonardo, A., Linke, S.P., Clarkin, K., Wahl, G.M., 1994. DNA damage triggers a prolonged p53-dependent G1 arrest and long-term induction of Cip1 in normal human fibroblasts. Genes Dev 8, 2540-2551.

DiVittorio, K.M., Johnson, J.R., Johansson, E., Reynolds, A.J., Jolliffe, K.A., Smith, B.D., 2006. Synthetic peptides with selective affinity for apoptotic cells. Org Biomol Chem 4, 1966-1976.

Dulic, V., Kaufmann, W.K., Wilson, S.J., Tlsty, T.D., Lees, E., Harper, J.W., Elledge, S.J., Reed, S.I., 1994. p53-dependent inhibition of cyclin-dependent kinase activities in human fibroblasts during radiation-induced G1 arrest. Cell 76, 1013-1023.

el-Deiry, W.S., Harper, J.W., O'Connor, P.M., Velculescu, V.E., Canman, C.E., Jackman, J., Pietenpol, J.A., Burrell, M., Hill, D.E., Wang, Y., et al., 1994. WAF1/CIP1 is induced in p53-mediated G1 arrest and apoptosis. Cancer Res 54, 1169-1174.

Glaser, M., Goggi, J., Smith, G., Morrison, M., Luthra, S.K., Robins, E., Aboagye, E.O., 2011. Improved radiosynthesis of the apoptosis marker (18)F-ICMT11 including biological evaluation. Bioorg Med Chem Lett 21, 6945-6949.

Golstein, P., Kroemer, G., 2007. Cell death by necrosis: towards a molecular definition. Trends Biochem Sci 32, 37-43.

Green, A.M., Steinmetz, N.D., 2002. Monitoring apoptosis in real time. Cancer J 8, 82-92.

Guo, M.F., Zhao, Y.Q., Tian, R., Li, L., Guo, L.M., Xu, F., Liu, Y.M., He, Y.B., Bai, S., Wang, J., 2009. In vivo 99mTc-HYNIC-annexin V imaging of early tumor apoptosis in mice after single dose irradiation. J Exp Clin Cancer Res 28, 136.

Hait, W.N., Jin, S., Yang, J.M., 2006. A matter of life or death (or both): understanding autophagy in cancer. Clin Cancer Res 12, 1961-1965.

Hong, H.Y., Choi, J.S., Kim, Y.J., Lee, H.Y., Kwak, W., Yoo, J., Lee, J.T., Kwon, T.H., Kim, I.S., Han, H.S., Lee, B.H., 2008. Detection of apoptosis in a rat model of focal cerebral ischemia using a homing peptide selected from in vivo phage display. J Control Release 131, 167-172.

Juweid, M.E., Cheson, B.D., 2006. Positron-emission tomography and assessment of cancer therapy. N Engl J Med 354, 496-507.

Kang, H., Cui, K., Zhao, K., 2004. BRG1 controls the activity of the retinoblastoma protein via regulation of p21CIP1/WAF1/SDI. Mol Cell Biol 24, 1188-1199.

Kartachova, M., Haas, R.L., Olmos, R.A., Hoebers, F.J., van Zandwijk, N., Verheij, M., 2004. In vivo imaging of apoptosis by 99mTc-Annexin V scintigraphy: visual analysis in relation to treatment response. Radiother Oncol 72, 333-339.

Kartachova, M., van Zandwijk, N., Burgers, S., van Tinteren, H., Verheij, M., Valdes Olmos, R.A., 2007. Prognostic significance of 99mTc Hynic-rh-annexin V scintigraphy during platinum-based chemotherapy in advanced lung cancer. J Clin Oncol 25, 2534-2539.

Kolesnick, R., Fuks, Z., 2003. Radiation and ceramide-induced apoptosis. Oncogene 22, 5897-5906.

Kondo, Y., Kanzawa, T., Sawaya, R., Kondo, S., 2005. The role of autophagy in cancer development and response to therapy. Nat Rev Cancer 5, 726-734.

Koslowsky, I., Shahhosseini, S., Von Guggenberg, E., Murray, D., Lavasanifar, A., Mercer, J., 2009. In vitro evaluation of a block copolymer as a potential transfection agent of [^{18}F]-labeled antisense oligonucleotides. J Nuclear Medicine 50, 265.

Koslowsky, I., Wilson, J., Murray, D., Mercer, J., 2007. An ^{18}F-labeled antisense oligonucleotide as an imaging probe to measure cellular response to radiation therapy. J Label Compd Radiopharm 50, S405.

Kuhnast, B., Hinnen, F., Boisgard, R., Tavitian, B., Dolle, F., 2003. Fluorine-18 labelling of oligonucleotides: Prosthetic labelling at the 50-end using the N-(4-[18F]fluorobenzyl)-2-bromoacetamide reagent. J Label Compd Radiopharm 46, 1093.

Langer, M., Beck-Sickinger, A.G., 2001. Peptides as carrier for tumor diagnosis and treatment. Curr Med Chem Anticancer Agents 1, 71-93.

Laumonier, C., Segers, J., Laurent, S., Michel, A., Coppee, F., Belayew, A., Elst, L.V., Muller, R.N., 2006. A new peptidic vector for molecular imaging of apoptosis, identified by phage display technology. J Biomol Screen 11, 537-545.

Linke, S.P., Clarkin, K.C., Wahl, G.M., 1996. p53 mediates permanent arrest over multiple cell cycles in response to gamma-irradiation. Cancer Research 57, 1171.

Mirzayans, R., Murray, D., 2007. Cellular Senescence: Implications for Cancer Therapy., in: Garvey, R.B. (Ed.), New Research on Cell Aging. Nova Science Publishers, Hauppauge, New York, pp. 1-64.

Mirzayans, R., Scott, A., Cameron, M., Murray, D., 2005. Induction of accelerated senescence by gamma radiation in human solid tumor-derived cell lines expressing wild-type TP53. Radiat Res 163, 53-62.

Mizushima, N., Yoshimori, T., 2007. How to interpret LC3 immunoblotting. Autophagy 3, 542-545.

Murakami, Y., Takamatsu, H., Taki, J., Tatsumi, M., Noda, A., Ichise, R., Tait, J.F., Nishimura, S., 2004. 18F-labelled annexin V: a PET tracer for apoptosis imaging. Eur J Nucl Med Mol Imaging 31, 469-474.

Nguyen, Q.D., Smith, G., Glaser, M., Perumal, M., Arstad, E., Aboagye, E.O., 2009. Positron emission tomography imaging of drug-induced tumor apoptosis with a caspase-3/7 specific [18F]-labeled isatin sulfonamide. Proc Natl Acad Sci U S A 106, 16375-16380.

Okada, H., Mak, T.W., 2004. Pathways of apoptotic and non-apoptotic death in tumour cells. Nat Rev Cancer 4, 592-603.

Quon, A., Gambhir, S.S., 2005. FDG-PET and beyond: molecular breast cancer imaging. J Clin Oncol 23, 1664-1673.

Radermacher, K.A., Boutry, S., Laurent, S., Elst, L.V., Mahieu, I., Bouzin, C., Magat, J., Gregoire, V., Feron, O., Muller, R.N., Jordan, B.F., Gallez, B., 2010. Iron oxide particles covered with hexapeptides targeted at phosphatidylserine as MR biomarkers of tumor cell death. Contrast Media Mol Imaging 5, 258-267.

Ran, S., Thorpe, P., 2002. Phosphatidylserine is a marker of tumor vasculature and a potential target for cancer imaging and therapy. Int. J. Radiation Oncology Biol. Phys. 54, 1479-1484.

Reshef, A., Shirvan, A., Waterhouse, R.N., Grimberg, H., Levin, G., Cohen, A., Ulysse, L.G., Friedman, G., Antoni, G., Ziv, I., 2008. Molecular imaging of neurovascular cell death in experimental cerebral stroke by PET. J Nucl Med 49, 1520-1528.

Reubi, J.C., Maecke, H.R., 2008. Peptide-based probes for cancer imaging. J Nucl Med 49, 1735-1738.

Roninson, I.B., 2003. Tumor cell senescence in cancer treatment. Cancer Res 63, 2705-2715.

Roninson, I.B., Broude, E.V., Chang, B.D., 2001. If not apoptosis, then what? Treatment-induced senescence and mitotic catastrophe in tumor cells. Drug Resist Updat 4, 303-313.

Rousseau, D., Cannella, D., Boulaire, J., Fitzgerald, P., Fotedar, A., Fotedar, R., 1999. Growth inhibition by CDK-cyclin and PCNA binding domains of p21 occurs by distinct mechanisms and is regulated by ubiquitin-proteasome pathway. Oncogene 18, 4313-4325.

Schmitt, C.A., Fridman, J.S., Yang, M., Lee, S., Baranov, E., Hoffman, R.M., Lowe, S.W., 2002. A senescence program controlled by p53 and p16INK4a contributes to the outcome of cancer therapy. Cell 109, 335-346.

Shao, R., Xiong, C., Wen, X., Gelovani, J.G., Li, C., 2007. Targeting phosphatidylserine on apoptotic cells with phages and peptides selected from a bacteriophage display library. Mol Imaging 6, 417-426.

Shay, J.W., Roninson, I.B., 2004. Hallmarks of senescence in carcinogenesis and cancer therapy. Oncogene 23, 2919-2933.

Shirvan, A., 2009. Apoptosis imaging with PET-18F-ML-10 for early assessment of response of brain metastases to radiotherapy. J Nucl Med 50, 118P.

Suzuki, M., Boothman, D.A., 2008. Stress-induced premature senescence (SIPS)--influence of SIPS on radiotherapy. J Radiat Res (Tokyo) 49, 105-112.

Thapa, N., Kim, S., So, I.S., Lee, B.H., Kwon, I.C., Choi, K., Kim, I.S., 2008. Discovery of a phosphatidylserine-recognizing peptide and its utility in molecular imaging of tumour apoptosis. J Cell Mol Med 12, 1649-1660.

van Engeland, M., Ramaekers, F.C., Schutte, B., Reutelingsperger, C.P., 1996. A novel assay to measure loss of plasma membrane asymmetry during apoptosis of adherent cells in culture. Cytometry 24, 131-139.

Vangestel, C., Van de Wiele, C., Mees, G., Peeters, M., 2009. Forcing cancer cells to commit suicide. Cancer Biother Radiopharm 24, 395-407.

Verheij, M., 2008. Clinical biomarkers and imaging for radiotherapy-induced cell death. Cancer Metastasis Rev 27, 471-480.

von Guggenberg, E., Shahhosseini, S., Koslowsky, I., Lavasanifar, A., Mercer, J., 2009. Evaluation of novel biodegradable vectors for improved cellular uptake of radiolabeled oligonucleotides. . J Label Compd Radiopharm 52, S324.

Wahl, R.L., Jacene, H., Kasamon, Y., Lodge, M.A., 2009. From RECIST to PERCIST: Evolving Considerations for PET response criteria in solid tumors. J Nucl Med 50 Suppl 1, 122S-150S.

Wang, Y., Blandino, G., Givol, D., 1999. Induced p21waf expression in H1299 cell line promotes cell senescence and protects against cytotoxic effect of radiation and doxorubicin. Oncogene 18, 2643-2649.

Weiner, R.E., Thakur, M.L., 2002. Radiolabeled peptides in the diagnosis and therapy of oncological diseases. Appl Radiat Isot 57, 749-763.

Weiner, R.E., Thakur, M.L., 2005. Radiolabeled peptides in oncology: role in diagnosis and treatment. BioDrugs 19, 145-163.

Weissleder, R., 2006. Molecular imaging in cancer. Science 312, 1168-1171.

Xiong, C., Brewer, K., Song, S., Zhang, R., Lu, W., Wen, X., Li, C., 2011. Peptide-based imaging agents targeting phosphatidylserine for the detection of apoptosis. J Med Chem 54, 1825-1835.

Zhang, X., Paule, M.G., Newport, G.D., Zou, X., Sadovova, N., Berridge, M.S., Apana, S.M., Hanig, J.P., Slikker, W., Jr., Wang, C., 2009. A minimally invasive, translational biomarker of ketamine-induced neuronal death in rats: microPET Imaging using 18F-annexin V. Toxicol Sci 111, 355-361.

Zhao, M., Zhu, X., Ji, S., Zhou, J., Ozker, K.S., Fang, W., Molthen, R.C., Hellman, R.S., 2006. 99mTc-labeled C2A domain of synaptotagmin I as a target-specific molecular probe for noninvasive imaging of acute myocardial infarction. J Nucl Med 47, 1367-1374.

Chapter 2

Evaluation of Novel Phosphatidylserine-binding Peptides Targeting Apoptotic Cells

2.1 Introduction

Apoptosis is extensively studied since it is associated with cancer and several other diseases. The ability of tumor cells to evade apoptosis is one of the hallmarks of cancer (Hanahan and Weinberg, 2000). Techniques for detection and assessment of apoptosis at the cellular level are well developed. Less well developed are molecular imaging modalities for assessing apoptosis at the clinical level particularly in the context of apoptosis induced by cancer therapies. One of the goals of personalized medicine in cancer therapy is the selection and tailoring of therapies that achieve maximum tumor destruction with minimum side effects. Rapid assessment of tumor response to therapy is clinically challenging and would be greatly aided by a reliable molecular imaging modality that targeted apoptosis.

Changes observed at the cellular level during apoptosis include phosphatidylserine (PS) externalization, caspase activation, chromatin and nucleus condensation, reduction in the volume of the cytoplasm and DNA degradation. A number of these changes, particularly caspase activation and PS externalization, provide selective targets for potential molecular imaging probes. PS is an attractive target for imaging apoptosis since it is on the exterior of the apoptotic cells, it represents a high capacity target, and PS externalization is an early marker of apoptosis (Denecker et al., 2000; Martin et al., 1995). PS targeting with fluorescent annexin V has been widely employed for *in vitro* imaging and i*n vivo* probes, based on labelling annexin V with radionuclides, have been developed to allow non-invasive imaging of apoptosis using nuclear medicine techniques (Kapty et al.,

2010; Kartachova et al., 2004; Kartachova et al., 2006). Radiolabelled annexin V however has failed to gain wide acceptance as a clinical imaging agent due to a variety of limitations including less than optimal biodistribution. The difficulties encountered with various forms of radiolabelled annexin V are reviewed by Kapty et al. (2010) and these issues illustrate the continued need to identify a robust and clinically acceptable molecular imaging probe for apoptosis.

In the search for alternative strategies for targeting PS externalization a variety of approaches have been exploited including peptide selection using phage libraries and phage display technology. Peptides have a number of potential advantages as radiotracers including small size, good tissue diffusion, rapid targeting, low antigenicity, easy synthesis, well developed radiolabeling, fast blood clearance, and inexpensive production (Langer and Beck-Sickinger, 2001; Reubi and Maecke, 2008; Weiner and Thakur, 2002, 2005). Recently, Burtea et al. (2009) isolated two peptides, LIKKPF[1] and PGDLSR, which have high affinity and specificity for PS. LIKKPF was further investigated as a conjugate with gadolinium-diethylenetriaminepentaacetic acid (Gd-DTPA) as a possible apoptosis imaging probe for use with magnetic resonance imaging (MRI). Preliminary MRI studies in an animal model of liver apoptosis and the $ApoE^{-/-}$ mouse model of atherosclerosis were conducted but were only moderately successful due to the low sensitivity of the peptide-Gd-DTPA imaging probe which limits detection of apoptosis in areas with low PS concentration.

[1] See Appendix A for single letter amino acid sequence designation.

The preliminary report of these peptides in animal models of apoptosis prompted us to investigate their application as radiopharmaceutical probes for Positron Emission Tomography (PET) imaging of apoptosis. We decided to incorporate an ^{18}F label using established prosthetic groups. The prosthetic groups N-succinimidyl-4-[^{18}F]fluorobenzoate ([^{18}F]SFB) and N-[6-(4-[^{18}F]fluorobenzylidene)aminooxyhexyl]maleimide ([^{18}F]FBAM) were investigated for ability to radiolabel the peptides with ^{18}F (Kapty et al., 2011) (discussed in Chapter 3). While ([^{18}F]SFB) is reactive with amines and can therefore be directly attached at the N-terminus of peptides we encountered a variety of problems with the radiochemistry using this approach and investigated the thiol reactive [^{18}F]FBAM where we achieved superior yields and purity of products. The [^{18}F]FBAM approach however required the modification of the 6-mer peptides (Burtea et al. 2009) to the 7-mer peptides CLIKKPF and CPGDLSR by the addition of a thiol-containing cysteine residue at the N-terminus. The affinity and specificity of these modified peptides was previously unknown. We here describe the evaluation of two novel peptides and two previously isolated peptides *in vitro* using a plate based assay system, using liposome mimics of cell membrane PS presentation and using a cell assay of apoptosis.

2.2 Materials and methods:

2.2.1 General

Human recombinant annexin V-FITC was obtained from BD Biosciences (New Jersey, USA) and was used according to the manufacturer's instructions.

1,2-dipalmitoyl-*sn*-glycero-3-phosphocholine (DPPC), 1,2-dipalmitoyl-*sn*-glycero-3-[phospho-L-serine] (sodium salt) (DPPS), and cholesterol were obtained from Avanti® Polar Lipids (Alabaster, AL, USA). Peptides LIKKPF, PGDLSR, CLIKKPF and CPGDLSR were purchased modified at the N-terminus with the fluorescent tag 5-carboxy fluorescein amidite (5-FAM) from LifeTein LLC (South Plainfield, NJ, USA) with >95% purity. Binding buffer contains 10 mM HEPES, 140 mM NaCl, and 2.5 mM $CaCl_2$. All other reagents used were of analytical grade.

2.2.2 Fluorescence plate assay

The plate assay was used to test the affinity of peptides 5-FAM-LIKKPF, 5-FAM-PGDLSR, 5-FAM-CLIKKPF and 5-FAM-CPGDLSR for PS. Annexin V-FITC was also used as a control. PS was immobilized on clear bottom 96 well microplates (Corning Inc, Corning, NY, USA) after solubilization in ethanol at a concentration of 1.0 mg/mL (Burtea et al., 2009). Wells were filled with 200 μL of this solution, and a film was formed after overnight evaporation of the ethanol at room temperature. The same procedure was used with phosphatidylcholine (PC) as control. PS- or PC-coated plates were incubated with 50 μL of peptide suspension for 1 h at 37 ºC in the dark. The plates were washed three times with 50 μL binding buffer. Bound peptide was detected by a fluorescence plate reader FLUOstar OPTIMA (BMG Labtech GmbH, Offenburg, Germany) and PC software version V1.30 R4 (BMG LABTECH GmbH, Offenburg, Germany) was used for data collection.

2.2.3 Determination of the dissociation constant

The dissociation constant (K_d) of each fluorescently labeled peptide was determined by saturation experiments performed by the method described above. Serial peptide dilutions ranging from 10^{-4} M to 10^{-12} M (annexin V dilutions ranged from 10^{-7} M to 10^{-13} M) were prepared in binding buffer. The quantity of bound peptide obtained from the relative fluorescence units (RFU) values was plotted against the logarithmic concentration of total peptide input, and the curve was fitted according to a sigmoidal dose response profile using GraphPad Prism Version 5.04 for Windows (GraphPad software, San Diego, CA, USA). The peptide concentration at half-saturation corresponds to the K_d as determined by non-linear regression which can be considered a modern method to determine the value of K_d.

2.2.4 Preparation of liposomes

For the PC liposome formulation (0 % PS) 1.2 mL of DPPC (20 mg/mL) and 1.2 mL cholesterol (4.89 mg/mL) were combined in a 250 mL round bottom flask. For 10% PS liposomes the solution was adjusted by the addition of 2.4 mL of DPPS (1.03 mg/mL). The solvent was removed under reduced pressure using a rotatory evaporator to form a thin film on the inside of the flask (Cabral et al., 2003). The dry lipid film was rehydrated in 2 mL of sodium acetate (1 M, pH 6.0). The solution was sonicated and extruded through polycarbonate membranes (pore size 2 µm, 25 mm; Nucleopore, Whatman, Piscataway, NJ, USA).

2.2.5 Confocal microscopy of liposomes

Confocal microscopy analysis of liposomes was used to visualize the binding of peptides 5-FAM-LIKKPF, 5-FAM-PGDLSR, 5-FAM-CLIKKPF, and 5-FAM-CPGDLSR to 10% PS liposomes. The liposome formulation (10% PS) was washed twice with 500 µL PBS. The liposome formulation was then suspended in 500 µL binding buffer and 200 µL of this suspension was transferred to an Eppendorf tube. Fluorescent peptides (0.1 nmol CLIKKPF and CPGDLSR, 0.01 nmol LIKKPF and PGDLSR) or annexin V-FITC (3 µL) was added to the tube followed by incubation in the dark for 15 minutes at 37 °C. After incubation 300 µL binding buffer was added to the tube. Peptides samples were then analyzed using the Zeiss LSM 710 confocal microscope (Plan-Apochromat 10x/0.45 M27**,** Argon 488 laser) using 200 µL of sample in a dish plate (MatTek Corporation, glass bottom microwell dishes, 35 mm Petri dish, 14 mm microwell, 1.5 coverglass, Ashland, MA, USA). Annexin V stained liposomes were analyzed using the Zeiss LSM 510 confocal microscopy (40x 1.3 oil, Argon 488 laser) using 200 µL of samples in a dish plate.

2.2.6 Confocal microscopy of cells

Confocal microscopy analysis of cells was used to determine the binding specificity of the peptides 5-FAM-CLIKKPF and 5-FAM-CPGDLSR to apoptotic cells and to determine the cellular localization. Apoptosis was induced in Jurkat cells by seeding cells (2×10^5 cells) on 24 well plates (500 µL per well) and

treatment with 2 µM camptothecin for 24 hours (Burtea et al., 2009). Cells were pelleted by centrifugation at 500 x *g* for 5 minutes. Cells were washed with binding buffer. Each sample was resuspended in 20 µL binding buffer. Peptide (1.9 µM for CLIKKPF, 7.9 µM for CPGDLSR) or annexin V was added to cell suspension and incubated in the dark for 15 min at room temperature. Samples were spotted onto a glass slide for a minimum of 10 minutes to allow cells to adhere to the glass. Then 50 µL of 4% paraformaldehyde was added to the cell droplet and allowed to incubate for 5 minutes at room temperature. Slides were immersed in 1 x PBS three times to wash samples. DAPI (20 µL of 0.3 µg/mL) was added to spotted samples for 3 minutes at room temperature. Slides were washed twice and allowed to dry before mounting. Slides were cured overnight to allow mounting media to set. Cells were then analyzed using the Leica SP5 confocal microscope (100X/1.44 oil objective, Argon laser 488 nm). The peptides were tested in apoptotic cells (camptothecin treatment) and healthy control cells (no camptothecin treatment).

2.3 Results

2.3.1 Fluorescence plate assay

The four fluorescently modified peptides were tested using a plate based assay with annexin V- FITC as a positive control. The peptides all bound to PS and the dissociation constant (K_d) for each peptide was determined (**Figure 2-1**). 5-FAM-CLIKKPF (K_d= 1.9 µM) and 5-FAM-CPGDLSR (K_d= 7.9 µM) have reduced affinity for PS compared to the original peptides 5-FAM-LIKKPF (K_d=

0.69 µM) and 5-FAM-PGDLSR (K_d= 0.40 µM) which do not contain an additional cysteine residue. Annexin V-FITC was found to have a dissociation constant of 6.6 nM in this assay and had a much higher affinity for PS when compared to the peptides (**Figure 2-2**).

2.3.2 Confocal microscopy analysis of liposomes stained with fluorescent peptides

The fluorescent peptides and annexin V-FITC were tested with 10% PS liposomes and 0% PS liposomes (PC liposomes) (**Figure 2-3 and Figure 2-4**). The images in Figure 2-3 and Figure 2-4 are representative images of liposomes stained with fluorescent peptides or annexin V. The peptides and annexin V-FITC did not bind to the PC liposomes but clearly demonstrated binding to the 10% PS liposomes (as indicated by green fluorescent staining) (**Figure 2-3 and Figure 2-4**). According to the confocal microscopy analysis peptides 5-FAM-LIKKPF, 5-FAM-CLIKKPF and 5-FAM-CPGDLSR, and annexin V-FITC bound at the membrane bilayer. However, the peptide 5-FAM-PGDLSR was distributed in the internal volume of the liposomes with less intense staining at the lipid bilayer.

2.3.3 Confocal microscopy analysis of cells stained with fluorescent peptides

Cell studies with the peptides 5-FAM-CLIKKPF, 5-FAM-CPGDLSR and with annexin V-FITC showed selective binding to apoptotic cells (camptothecin treated) and the absence of binding to healthy cells (**Figure 2-5**). Not all the cells in the treated sample underwent the process of apoptosis however several cells were apoptotic. The images in Figure 2-5 are representative cells undergoing

apoptosis (for treated samples). Annexin V-FITC was observed only at the cell membrane in the apoptotic cells while the peptides 5-FAM-CLIKKPF and 5-FAM-CPGDLSR showed membrane binding as well as generalized uptake in the cytosol.

2.4 Discussion

Despite intensive investigation there is not yet a clinically acceptable molecular imaging agent targeting apoptosis. However the recognition that apoptosis is an important process in human disease whether caused by a pathological process such as a heart attack or whether induced through treatment such as chemotherapy continues to encourage research in this area. The desired characteristics of an imaging agent for apoptosis include; a) rapid uptake and retention in apoptotic tissue; b) rapid blood clearance of unbound tracer and rapid excretion; c) selectivity for apoptotic cells and minimal uptake in healthy tissues; d) generation of an on-target signal suitable for high contrast molecular imaging; e) clinical acceptability in terms of availability, ease of preparation, cost effectiveness and biological compatibility. Peptides labelled with imaging radionuclides, and particularly PET based probes, are an attractive option that can be potentially designed and selected to satisfy many of these requirements. The development of peptide-based imaging agents has been particularly fueled by the advent of phage display technology and its ability to identify binding sequences to a particular target from large libraries of random-sequence peptides. In this study we investigated two PS binding peptides described previously (Burtea et al., 2009)

(LIKKPF and PGDLSR) and two novel peptides produced by the addition of a cysteine residue (CLIKKPF and CPGDLSR). The addition of the cysteine residue provided a free thiol suitable for mild reaction with the ^{18}F-containing prosthetic group [^{18}F]FBAM. We have also evaluated these peptides to determine the binding characteristics using a plate assay and a liposomes assay to assess binding to PS.

Burtea et al. (2009) used an enzyme-linked immunosorbent assay (ELISA) plate assay to test binding affinity of phages to PS. We have modified this method to allow affinity determination of our peptides by fluorescence measurements. Peptides can be readily modified to include a fluorescent tag for affinity studies with the advantage that these compounds can be used for further cell-based evaluation with confocal microscopy and flow cytometry. This method is applicable not only for peptides but also proteins and oligonucleotides. Calcium is required for all four peptides and annexin V to bind to PS. Only background signal was observed when calcium was removed from the buffer.

The plate assay indicates that all four peptides bind to PS. The binding affinity of 5-FAM-CLIKKPF and 5-FAM-CPGDLSR is lower than the original peptides (5-FAM-LIKKPF and 5-FAM-PGDLSR). This is likely due to the addition of the cysteine residue at the N-terminus which could modify the PS-binding site on the small peptide. According to the methods used by Burtea *et al.* (2009) the phage displayed LIKKPF has a K_d= 2 nM and phage displayed PGDLSR has a K_d= 1 nM. This is much higher affinity for PS than we determined for the peptides 5-FAM-LIKKPF (K_d= 0.69 μM) and 5-FAM-PGDLSR (K_d= 0.40

μM). However, the assay used by Burtea et al. (2009) is an absorbance based ELISA technique using phages (unmodified) identified by anti-M13 monoclonal antibody conjugated to horseradish peroxidase. It has been previously reported that the binding affinity of the peptide is often lower than the original phage displayed peptide (Laumonier et al., 2006). This can be due to two reasons; firstly, a phage carries five copies of the hexapeptide that are able to interact with PS on the plate compared to a single peptide sequence where only one copy interacts with PS. The second possible reason for increased affinity of the phage is that the phage coat protein may induce a conformational change in the peptide that results in a higher affinity for PS than compared to the conformation of the free peptide. In our study we tested the purified free peptide and Burtea et al. (2009) reports the dissociation constant values for the phage displayed peptides. The distinction between the phage and the peptide is important since the use of phages *in vivo* is highly unlikely since they are immunogenic.

According to previous reports human recombinant annexin V has a K_d= 0.5 nM (Andree et al., 1990). Our determined value of annexin V-FITC in this plate assay was 6.6 nM. There are a few possibilities to explain this difference from the previous literature. It is known that the addition of a fluorescein modification alters the binding affinity of annexin V (Tait et al., 2006). The affinity of annexin V to PS decreases as more amino groups are modified by the addition of a FITC molecule (Tait et al., 2006). According to the supplier there are two fluorescein labels per annexin protein which may account for the reduced affinity of annexin V-FITC compared to human recombinant annexin V.

The liposome construct is designed to be similar to apoptotic cells with respect to PS externalization; and in this regard can be considered a mimic of apoptotic cells with externalized PS. In cells PS constitutes approximately 10% of total phospholipids in the lipid membrane (Devaux, 1991; Stuart et al., 1998; Vance and Steenbergen, 2005) and during apoptosis PS is externalized to the outer membrane layer of the cell. The results of the liposome assay indicate that all four peptides and annexin V bind to 10% PS liposomes but do not bind to PC liposomes (0% PS) according to confocal microscopy analysis. These results are in agreement with previous literature (Burtea et al., 2009) which show that LIKKPF and PGDLSR bind to plate immobilized PS. The results of the liposome assay support the data from the fluorescence plate assay in that all of the peptides bind to PS but not to PC at the concentrations tested.

The liposome assay presents a readily prepared formulation which provides a population that is similar to apoptotic cells with respect to the membrane presentation of PS. This assay has a number of advantages over conventional cell based assays including the ease of preparation, the ability to modify PS concentration, and the elimination of the requirement to induce and track the progress of apoptosis in cell studies. Liposomes can be analyzed by confocal microscopy or flow cytometry since they are sufficient size for these analytical methods. The designed composition of the liposomes provides a reproducible test system for comparing and contrasting results between labs working on PS binding constructs.

The cell assay indicates that 5-FAM-CLIKKPF and 5-FAM-CPGDLSR bind specifically to apoptotic cells and do not bind to healthy cells. Microscopy imaging indicates that 5-FAM-CLIKKPF and 5-FAM-CPGDLSR are localized at the membrane bilayer and are also present in the cytosol. This is possibly due to the small size of the peptides, relative to annexin V, which may allow them to cross the cell membrane but the exact nature of the uptake and retention of the probes is unknown. Notably, fluorescence from the PS targeted peptides was only observed in the apoptotic cells and not at the membrane or in the cytosol of healthy cells. Annexin V localized as expected in our studies at the cell membrane of apoptotic cells and was not evident in the cytosol. The cell-based studies serve to support the results of the plate and liposome assay providing strong evidence that CLIKKPF and CPGDLSR are PS-binding peptides that have a high specificity for apoptotic cells. The cell data also provides a validation of the simpler assay techniques provided by plate immobilized PS and by PS liposomes. The peptides LIKKPF and PGDLSR were not tested to determine if they bind to apoptotic cells since this was previously reported (Burtea et al., 2009).

Both of the non-cell assays can be easily reproduced, can be used to test a wide variety of concentrations of a compound and do not require extensive lab material and equipment required for cell culture techniques. These assays can also be applied with other classes of compounds such as small molecules, proteins and oligonucleotides. The plate assay has been used previously by our group to screen several nucleotide sequences derived by computational modeling which were designed to bind to PS (Tseng et al., 2011). These assays have allowed us to

rapidly test modifications made to our lead compounds to determine if binding affinity is improved or impaired. Both of these assays may prove to be valuable tools in the rapid *in vitro* assessment of potential apoptosis targeting probes which bind to PS and could help to accelerate discovery of compounds which can be used to image apoptosis. The two novel PS-binding peptides described in this study are presently being evaluated in a murine tumor model of apoptosis as candidates for molecular imaging as their ^{18}F-labelled analogs.

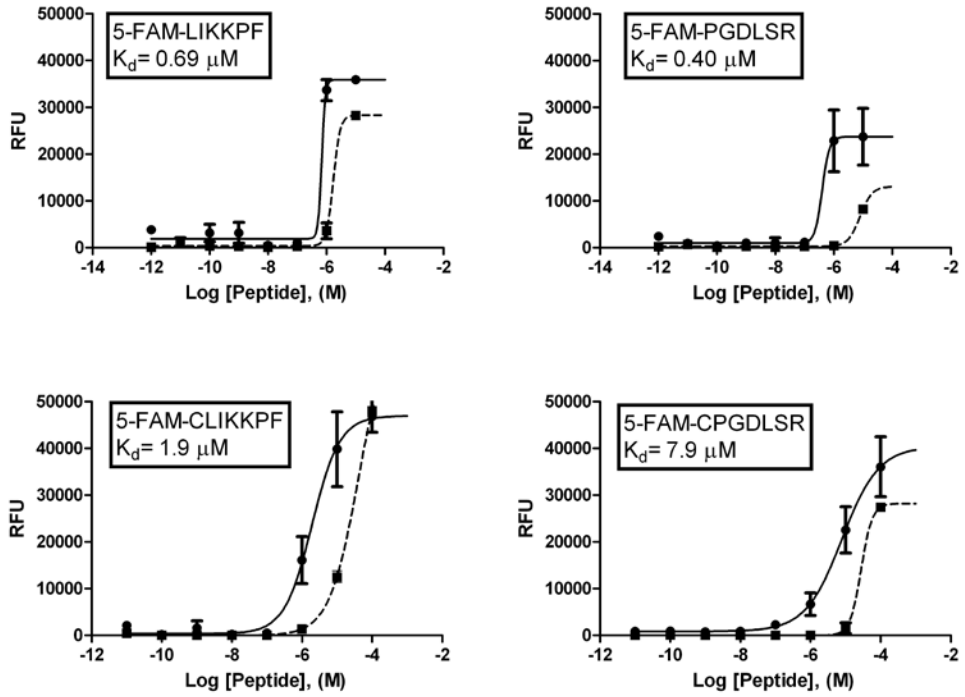

Figure 2-1. Binding curves for fluorescently labeled PS-binding peptides. Relative fluorescence units (RFU). PS- dark circles and solid line. PC- dark boxes and dashed line. X axis measurements in Log [Peptide], (M). The K_d in each box is for PS.

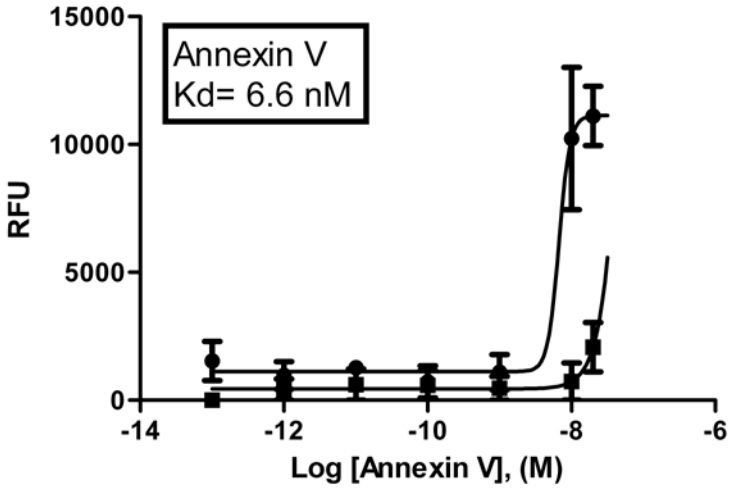

Figure 2-2. Binding curve for annexin V-FITC. Relative fluorescence units (RFU). PS- dark circles. PC- dark boxes. X axis measurements in Log [annexin V], (M). K_d= 6.6 nM is for PS.

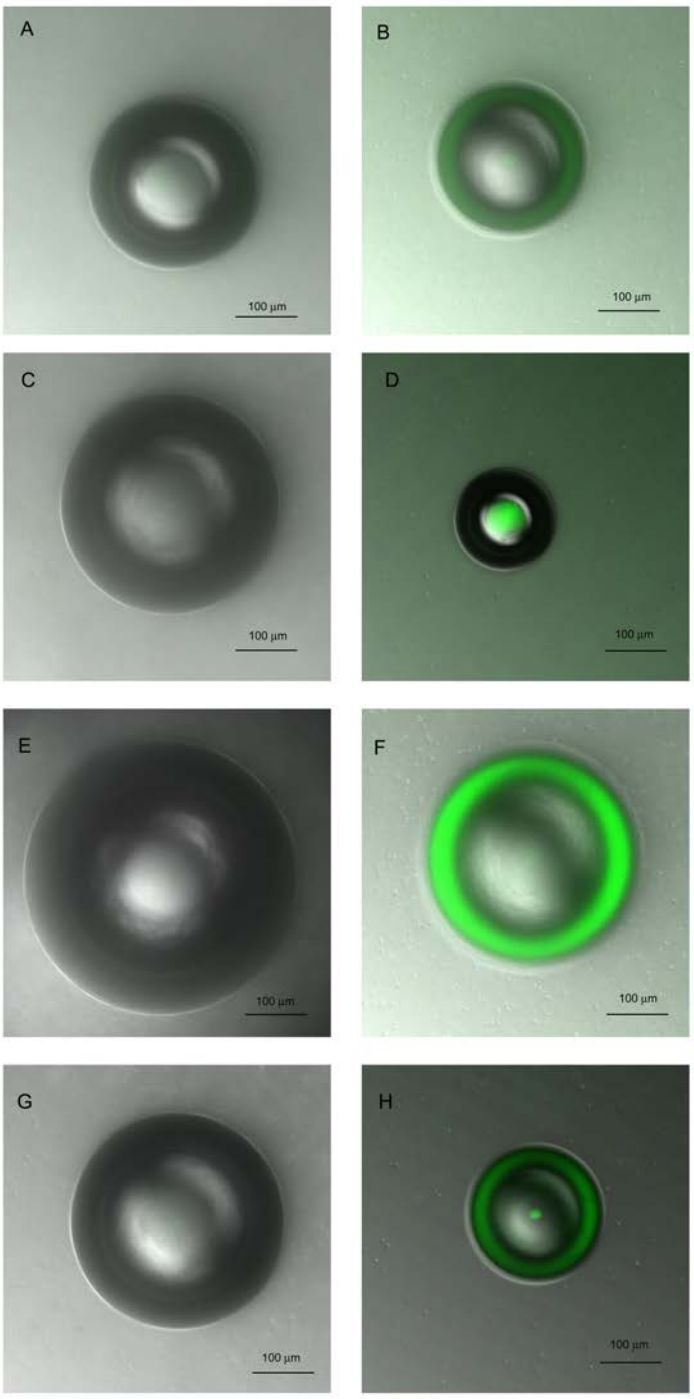

Figure 2-3. Confocal microscopy images of liposomes stained with fluorescent peptides. A) PC liposome with 5-FAM-LIKKPF. B) PS liposome with 5-FAM-LIKKPF. C) PC liposome with 5-FAM-PGDLSR. D) PS liposome with 5-FAM-PGDLSR. E) PC liposome with 5-FAM-CLIKKPF. F) PS liposome with 5-FAM-CLIKKPF. G) PC liposome with 5-FAM-CPGDLSR. H) PS liposome with 5-

FAM-CPGDLSR. These are representative images of liposomes stained with fluorescent peptides.

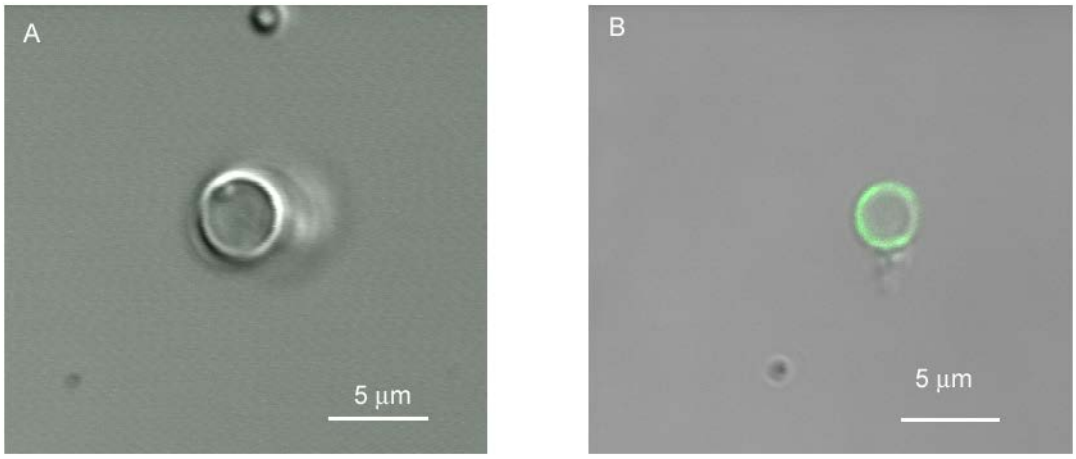

Figure 2-4. Confocal microscopy images of liposomes stained with annexin V-FITC. A) PC liposome. B) PS liposome. These are representative images of liposomes stained with annexin V-FITC.

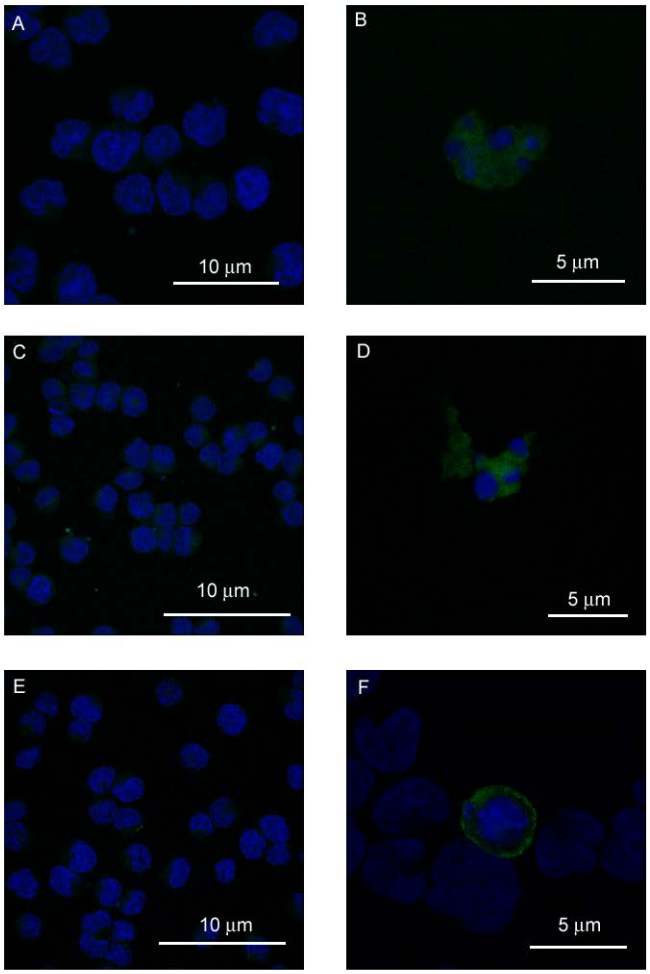

Figure 2-5. Localization of fluorescent peptides in Jurkat cells. Laser-scanning confocal microscope images were obtained to show staining of annexin V-FITC (green) or fluorescent peptides (green) in healthy and camptothecin treated cells. Cells were also stained with DAPI (blue) which binds to DNA. A) Healthy cells with 5-FAM-CLIKKPF. B) Camptothecin treated cells with 5-FAM-CLIKKPF. C) Healthy cells with 5-FAM-CPGDLSR. D) Camptothecin treated cells with 5-FAM-CPGDLSR. E) Healthy cells with annexin V. F) Camptothecin treated cells with annexin V. These are representative images of cells undergoing apoptosis (for samples that received treatment).

2.5 References:

Andree, H.A., Reutelingsperger, C.P., Hauptmann, R., Hemker, H.C., Hermens, W.T., Willems, G.M., 1990. Binding of vascular anticoagulant alpha (VAC alpha) to planar phospholipid bilayers. J Biol Chem 265, 4923-4928.

Burtea, C., Laurent, S., Lancelot, E., Ballet, S., Murariu, O., Rousseaux, O., Port, M., Vander Elst, L., Corot, C., Muller, R.N., 2009. Peptidic targeting of phosphatidylserine for the MRI detection of apoptosis in atherosclerotic plaques. Mol Pharm 6, 1903-1919.

Cabral, E.C., Hennies, P.T., Correia, C.R., Zollner, R.L., Santana, M.H., 2003. Preparation and characterization of diacetylene polymerized liposomes for detection of autoantibodies. J Liposome Res 13, 199-211.

Denecker, G., Dooms, H., Van Loo, G., Vercammen, D., Grooten, J., Fiers, W., Declercq, W., Vandenabeele, P., 2000. Phosphatidyl serine exposure during apoptosis precedes release of cytochrome c and decrease in mitochondrial transmembrane potential. FEBS Lett 465, 47-52.

Devaux, P.F., 1991. Static and dynamic lipid asymmetry in cell membranes. Biochemistry 30, 1163-1173.

Hanahan, D., Weinberg, R.A., 2000. The hallmarks of cancer. Cell 100, 57-70.

Kapty, J., Kniess, T., Wuest, F., Mercer, J.R., 2011. Radiolabeling of phosphatidylserine-binding peptides with prosthetic groups N-[6-(4-[18F]fluorobenzylidene)aminooxyhexyl]maleimide ([18F]FBAM) and N-succinimidyl-4-[18F]fluorobenzoate ([18F]SFB). Appl Radiat Isot 69, 1218-1225.

Kapty, J., Murray, D., Mercer, J., 2010. Radiotracers for noninvasive molecular imaging of tumor cell death. Cancer Biother Radiopharm 25, 615-628.

Kartachova, M., Haas, R.L., Olmos, R.A., Hoebers, F.J., van Zandwijk, N., Verheij, M., 2004. In vivo imaging of apoptosis by 99mTc-Annexin V scintigraphy: visual analysis in relation to treatment response. Radiother Oncol 72, 333-339.

Kartachova, M.S., Valdes Olmos, R.A., Haas, R.L., Hoebers, F.J., van den Brekel, M.W., van Zandwijk, N., Herk, M., Verheij, M., 2006. Mapping of treatment-induced apoptosis in normal structures: 99mTc-Hynic-rh-annexin V SPECT and CT image fusion. Eur J Nucl Med Mol Imaging 33, 893-899.

Langer, M., Beck-Sickinger, A.G., 2001. Peptides as carrier for tumor diagnosis and treatment. Curr Med Chem Anticancer Agents 1, 71-93.

Martin, S.J., Reutelingsperger, C.P., McGahon, A.J., Rader, J.A., van Schie, R.C., LaFace, D.M., Green, D.R., 1995. Early redistribution of plasma membrane phosphatidylserine is a general feature of apoptosis regardless of the initiating stimulus: inhibition by overexpression of Bcl-2 and Abl. J Exp Med 182, 1545-1556.

Reubi, J.C., Maecke, H.R., 2008. Peptide-based probes for cancer imaging. J Nucl Med 49, 1735-1738.

Stuart, M.C., Reutelingsperger, C.P., Frederik, P.M., 1998. Binding of annexin V to bilayers with various phospholipid compositions using glass beads in a flow cytometer. Cytometry 33, 414-419.

Tait, J.F., Smith, C., Levashova, Z., Patel, B., Blankenberg, F.G., Vanderheyden, J.L., 2006. Improved detection of cell death in vivo with annexin V radiolabeled by site-specific methods. J Nucl Med 47, 1546-1553.

Tseng, C.Y., Ashrafuzzaman, M., Mane, J.Y., Kapty, J., Mercer, J.R., Tuszynski, J.A., 2011. Entropic fragment-based approach to aptamer design. Chem Biol Drug Des 78, 1-13.

Vance, J.E., Steenbergen, R., 2005. Metabolism and functions of phosphatidylserine. Prog Lipid Res 44, 207-234.

Weiner, R.E., Thakur, M.L., 2002. Radiolabeled peptides in the diagnosis and therapy of oncological diseases. Appl Radiat Isot 57, 749-763.

Weiner, R.E., Thakur, M.L., 2005. Radiolabeled peptides in oncology: role in diagnosis and treatment. BioDrugs 19, 145-163.

Chapter 3

Radiolabeling of Phosphatidylserine-binding Peptides with Prosthetic Groups *N*-[6-(4-[^{18}F]fluorobenzylidene)aminooxyhexyl]maleimide ([^{18}F]FBAM) and *N*-succinimidyl-4-[^{18}F]fluorobenzoate ([^{18}F]SFB)

A version of this chapter has been published. **Kapty, J**., Kniess, T., Wuest, F., Mercer, J. *Applied Radiation and Isotopes,* (Sept 2011) 69(9): 1218-1225.

3.1 Introduction

Peptides play vital roles in regulatory functions in the human body and have proven applications in diagnostic imaging and radiotherapy. Both single photon emitting radionuclides and positron emitting radionuclides have been investigated for radiolabeling peptides with increasing interesting the positron emitters due to advantages of the positron emission tomography (PET) imaging technique (Tolmachev and Stone-Elander, 2010). ^{18}F-Fluorine is the preferred radionuclide for labeling and use in clinical PET imaging due to its increasing availability and advantages such as low positron energy (0.64 MeV) and favorable half life (109.8 min) (Okarvi, 2001). The inherent sensitivity of most peptides to the chemistry conditions used in standard direct fluorination procedures has resulted in the adoption of milder labeling procedures using ^{18}F labeled prosthetic groups. The most widely used ^{18}F-prosthetic group for labeling peptides and proteins is *N*-succinimidyl-4-[^{18}F]fluorobenzoate ([^{18}F]SFB) which reacts with primary amine groups under mild pH and temperatures (Vaidyanathan and Zalutsky, 1992; Wester et al., 1996; Wuest et al., 2003; Zijlstra et al., 2003). [^{18}F]SFB is a suitable acylation agent not only for the radiolabeling of peptides but also proteins, antibodies, and oligonucleotides, and thus has the potential to aid in the development of novel PET tracers.

Despite the versatility of [^{18}]SFB, it has been observed that reactions with [^{18}F]SFB can produce poor or no yield of labeled peptides in some situations such as where amine groups are subject to steric hindrance (Wuest et al., 2009). It may also be difficult to achieve chemo-selective radiolabeling with [^{18}F]SFB if the

peptide of interest contains several reactive amine groups, for example in lysine residues, in addition to that of the N-terminus. It may also be difficult to radiolabel the N-terminus of a peptide if the residue is proline since there is no primary amine group available for reaction with [^{18}F]SFB.

An alternative ^{18}F prosthetic group for peptide labeling is the thiol reactive N-[6-(4-[^{18}F]fluorobenzylidene)aminooxyhexyl]maleimide ([^{18}F]FBAM). The automated radiosynthesis of [^{18}F]FBAM has been recently published (Kniess et al., 2011). Although free thiol groups are not typically found in most peptides and proteins these molecules can be modified to include a cysteine residue or a thiol group to enable site-specific labeling with [^{18}F]FBAM (Wuest et al., 2009).

Our interest in radiolabeling peptides with ^{18}F resulted from the recent report of two peptides that were identified using phage display technology and which showed high binding affinity and specificity to the phospholipid phosphatidylserine (PS) (Burtea et al., 2009). The peptides of interest and their respective affinity to PS are: LIKKPF (K_d= 0.69 µM), PGDLSR (K_d= 0.40 µM), CLIKKPF (K_d= 1.9 µM), and CPGDLSR (K_d= 7.9 µM) (as discussed in Chapter 2). PS externalization is an early event in apoptosis which is a mechanism of programmed cell death (Vance and Steenbergen, 2005). Thus PS is a target that has been exploited in a number of attempts to image apoptosis (Kapty et al., 2010). Therefore, peptides that bind to PS on apoptotic cells represent attractive compounds for development of radiotracers for molecular imaging of apoptosis.

In this report, we examine the scope and limitations of [^{18}F]SFB and [^{18}F]FBAM as prosthetic groups for the mild and efficient ^{18}F-radiolabeling of the two PS-

binding peptides identified by Burtea et al (2009). We describe a modified synthesis of the bifunctional labeling agent [^{18}F]SFB in a remotely-controlled synthesis unit and a comparison of this popular amine-reactive prosthetic group (Lapi et al., 2009; Liu et al., 2010; Ren et al., 2009) with the novel thiol-reactive prosthetic group [^{18}F]FBAM.

3.2 Materials and methods

3.2.1 General

Binding peptides (LIKKPF, PGDLSR), peptides augmented by addition of a terminal cysteine residue for subsequent FBAM labeling (CLIKKPF, CPGDLSR) and peptides coupled with fluorobenzoate (FB-LIKKPF and FB-PGDLSR) were obtained from Hanhong Chemical Co. (Shanghai, China) with purity of >95%. All chemicals were reagent grade and were used without further purification. Mass spectrometric (MS) analysis was carried out with a Triple-Quattro LC/MS (Micromass, UK) with electrospray ionization (ESI).

3.2.1.1 [^{18}F]SFB experiments

Radio-thin layer chromatography (radio-TLC) was performed with silica gel MK6F plates (Whatman, Piscataway, NJ, USA) developed with *n*-butanol/water/acetic acid (4/1/1) (Wuest et al., 2003) and radioactive compounds were detected with an AR-2000 imaging scanner (Bioscan Inc, Washington, DC, USA) (Method A).

Reverse phase high pressure liquid chromatography (HPLC) analyses of [^{18}F]SFB were carried out with a Beckman Coulter Inc system consisting of a Model 168 Diode Array UV detector; a Model 126 analytical dual pump; a radioactivity detector (Ortec, TN, USA): ACE *Mate*™ Single Channel Analyzer and using a Machery Nagel VP250/10 Nucleosil 100-5 C18 Nautilus HPLC column with a flow rate of 2 mL/min. Solvent A: water 0.2% TFA; solvent B: ethanol. The following gradient was used: 0 min 60% B, 12 min 70% B, 15 min 70% B, 18 min 80% B, 19 min 80% B (System A). The addition of [^{18}]SFB to peptide was monitored by radio-TLC and radio-HPLC.

3.2.1.2 [^{18}F]FBAM experiments

In cartridge purified [^{18}F]FBAM experiments radio-TLC was performed with silica gel F-254 aluminum plates (Merck, Darmstadt, Germany) developed with acetonitrile/water (80:20) and radioactive compounds detected with a BAS 2000 scanner (FUJIX, Tokyo, Japan) (Method B).

In HPLC purified [^{18}F]FBAM experiments radio-TLC was performed with silica gel aluminum plates (Fluka, Sigma-Aldrich, Oakville, ON, Canada) developed with acetonitrile/water (80:20) and radioactive compounds detected with an AR-2000 imaging scanner (Bioscan Inc, Washington, DC, USA) (Method C).

HPLC analyses of cartridge purified [^{18}F]FBAM were carried out with an Agilent 1200 Series HPLC and a Machery Nagel EC250/4 Nucleosil 100-5 C18 PPN column with a flow rate of 1 mL/min. Solvent A: acetonitrile 0.1% TFA;

solvent B water 0.1% TFA. The following gradient was used: 0 min 10% A, 20 min 70% A, 30 min 70% A (System B). The products were monitored by a UV detector at 220 nm and by gamma detection with a scintillation detector GABI (X-RAYTEST). The reaction of [^{18}F]FBAM with peptide was monitored by radio-TLC and radio-HPLC.

3.2.2 Preparation of FBAM- reference compounds.

The non-radioactive reference compounds FBAM-CLIKKPF and FBAM-CPGDLSR were prepared by the addition of 0.5 mg (1.6 µmol) of cold FBAM in 30 µL acetonitrile to 2 mg of CLIKKPF or CPGDLSR dissolved in phosphate buffer (30 µL, pH 7.2). The reaction mixtures were incubated for 2 h at 60 ºC. HPLC purification of the products was accomplished using System B. Retention time for FBAM-CLIKKPF was 14.8 min. MW calculated 1166.46, found ESI-MS 1167.28 $[M + H]^+$. Retention time for FBAM-CPGDLSR was 13.8 min, MW calculated 1064.18, found ESI-MS 1066.00 $[M + H]^+$.

3.2.3 Radiosynthesis of [^{18}F]SFB

No carrier added aqueous [^{18}F]fluoride ion was produced on a TR-19/9 cyclotron (Advanced Cyclotron Systems, Burnaby, BC, Canada) by irradiation of [^{18}O]H_2O *via* the $^{18}O(p,n)^{18}F$ nuclear reaction.

[^{18}F]SFB was prepared using a modified commercially available automated synthesis unit (General Electric Tracerlab FX_{FDG}). The synthesis employed a three step/two pot synthesis sequence involving fluoride incorporation

into *tert*-butyl 4-*N*,*N*,*N*-trimethylammoniumbenzoate, acidic hydrolysis, and subsequent conversion of 4-[^{18}F]fluorobenzoic acid ([^{18}F]FBA) into [^{18}F]SFB (Mading et al., 2005). Modifications included changes to the fluoride drying method, a redesign of the reaction train and changes in the methods of reagent addition. Modifications to the reaction train were as follows: the two separate reaction trains of the GE TRACERlab FX_{FDG} were linked together to transfer synthesized [^{18}F]FBA directly from reactor 1 to reactor 2. Modifications to the reagent addition were as follows: tetramethylammonium hydroxide was added directly to reactor 2 instead of to vial 7. Crude [^{18}F]SFB was washed with 5% acetic acid and water after trapping on a Sep Pak plus C18 cartridge (55-105 µm) (Waters, Milford, MA, USA) and eluted with acetonitrile.

3.2.4 Radiosynthesis of cartridge purified [^{18}F]FBAM

No carrier added aqueous [^{18}F]-fluoride ion was produced in an IBA CYCLONE 18/9 cyclotron by the irradiation of [^{18}O] H_2O via the $^{18}O(p,n)^{18}F$ nuclear reaction. The radiosynthesis of [^{18}F]FBAM was performed in an automated nucleophilic fluorination module (General Electric Tracerlab FX_{FDG}). Radiosynthesis of [^{18}F]FBAM was performed by a two step procedure involving synthesis and solid phase extraction of 4-[^{18}F]fluorobenzaldehyde and subsequent Schiff-base reaction with the corresponding aminooxy precursor. The [^{18}F]FBAM was trapped on a RP18 cartridge (LiChrolut, Merck, Darmstadt, Germany) and after washing with acetonitrile/water eluted with pure acetonitrile (Kniess et al., 2011).

3.2.5 Radiosynthesis of HPLC purified [^{18}F]FBAM

No carrier added aqueous [^{18}F]fluoride ion was produced on a TR-19/9 cyclotron (Advanced Cyclotron Systems, Burnaby, BC, Canada) by irradiation of [^{18}O]H_2O *via* the $^{18}O(p,n)^{18}F$ nuclear reaction. [^{18}F]FBAM was prepared as above; however, following automated synthesis it was subjected to further HPLC-purification. Isolation of [^{18}F]FBAM was carried out with a Beckman Coulter Inc. system consisting of a Model 168 Diode Array UV detector; a Model 126 analytical dual pump; a radioactivity detector (Ortec, TN, USA): ACE *Mate*^{TM} Single Channel Analyzer and using a Luna C18(2) 100 A (250 x 10 mm) reverse phase HPLC column with a flow rate of 3 mL/min. Solvent A: acetonitrile; solvent B: water. The following gradient was used: 0 min 50% B, 8 min 70% B, 9 min 70% B, 30 min 70% B (System C). Retention time for [^{18}F]FBAM was 24.0 min.

3.2.6 Peptide radiolabeling with [^{18}F]SFB

Peptide labeling reactions are shown in **Figure 3-1**. For optimization experiments [^{18}F]SFB in acetonitrile (100 µL, 20 MBq) was added to 300 µL peptide (LIKKPF or PGDLSR) solution in buffer (Kolthoff buffer pH 7.6, Kolthoff buffer pH 8.4, or sodium phosphate buffer 0.05 M pH 9.0) and was incubated at various temperatures (40 or 60 ºC). The final peptide concentration was 2.0 mg/mL. The progress of the reaction was determined by monitoring the consumption of [^{18}F]SFB and the formation of labeled peptides by radio-TLC

after 20, 40, 60 min. Radio-TLC: R_f [^{18}F]SFB= 0.85, R_f [^{18}F]-LIKKPF= 0.2-0.4, R_f [^{18}F]-PGDLSR= 0.2-0.4, *n*-BuOH/H_2O/HOAc (4/1/1).

Preparative scale radiolabeling of peptides with [^{18}F]SFB was performed and evaluated using radio-HPLC. [^{18}F]SFB 100 µL (300 MBq) in acetonitrile was added to peptide LIKKPF (1.5 mg, concentration of 5 mg/mL) dissolved in 300 µL Kolthoff buffer (pH 8.4) and was incubated at 40 °C for 1 h. [^{18}F]SFB 100 µL (74-472 MBq) in acetonitrile was added to peptide PGDLSR (1.0-1.7 mg, concentration of 3.3-5.6 mg/mL) dissolved in 300 µL Kolthoff buffer (pH 8.4) and was incubated at 40 ºC for 40 min. Radio-HPLC analysis was performed to determine radiochemical purity.

3.2.7 Peptide radiolabeling with cartridge purified [^{18}F]FBAM

Optimization of reaction conditions for radiolabeling peptides with [^{18}F]FBAM were evaluated using radio-TLC. The synthetic scheme for radiolabeling of cysteine-containing peptides (CLIKKPF and CPGDLSR) using the bifunctional labeling agent [^{18}F]FBAM is shown in **Figure 3-2**. PS-binding peptides were modified to include a reactive thiol group by the addition of a cysteine residue at the N-terminus of each peptide. Cartridge purified [^{18}F]FBAM in acetonitrile (20-30 µL, 2-20 MBq) was added to 20-30 µL peptide (CLIKKPF or CPGDLSR) solution in phosphate buffer (pH 7.2) and was incubated at various temperatures (40 or 60 ºC). The final peptide concentrations were 0.05 mg/mL, 0.25 mg/mL, 0.5 mg/mL, 2.5 mg/mL, 5 mg/mL, 10 mg/mL, and 20 mg/mL. The consumption of [^{18}F]FBAM and production of labeled peptide was monitored by

radio-TLC after 20, 40, and 60 min. Radio TLC: [^{18}F]FBAM R_f= 0.8, [^{18}F]FBAM-CLIKKPF R_f= 0.08-0.12, [^{18}F]FBAM-CPGDLSR R_f= 0.17-0.28, acetonitrile/water (80:20) (Method B).

Preparative scale radiolabeling of peptides with [^{18}F]FBAM was performed and evaluated using radio-HPLC. [^{18}F]FBAM 60 µL (18-21 MBq) in acetonitrile was added to peptide (concentration of 5 mg/mL) dissolved in 60 µL PBS buffer (pH 7.2) and was incubated at 60 ºC for 1 h. Radio-HPLC analysis was performed to determine radiochemical purity. The chemical stability of [^{18}F]FBAM -CLIKKPF and [^{18}F]FBAM –CPGDLSR, with PBS (pH 7.2) as solvent at 37 °C, was investigated at 1 h, 2 h and 3 h after radiolabelling.

3.2.8 Peptide radiolabeling with HPLC purified [^{18}F]FBAM

Reactions were also investigated using HPLC purified [^{18}F]FBAM after evidence that non-radioactive impurities in the cartridge purified product influenced the reaction. Thus HPLC purified [^{18}F]FBAM in acetonitrile (300 µL, 1-2 MBq) was added to 300 µL peptide (CLIKKPF or CPGDLSR) solution in phosphate buffer (pH 7.2) and was incubated at 60 °C for 60 min. The final peptide concentrations were 0.05 mg/mL, 0.25 mg/mL, 0.5 mg/mL, and 2.5 mg/mL. Peptide CLIKKPF was also tested at a concentration of 5 mg/mL. Conversion was monitored by radio-TLC after 60 min. Radio TLC: [^{18}F]FBAM R_f=0.8. [^{18}F]FBAM-CLIKKPF R_f=0.25, [^{18}F]FBAM-CPGDLSR R_f=0.23, acetonitrile/water (80:20) (Method C).

3.2.9 Evaluation of kinetics of isomerisation equilibrium for FBAM-CLIKKPF

[^{18}F]FBAM-CLIKKPF was evaluated using HPLC analysis at 0, 1, 2, and 3 h after completion of reaction and the percentages of each E- and Z-isomer were determined.

3.3 Results

3.3.1 Radiosynthesis of [^{18}F]SFB

[^{18}F]SFB was synthesized with an average radiochemical yield of 29% ± 8% (n=51), decay corrected; 19% ± 5% (n=51), non-decay corrected. The synthesis time was 50-55 minutes including the purification time which is an improvement over the previously reported synthesis time of 68 minutes (Mading et al., 2005). The radiochemical purity of [^{18}F]SFB was 92% ± 8% (n=51) as determined by radio-TLC. It was possible to obtain high radiochemical purity without column chromatography by washing the crude [^{18}F]SFB with 5% acetic acid and water after trapping on a C18 cartridge and final elution of the purified product with acetonitrile.

3.3.2 Optimization of peptide radiolabeling with [^{18}F]SFB

Small scale reactions between peptides and [^{18}F]SFB were evaluated using radio-TLC. The loss of activity at the R_f value corresponding to the prosthetic group and appearance of activity at other peak positions was used to estimate the progress of the radiolabeling reactions as outlined in **Tables 3-1 and 3-2**. The

reaction between [^{18}F]SFB and the peptides was evaluated with respect to time of reaction and pH.

As indicated in **Tables 3-1 and 3-2** the progress of the reactions showed dependence on the pH of the buffer solutions and allowed selection of preferred conditions for subsequent larger scale reactions. Further analysis by HPLC however, indicated that the reactions between [^{18}F]SFB and the peptides produced mixtures of labeled products rather than a single labeled peptide product (Sections 3.3 and 3.4). In summary, radio-TLC results indicated that the reaction in Kolthoff buffer at pH 8.4 and 40 °C for 40 min (n=3 for all reaction conditions) are optimized conditions for [^{18}F]SFB radiolabeling of the peptides LIKKPF and PGDLSR.

3.3.3 Preparative scale radiolabeling of LIKKPF with [^{18}F]SFB

Preparative scale radiolabeling of LIKKPF with [^{18}F]SFB was performed and evaluated using radio-HPLC. The radiolabeling of LIKKPF (5 mg/mL) with 300 MBq [^{18}F]SFB resulted in a radiochemical yield of [^{18}F]FB-LIKKPF (N-terminus labeled) of 18% after 1 h at 40 °C. [^{18}F]FB-LIKKPF has a retention time of 24.0 min according to HPLC analysis (System A) which is consistent with cold reference FB-LIKKPF. Many other radioactive peaks were visible on the HPLC radiotrace. While radio-TLC analysis indicates good radiolabeling yield (75%) after 40 min at 40 ºC, the HPLC analysis proves that the yield of LIKKPF radiolabeled at the N-terminus is only 18%. N-terminus labeling is preferred because on that position the prosthetic group is less likely to interfere with the

binding interaction of the peptide and phosphatidylserine. The additional radioactive peaks likely represent singly or multiply derivatized peptide products produced by the reaction between [^{18}F]SFB or the accompanying nonradioactive [^{19}F]SFB and the free amino groups of the two lysine residues in the peptide. These radioactive products were not further analyzed.

3.3.4 Preparative scale radiolabeling of PGDLSR with [^{18}F]SFB

Preparative scale radiolabeling of PGDLSR with [^{18}F]SFB was performed and evaluated using radio-HPLC. The radiolabeling of PDGLSR (4.6 mg/mL) with 74 MBq [^{18}F]SFB resulted in a yield of [^{18}F]FB-PGDLSR of 19% after 40 min at 40 °C. [^{18}F]FB-PGDLSR has a retention time of 16.2 min according to HPLC analysis (System A) which is consistent with the cold reference compound FB-PGDLSR. A second radioactive peak was observed at 7.3 min (58%). Further analysis indicated that initially formed [^{18}F]FB-PGDLSR was unstable and rapidly degraded to produce the unidentified product with HPLC retention time of 7.3 minutes. Five additional tests of the experiment confirmed that no desired product remained in the reaction mixture after 30 minutes. Radiolabeling of PGDLSR with [^{18}F]SFB resulted in a very unstable radiochemical species which could not be collected or purified with HPLC.

3.3.5 Radiosynthesis of [^{18}F]FBAM

In a typical experiment, 2978 MBq of [^{18}F]fluoride was converted into 584 MBq of [^{18}F]FBAM within 43 minutes including cartridge-based purification. The

controlled manufacturing process allowed the convenient synthesis of [^{18}F]FBAM with a radiochemical yield with a range of 14-30% (decay corrected); 11-23% (non-decay corrected) and radiochemical purity ranging from 92-99.5% (N= 7), as verified by radio-HPLC and radio-TLC (R_f= 0.8) (see **Figure 3-3** for HPLC trace). HPLC retention time for [^{18}F]FBAM was 23.3 minutes (System B) which is consistent with cold FBAM.

3.3.6 Optimization of CLIKKPF radiolabeling with cartridge purified [^{18}F]FBAM

Optimization of reaction conditions for radiolabeling CLIKKPF with cartridge purified [^{18}F]FBAM was evaluated using radio-TLC. The reaction was optimized with respect to temperature, time of reaction, and peptide concentration. The R_f of [^{18}F]FBAM-CLIKKPF was 0.08-0.12 (method B). After 1 h at temperatures of 20 °C, 40 °C and 60 °C, CLIKKPF was not radiolabeled with [^{18}F]FBAM when reacted at concentrations of 0.05 mg/mL, 0.25 mg/mL, and 0.5 mg/mL. By increasing the peptide concentration to 2.5 mg/mL after 20 min at 20 °C the labeling reagent [^{18}F]FBAM was converted into 2% radiolabeled peptide. With this peptide concentration at 60 °C in 60 min a maximum labeling yield of 6% was observed. By using a higher peptide concentration of 5.0 mg/mL an almost quantitative consumption of [^{18}F]FBAM was detected already after 20 min at 20 °C (**Table 3-3**). With even higher peptide concentrations such as 10 or 20 mg/mL peptide the labeling reagent [^{18}F]FBAM was converted into 98-99% [^{18}F]FBAM-CLIKKPF after 1 h at 60 °C according to radio-TLC analysis. The

most important factor for radiolabeling with cartridge purified [^{18}F]FBAM turned out to be the concentration of peptide.

3.3.7 Optimization of CLIKKPF radiolabeling with HPLC purified [^{18}F]FBAM

Optimization of the reaction conditions for radiolabeling CLIKKPF with HPLC purified [^{18}F]FBAM was evaluated using radio-TLC. The R_f of [^{18}F]FBAM-CLIKKPF was 0.25 (Method C). At a peptide concentration of 0.05 mg/mL after 60 min at 60 °C the labeling reagent [^{18}F]FBAM was converted into 53% radiolabeled peptide (**Table 3-3**). By increasing the peptide concentration to 0.25 mg/mL after 60 min at 60 °C the labeled reagent [^{18}F]FBAM was converted into 82% radiolabeled peptide. At concentrations of 0.50 mg/mL, 2.5 mg/mL, and 5.0 mg/mL there was an almost quantitative reaction of [^{18}F]FBAM into radiolabeled peptide (96-98%).

3.3.8 Optimization of CPGDLSR radiolabeling with cartridge purified [^{18}F]FBAM

Optimization of reaction conditions for radiolabeling CPGDLSR with [^{18}F]FBAM was evaluated using radio-TLC. The reaction was optimized with respect to temperature, time of reaction, and peptide concentration. The R_f of [^{18}F]FBAM-CPGDLSR was 0.17-0.28 (Method B). After 1 h at various temperatures, CPGDLSR was not radiolabeled with [^{18}F]FBAM when reacted at concentrations of 0.05 mg/mL, 0.25 mg/mL, 0.5 mg/mL, and 2.5 mg/mL. Using peptide concentration 5 mg/mL after 20 min at 20 °C resulted in 97% labeling

product. After 1 h at 60 ºC with 5, 10, or 20 mg/mL peptide, the labeling reagent [^{18}F]FBAM was converted into 96-98% [^{18}F]FBAM-CPGDLSR according to radio-TLC analysis.

After reacting for 1 h at 60 ºC with 20 mg/mL peptide, radio-HPLC found [^{18}F]FBAM-CPGDLSR (R_t=14.1 min) with a radiochemical yield of >99%. The reaction conditions of 5 mg/mL for 1 h at 40 ºC and 5 mg/mL for 1 h at 20 ºC, also resulted in nearly quantitative radiochemical yield [^{18}F]FBAM-CPGDLSR (R_t=14.1 min). There was no remaining [^{18}F]FBAM according to HPLC.

3.3.9 Optimization of CPGDLSR radiolabeling with HPLC purified [^{18}F]FBAM

Optimization of reaction conditions for radiolabeling CPGDLSR with HPLC purified [^{18}F]FBAM was evaluated using radio-TLC. The R_f of [^{18}F]FBAM-CPGDLSR was 0.23 (Method C). At concentrations of 0.05 mg/mL, 0.25 mg/mL, 0.50 mg/mL and 2.5 mg/mL there was an almost quantitative reaction of [^{18}F]FBAM into radiolabeled peptide (97-99%) (**Table 3-3**).

3.3.10 Preparative scale radiolabeling of CLIKKPF with [^{18}F]FBAM

Preparative scale radiolabeling of CLIKKPF with [^{18}F]FBAM was performed and evaluated using radio-HPLC. The radiolabeling of CLIKKPF (5 mg/mL) with [^{18}F]FBAM resulted in a yield of [^{18}F]FBAM-CLIKKPF of >99% (N= 4). The [^{18}F]FBAM-CLIKKPF, 10 µL, was co-injected with 50 µL cold FBAM-CLIKKPF reference peptide. The [^{18}F]FBAM-CLIKKPF has a retention time of 15.2 min according to HPLC analysis which is consistent with cold

FBAM-CLIKKPF reference peptide and confirms the radiolabeling result. All of the [^{18}F]FBAM reacted with CLIKKPF to form [^{18}F]FBAM-CLIKKPF with an excellent radiochemical yield of >99%.

3.3.11 Preparative scale radiolabeling of CPGDLSR with [^{18}F]FBAM

Preparative scale radiolabeling of CPGDLSR with [^{18}F]FBAM was performed and evaluated using radio-HPLC. The radiolabeling of CPGDLSR (5 mg/mL) with [^{18}F]FBAM resulted in a yield of [^{18}F]FBAM-CPGDLSR of >99% (N=7). The [^{18}F]FBAM-CPGDLSR, 10 µL, was co-injected with 50 µL cold FBAM-CPGDLSR reference peptide. The [^{18}F]FBAM-CPGDLSR has a retention time to 14.15 min according to HPLC analysis which is consistent with cold FBAM-CPGDLSR reference peptide and confirms the radiolabeling result. All of the [^{18}F]FBAM reacted with CPGDLSR to form [^{18}F]FBAM-CPGDLSR with an excellent radiochemical yield of >99%.

3.3.12 Chemical stability of peptides radiolabeled with [^{18}F]FBAM

Preliminary studies of the chemical stability of [^{18}F]FBAM-CLIKKPF and [^{18}F]FBAM-CPGDLSR as a function of time (at 1 h, 2 h and 3 h after radiolabeling) were performed in PBS (pH 7.2) at 37 °C by radio-HPLC analysis. Both radiolabeled peptides proved to be very stable under these conditions with >99% of the radioactivity associated with the HPLC retention positions of the peptide conjugates.

3.3.13 Isomerisation of FBAM-CLIKKPF

There is evidence of equilibrium between the E- and Z- isomers at the oxime functional group of FBAM in FBAM-CLIKKPF. In previous studies where [^{18}F]FBAM was used to radiolabel peptides and proteins, only radio-TLC was performed (Hultsch et al., 2007) or only one isoform was formed in the reaction (Wuest et al., 2009); therefore, these studies did not reveal the E- and Z- isomers. HPLC has better resolution and allows for detection of the effects due to isomerisation. The formation of oxime E- and Z- isomers has previously been reported (Berndt et al., 2007; Toyokuni et al., 2003; Wuest et al., 2008).

Reaction of [^{18}F]FBAM with CLIKKPF results in a yield of >99% [^{18}F]FBAM-CLIKKPF but with two peaks of similar retention time (0.3 min separation) observed by HPLC analysis. We propose that the observed peaks are the E- and Z- oximes. Immediately following the chemical reaction, isomer 1 is present at 89% (R_t= 15.2 min) and isomer 2 at 11% (R_t= 14.9 min). Over time the isomers equilibrate to about 70% isomer 1 and 30% isomer 2 (**Table 3-4**). Mass spectrometric analysis (ESI-MS) of the isolated compounds at R_t= 15.2 min and R_t= 14.9 min showed identical mass peaks of *m/z* 1167.28 ($[M + H]^+$) suggesting the existence of two isomers. The demonstration of an apparent equilibrium between the two peaks with similar retention times on HPLC and the identical masses of the two products allows us to propose that the two peaks are the E and Z isomers.

3.4 Discussion

In this report, we present the scope and limitations of the two ^{18}F-labeled prosthetic groups, [^{18}F]SFB and [^{18}F]FBAM, for the ^{18}F-radiolabeling of two PS-binding peptides. We radiolabeled our peptides of interest and compared radiolabeling yield and chemoselectivity of each prosthetic group. It has been proposed that the PS-binding peptides, LIKKPF and PGDLSR, bind to the headgroup of phosphatidylserine using the amino acid residues in the middle of the sequence (Burtea et al., 2009). Therefore, we do not anticipate a negative effect on peptide binding due to chemical modifications made to the N-terminus (due to prosthetic group labeling with [^{18}F]SFB or [^{18}F]FBAM). We modified the peptides to include a cysteine residue at the N-terminus for the purpose of labeling with [^{18}F]FBAM.

[^{18}F]SFB is a very popular compound for radiolabeling peptides and is easily produced using an automated synthesis unit. We have developed an efficient automated synthesis of [^{18}F]SFB which requires 50-55 min for production compared to 68 min described previously (Mading et al., 2005). We modified the cartridge-based purification method which resulted in [^{18}F]SFB with very high radiochemical purity. We also have a rapid automated synthesis of [^{18}F]FBAM which only requires 43 min for production and cartridge-based purification resulting in high radiochemical purity and good radiochemical yield (Kniess et al., 2011). Both of these automated methods do not require the use of HPLC for purification which reduces the time required to obtain purified [^{18}F]SFB and [^{18}F]FBAM and thus the overall time to final [^{18}F]-peptide.

However, as discussed below, HPLC purification of the prosthetic groups may be required if the presence of chemical impurities impacts on the reaction of the prosthetic groups with their peptide targets.

In a peptide with several primary amine groups available for reaction with [^{18}F]SFB, it is challenging to achieve chemoselective radiolabeling and the yield of a particular product may be low. The initial indication in the radiolabeling of the peptide LIKKPF with [^{18}F]SFB was that a high yield of radiolabeled product was obtained at optimized conditions as indicated by TLC. However, there are three possible reaction sites where [^{18}F]SFB can radiolabel this peptide since there are two lysine residues and the N-terminus which have reactive amine groups. The limitation of radio-TLC analysis is that the different labeled radiochemical species cannot be differentiated; only the total amount of radiolabeled peptide can be measured. HPLC analyses indicated that only 18% of the activity in the crude product corresponded to N-terminus labeled product accompanied by multiple other products representing addition of SFB (F-18/F-19) singly or multiply to the other available reaction sites.

Problems were also encountered in our attempts to radiolabel the peptide PGDLSR with [^{18}F]SFB. The proline residue at the N-terminus, as a secondary amine, is unreactive to SFB and to our our knowledge this group has not been successfully radiolabeled with [^{18}F]SFB. While the side chain of the arginine residue is potentially reactive with SFB, the strongly basic guanidine group has a pK_a >12 and would generally be protonated, positively charged and un-reactive with SFB. [^{18}F]SFB was able to react with the side chain of serine; however this

reaction is readily reversible since [^{18}F]SFB can be removed by hydrolysis. Due to this phenomenon we were not able to isolate this product. This is likely to occur with nucleophilic solvents including the currently used HPLC solvent system. Hydrolysis of the prosthetic group would generate ^{18}F-fluorobenzoic acid which is quite polar and would have a shorter retention time on reverse phase HPLC and this effect was observed in our experiments.

As a consequence of the less than optimal radiolabeling with [^{18}F]SFB, an alternative prosthetic group [^{18}F]FBAM, which reacts with sulfhydryl groups, was investigated for labeling our two peptides. [^{18}F]FBAM has recently been efficiently produced using automated synthesis and solid phase extraction (Kniess et al., 2011). Since neither of our peptides of interest contained a sulfhydryl group they were modified by the addition of a cysteine residue at the N-terminus. The radiolabeling reaction for both peptides with cartridge purified [^{18}F]FBAM was strongly dependent on peptide concentration in agreement with previously published observations (Berndt et al., 2007; Wuest et al., 2003). We report a higher concentration of peptide required for radiolabeling with cartridge purified [^{18}F]FBAM compared to previous research (Hultsch et al., 2007) and compared to HPLC purified [^{18}F]FBAM. Radiolabeling with [^{18}F]FBAM proceeds at room temperature and short reaction time (20 min) resulting in a single radiolabeled product for both peptides and high radiochemical yield. Thus using [^{18}F]FBAM, peptides CLIKKPF and CPGDLSR were chemoselectively labeled at the thiol group of the terminal cysteine. Based on the results of this study, it can be

concluded that [^{18}F]FBAM has the potential to play an important role for the radiolabeling of cysteine-containing peptides.

Cartridge-based purifications for ^{18}F-labeled prosthetic groups are attractive due to their speed and simplicity but they must be able to provide products with appropriate chemical and radiochemical purity. The high concentrations of the peptides required for the reactions with cartridge purified [^{18}F]FBAM is due to the presence of chemical impurities that preferentially react with the peptides (**Figure 3-3**). To confirm this we conducted a series of reactions with HPLC purified [^{18}F]FBAM and were able to demonstrate that a high yield of labeled peptides was obtained even at the lowest concentrations of peptides evaluated in the reaction. This is one disadvantage of using cartridge purified [^{18}F]FBAM especially if there is only a small amount of peptide available for the labeling reaction. In order to remove unwanted cold peptide by-products, the radiolabeled peptide needs to be purified by HPLC to eliminate these and other chemical impurities. HPLC purification of radiolabeled peptide also helps to reduce possible toxicity due to chemical impurities and to maintain high specific activity of radiolabeled peptides.

While [^{18}F]SFB remains a popular prosthetic group our studies have demonstrated some of the problems that may arise depending on the nature of the peptide to be labeled. The presence of multiple reactive primary amino groups in a peptide can lead to a complex mixture of singly and multiply labeled products and thus poor chemoselectivity to labeling at the N-terminus. N-terminus labeling will generally be preferred as addition of prosthetic groups at this position is less likely

to perturb the biological binding behaviour of the peptides. In addition to poor radiochemical yields, it can be very difficult to isolate one radiochemical species from a sample containing various radiolabeled compounds all with very similar chemical properties. We also encountered problems in radiolabeling PGDLSR due to the absence of a primary amine for [^{18}F]SFB reaction. For these peptides in particular, overall radiolabeling with [^{18}F]FBAM is superior to radiolabeling with [^{18}F]SFB due to higher radiolabeling yield and due to the ability to chemoselectively radiolabel the peptides. Prosthetic group labeling has proven applicability with a variety of biologically relevant molecules including peptides, proteins and oligonucleotides and this approach will certainly see continued developments and improvements. Our experience points out the advantage of access to several prosthetic groups since the required selectivity, specificity and yield may be suboptimal in the reaction between a selected target molecule and a particular prosthetic group.

Further investigations will focus on radiopharmacologic studies of the *in vitro* and *in vivo* stability of peptides CLIKKPF and CPGDLSR radiolabeled with [^{18}F]FBAM. Our goal is to develop these peptides into novel PET imaging agents to image apoptosis in tumors and to explore their potential to evaluate tumor response to therapy.

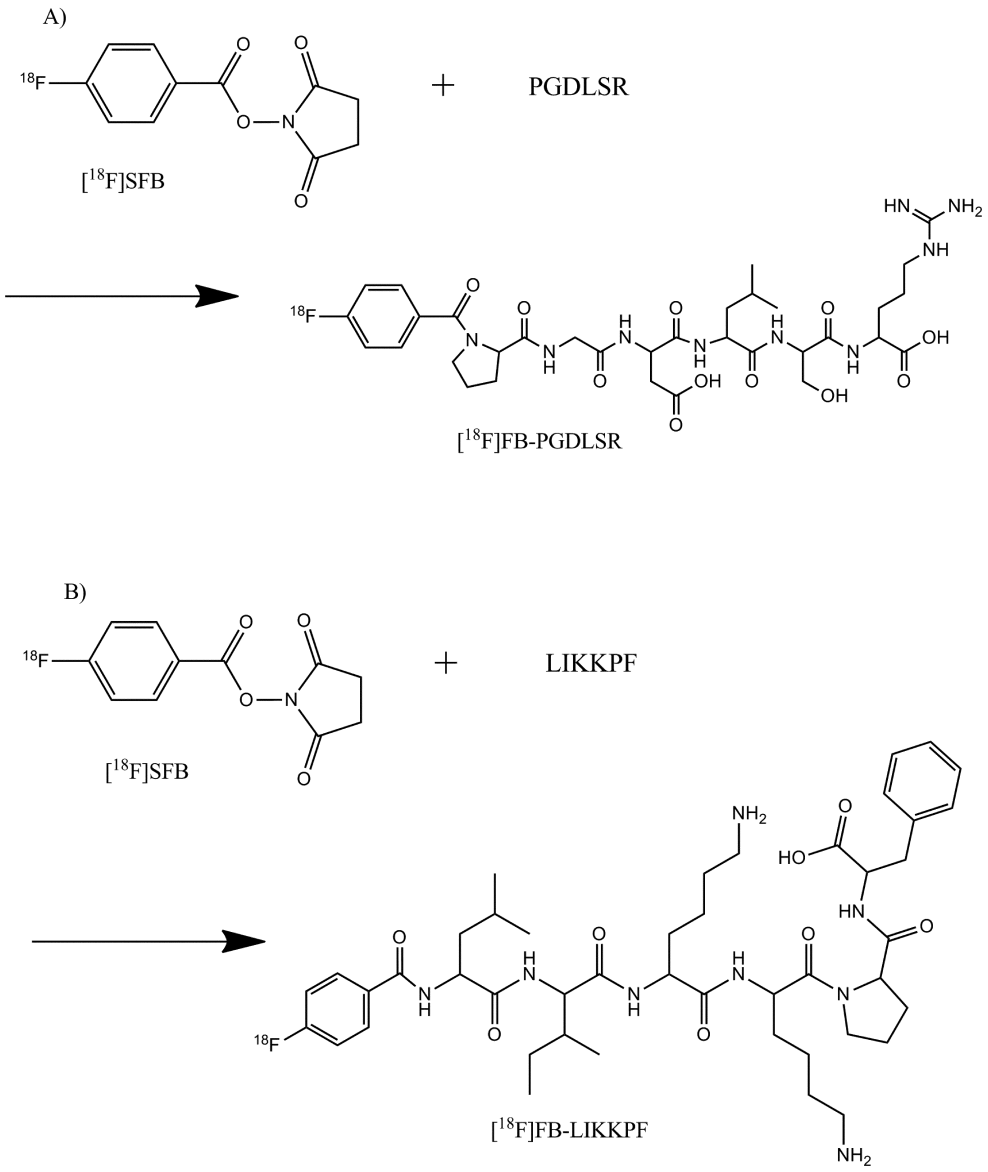

Figure 3-1. A) PGDLSR radiolabeled with [^{18}F]SFB resulting in [^{18}F]FB-PGDLSR. B) LIKKPF radiolabeled with [^{18}F]SFB resulting in [^{18}F]FB-LIKKPF.

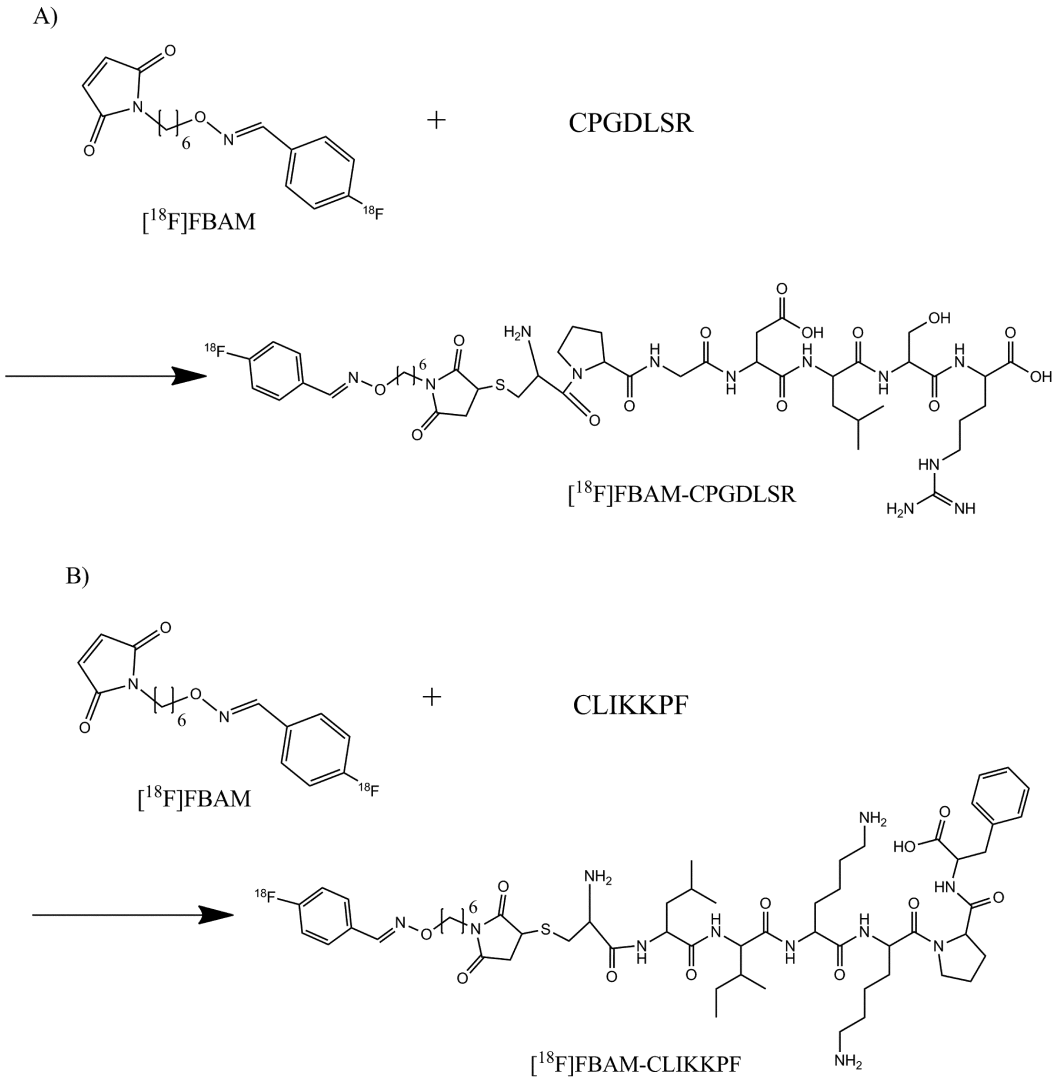

Figure 3-2. A) CPGDLSR radiolabeled with [^{18}F]FBAM resulting in [^{18}F]FBAM-CPGDLSR. B) CLIKKPF radiolabeled with [^{18}F]FBAM resulting in [^{18}F]FBAM-CLIKKPF.

A)

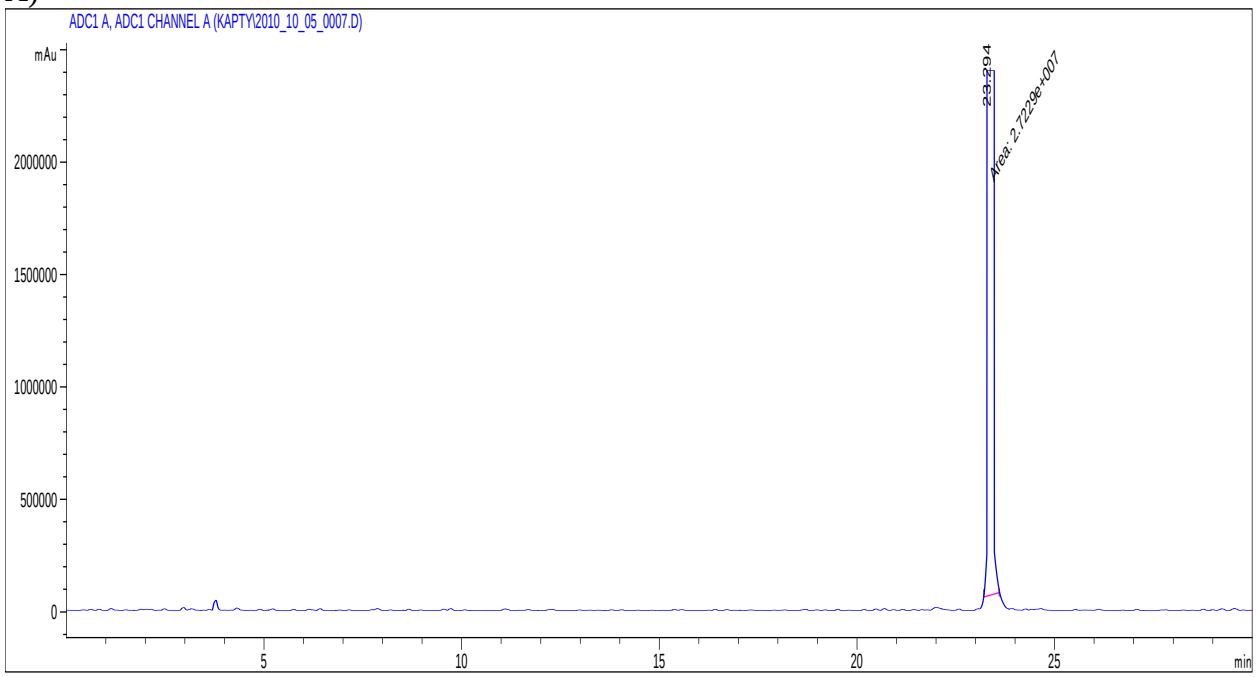

B)

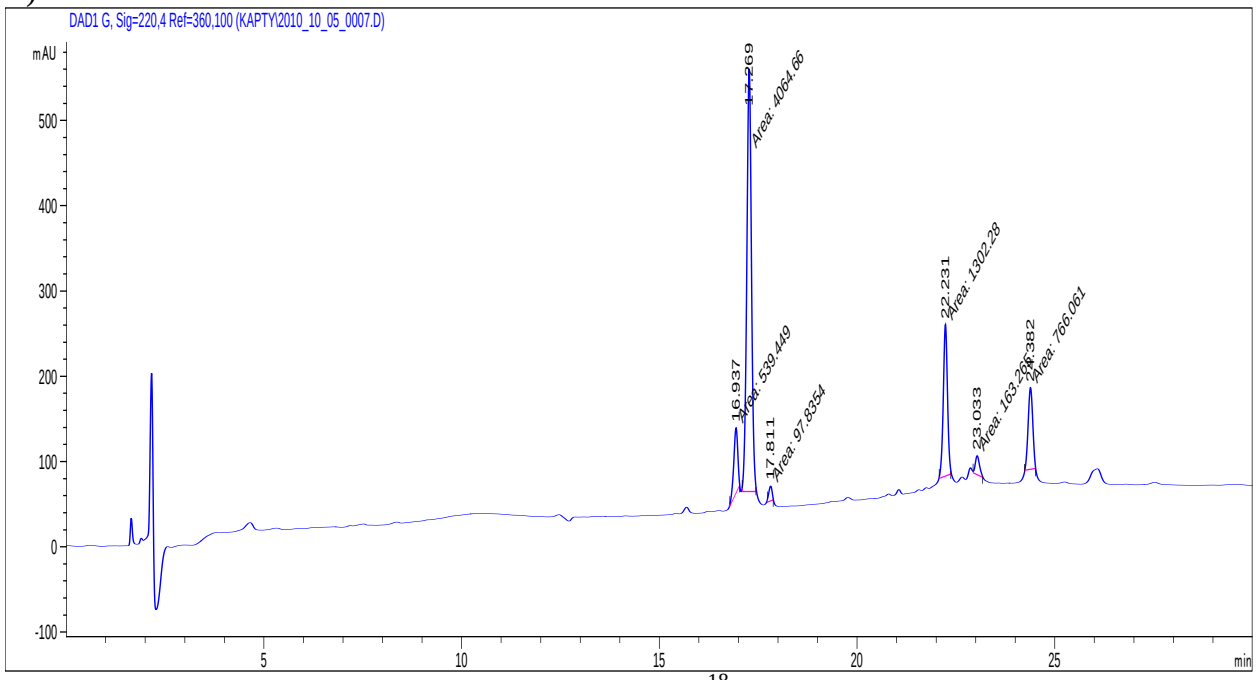

Figure 3-3. A) HPLC radiotrace of cartridge purified [^{18}F]FBAM. B) HPLC UV trace (220 nm) of cartridge purified [^{18}F]FBAM.

Table 3-1. Optimization of Reaction Conditions for radiolabeling of LIKKPF with [^{18}F]SFB.

Time (min)	**Radiochemical yield* (%) at different reaction conditions**		
	pH 7.6 40 ºC	**pH 8.4 40 ºC**	**pH 9.0 60 ºC**
20	67	63	55
40	70	**75**	57
60	66	72	58

*Radiochemical yield refers to the mixture of radiolabeled peptides produced. Results are the average of N=3.

Table 3-2. Optimization of Reaction Conditions for radiolabeling of PGDLSR with [^{18}F]SFB.

Time (min)	**Radiochemical yield* (%) at different reaction conditions**		
	pH 7.6 60 ºC	**pH 8.4 40 ºC**	**pH 9.0 60 ºC**
20	24	40	21
40	28	**49**	27
60	37	43	22

*Radiochemical yield refers to the mixture of radiolabeled peptides produced. Results are the average of N=3.

Table 3-3. Radiolabeling of Peptides (CLIKKPF and CPGDLSR) with cartridge purified (CP) and HPLC-purified [^{18}F]FBAM. Reacted at 60 °C for 60 min.

Peptide Concentration (mg/mL)	**Radiochemical Yield (%)* (CLIKKPF)**		**Radiochemical Yield (%)* (CPGDLSR)**	
	CP	**HPLC**	**CP**	**HPLC**
0.05	0	53	0	99
0.25	0	82	0	>99
0.50	0	97	0	>99
2.5	6	96	0	97
5.0	98	98	97	-

***** Results are the average of N=3.

Table 3-4. [^{18}F]FBAM-CLIKKPF isomerisation equilibration over time (N=1).

Time after reaction completed (hrs)	**Isomer 1 (%) HPLC, R_t= 15.2**	**Isomer 2 (%) HPLC, R_t= 14. 9**
0	89	11
1	68	32
2	70	30
3	68	32

3.5 References:

Berndt, M., Pietzsch, J., Wuest, F., 2007. Labeling of low-density lipoproteins using the 18F-labeled thiol-reactive reagent N-[6-(4-[18F]fluorobenzylidene)aminooxyhexyl]maleimide. Nucl Med Biol 34, 5-15.

Burtea, C., Laurent, S., Lancelot, E., Ballet, S., Murariu, O., Rousseaux, O., Port, M., Vander Elst, L., Corot, C., Muller, R.N., 2009. Peptidic targeting of phosphatidylserine for the MRI detection of apoptosis in atherosclerotic plaques. Mol Pharm 6, 1903-1919.

Hultsch, C., Berndt, M., Bergmann, R., Wuest, F., 2007. Radiolabeling of multimeric neurotensin(8-13) analogs with the short-lived positron emitter fluorine-18. Appl Radiat Isot 65, 818-826.

Kapty, J., Murray, D., Mercer, J., 2010. Radiotracers for noninvasive molecular imaging of tumor cell death. Cancer Biother Radiopharm 25, 615-628.

Kniess, T., Kuchar, M., Pietzsch, J., 2011. Automated radiosynthesis of the thiol-reactive labeling agent N-[6-(4-[^{18}F]fluorobenzylidene)aminooxyhexyl]maleimide ([^{18}F]FBAM) Appl Radiat Isotopes.

Lapi, S.E., Wahnishe, H., Pham, D., Wu, L.Y., Nedrow-Byers, J.R., Liu, T., Vejdani, K., VanBrocklin, H.F., Berkman, C.E., Jones, E.F., 2009. Assessment of an 18F-labeled phosphoramidate peptidomimetic as a new prostate-specific membrane antigen-targeted imaging agent for prostate cancer. J Nucl Med 50, 2042-2048.

Liu, S., Liu, Z., Chen, K., Yan, Y., Watzlowik, P., Wester, H.J., Chin, F.T., Chen, X., 2010. 18F-labeled galacto and PEGylated RGD dimers for PET imaging of alphavbeta3 integrin expression. Mol Imaging Biol 12, 530-538.

Mading, P., Fuchtner, F., Wust, F., 2005. Module-assisted synthesis of the bifunctional labelling agent N-succinimidyl 4-[(18)F]fluorobenzoate ([(^{18})F]SFB). Appl Radiat Isot 63, 329-332.

Okarvi, S.M., 2001. Recent progress in fluorine-18 labelled peptide radiopharmaceuticals. Eur J Nucl Med 28, 929-938.

Ren, G., Liu, Z., Miao, Z., Liu, H., Subbarayan, M., Chin, F.T., Zhang, L., Gambhir, S.S., Cheng, Z., 2009. PET of malignant melanoma using 18F-labeled metallopeptides. J Nucl Med 50, 1865-1872.

Tolmachev, V., Stone-Elander, S., 2010. Radiolabelled proteins for positron emission tomography: Pros and cons of labelling methods. Biochim Biophys Acta 1800, 487-510.

Toyokuni, T., Walsh, J.C., Dominguez, A., Phelps, M.E., Barrio, J.R., Gambhir, S.S., Satyamurthy, N., 2003. Synthesis of a new heterobifunctional linker, N-[4-(aminooxy)butyl]maleimide, for facile access to a thiol-reactive 18F-labeling agent. Bioconjug Chem 14, 1253-1259.

Vance, J.E., Steenbergen, R., 2005. Metabolism and functions of phosphatidylserine. Prog Lipid Res 44, 207-234.

Wuest, F., Berndt, M., Bergmann, R., van den Hoff, J., Pietzsch, J., 2008. Synthesis and application of [18F]FDG-maleimidehexyloxime ([18F]FDG-MHO): a [18F]FDG-based prosthetic group for the chemoselective 18F-labeling of peptides and proteins. Bioconjug Chem 19, 1202-1210.

Wuest, F., Hultsch, C., Bergmann, R., Johannsen, B., Henle, T., 2003. Radiolabelling of isopeptide N epsilon-(gamma-glutamyl)-L-lysine by conjugation with N-succinimidyl-4-[18F]fluorobenzoate. Appl Radiat Isot 59, 43-48.

Wuest, F., Kohler, L., Berndt, M., Pietzsch, J., 2009. Systematic comparison of two novel, thiol-reactive prosthetic groups for 18F labeling of peptides and proteins with the acylation agent succinimidyl-4-[18F]fluorobenzoate ([^{18}F]SFB). Amino Acids 36, 283-295.

Chapter 4

In vivo Dynamic Imaging of Chemotherapy Induced Tumor Apoptosis with Radiolabeled Phosphatidylserine-binding Peptides

4.1 Introduction

Apoptosis is a genetically controlled process that is characterized by distinct biochemical and morphological changes including nuclear condensation, phosphatidylserine (PS) externalization, cytoplasm shrinkage, nonrandom DNA degradation, plasma membrane blebbing, and fragmentation of the cell into small apoptotic bodies (Vangestel et al., 2009). Chemotherapy and radiation therapy aim to induce apoptosis; however, the deregulation and suppression of apoptosis in tumors results in increased proliferative capacity and resistance to therapy. Currently there is no clinically available method to assess the level of apoptosis in a tumor after therapy. Rapid assessment of tumor response to therapy would be greatly aided by a reliable molecular imaging probe that targeted apoptosis. The changes in biochemical processes during apoptosis provide attractive targets for molecular imaging. PS is externalized early in the apoptotic process (Devaux, 1991; Vance and Steenbergen, 2005) and this attractive target has led to the development of molecular imaging probes for apoptosis that bind to externalized PS such as annexin V probes.

PS targeting with fluorescent annexin V has been widely employed for *in vitro* imaging and *in vivo* probes based on labeling annexin V with radionuclides have been developed to allow non-invasive imaging of apoptosis using nuclear medicine techniques (Kapty et al., 2010; Kartachova et al., 2004; Kartachova et al., 2006). Radiolabeled annexin V however has failed to gain wide acceptance as a clinical imaging agent due to a variety of limitations including less than optimal biodistribution. The difficulties encountered with various forms of radiolabeled

annexin V are reviewed by Kapty *et al.* (2010) and these issues illustrate the continued need to identify a robust and clinically acceptable molecular imaging probe for apoptosis.

One alternative approach is to develop a molecular imaging probe based on radiolabeled peptides which bind to externalized PS. Peptides may provide advantages as imaging agents because they are smaller than the PS-binding annexin V and this may contribute to a more favorable biodistribution for imaging purposes. Peptides have a number of potential advantages as radiotracers including small size, good tissue diffusion, rapid targeting, low antigenicity, easy synthesis, well developed radiolabeling, fast blood clearance, and inexpensive production (Langer and Beck-Sickinger, 2001; Reubi and Maecke, 2008; Weiner and Thakur, 2002, 2005). We propose that PS-binding peptides radiolabeled with ^{18}F could be effective radiotracers for imaging apoptosis *in vivo*.

Recently, Burtea *et al*. (2009) isolated two phages displaying the peptides LIKKPF and PGDLSR, which have high affinity and specificity for PS. The preliminary report of these peptides prompted us to investigate their application as possible molecular imaging probes for use with Positron Emission Tomography (PET). We have previously reported the evaluation of the peptides LIKKPF and PGDLSR (Burtea et al., 2009) and two modified peptides CLIKKPF and CPGDLSR for binding to PS and to apoptotic cells (see Chapter 2). We have also reported results for radiolabeling CLIKKPF and CPGDLSR with the ^{18}F-prosthetic group N-[6-(4-[^{18}F]fluorobenzylidene)aminooxyhexyl]maleimide ([^{18}F]FBAM) in order to incorporate a positron emitting radionuclide into the

peptide (Kapty et al., 2011) required for future imaging as a PET tracer (see Chapter 3).

The current study aims to investigate [^{18}F]FBAM-CLIKKPF and [^{18}F]FBAM-CPGDLSR *in vitro* and *in vivo* as possible radiotracers able to bind to apoptotic cells and we aim to image chemotherapy induced apoptosis using the radiopeptides as novel PET probes. We report the first experiments where PS-binding peptides were radiolabeled with ^{18}F and evaluated as possible radiotracers for imaging apoptosis.

4.2 Materials and methods

4.2.1 General

Peptides CLIKKPF and CPGDLSR were obtained from Institute for Biomolecular Design (University of Alberta, Edmonton, AB, Canada) with >95% purity. Cyclophosphamide and etoposide were obtained from Sigma. Sterile saline (0.9% w/v NaCl) was obtained from Hospira Healthcare (Montreal, Quebec, Canada). All chemicals were reagent grade and were used without further purification. Mass spectrometric (MS) analysis was carried out with a Voyager Elite MALDI (AB Sciex, Foster City, CA, USA). Cells were obtained from in house stocks (Jurkat cells) or purchased from American Type Culture Collection (ATCC) (EL4 cells) and expanded as required. HPLC purification of products was carried out with a Beckman Coulter Inc. system consisting of a Model 168 Diode Array UV detector; a Model 126 analytical dual pump; a radioactivity detector (Ortec, TN, USA):ACE MateTM Single Channel Analyzer and using a Machery

Nagel VP250/10 Nucleosil 100-5 C18 Nautilus HPLC column with a flow rate of 2 mL/min. Solvent A: water; solvent B: acetonitrile. The following gradient was used: 0 min 10% B, 20 min 80% B, 33 min 80% B (System A).

4.2.2 Preparation of FBAM- reference compounds

The non-radioactive reference compounds FBAM–CLIKKPF and FBAM–CPGDLSR were prepared by the addition of 2 mg of cold FBAM in 120 µL acetonitrile to 8 mg of CLIKKPF or CPGDLSR dissolved in phosphate buffer (120 µL, pH 7.4). The reaction mixtures were incubated for 2 h at 60 °C. HPLC purification of the products was accomplished using SystemA. Retention time for FBAM–CLIKKPF was 17.8 min. MW calculated 1166.46, found MS 1165.74 $[M+H]^+$. Retention time for FBAM– CPGDLSR was 20.8 min. MW calculated 1064.18, found MS 1065.59 $[M+H]^+$.

4.2.3 Radiosynthesis of [^{18}F]FBAM

No carrier added aqueous [^{18}F]fluoride ion was produced on a TR-19/9 cyclotron (Advanced Cyclotron Systems, Burnaby, BC, Canada) by irradiation of [^{18}O]H_2O via the $^{18}O(p,n)^{18}F$ nuclear reaction. The radiosynthesis of [^{18}F]FBAM was performed in an automated nucleophilic fluorination module (General Electric Tracerlab FX_{FDG}) using the previously reported method (Berndt et al., 2007; Kapty et al., 2011). Radiosynthesis of [^{18}F]FBAM was performed by a two-step procedure involving synthesis and solid phase extraction of 4-[^{18}F]fluorobenzaldehyde and subsequent Schiff-base reaction with the

corresponding aminooxy precursor. The [^{18}F]FBAM was trapped on an RP18 cartridge (SepPak tC18plus, Waters, Milford, MA, USA) and after washing with acetonitrile/water it was eluted with pure acetonitrile. [^{18}F]FBAM was purified by radio-HPLC (System A). Retention time for [^{18}F]FBAM was 29.8 min which is consistent with cold FBAM. After HPLC purification, [^{18}F]FBAM was dried on a mini-rotovap for 10 min at 20 °C to reduce the solution volume.

4.2.4 Radiolabeling of peptides with [^{18}F]FBAM

Both peptides CLIKKPF and CPGDLSR were radiolabeled with [^{18}F]FBAM and purified by radio-HPLC. For the CLIKKPF reaction, HPLC purified [^{18}F]FBAM in acetonitrile (44-270 MBq) was added to 1 mg CLIKKPF solution in phosphate buffer (200 µL, pH 7.4) and was incubated at room temperature for 45 min. The final peptide concentrations were in the range of 1.0-2.5 mg/mL. For the CPGDLSR reaction, HPLC purified [^{18}F]FBAM in acetonitrile (84-557 MBq) was added to 1 mg CPGDLSR solution in phosphate buffer (200 µL, pH 7.4) and was incubated at room temperature for 45 min. The final peptide concentrations were in the range of 1.0-2.0 mg/mL. The radiolabeled peptides were purified and isolated using radio-HPLC (System A). HPLC retention time for [^{18}F]FBAM-CLIKKPF was 18.0 min and the retention time for [^{18}F]FBAM-CPGDLSR was 20.7 min. The HPLC purified radiopeptide in solution of acetonitrile/water was then processed in a mini-rotovap for 15 min at 40 °C to remove all solvent. Ethanol (0.5 mL) was added to redissolve the radiopeptide and the solution was transferred to an Eppendorf tube. One variation

in the method for the cell experiments is that instead of 0.5 mL ethanol, 0.5 mL binding buffer was added to redissolve the radiopeptide and this solution was used for subsequent cell studies. The ethanol was evaporated using nitrogen gas and heating at 40 °C for 20 min. The remaining radiopeptide was dissolved in 100 µL sterile saline for subsequent animal experiments.

4.2.5 Cell culture

Jurkat cells were used for the *in vitro* binding assay, and EL4 murine cells were employed for the tumor model. The cells were grown using T75 flasks in RPMI medium supplemented with 10% fetal bovine serum (Gibco, Invitrogen, Carlsbad, CA, USA), 2 mM glutamine (Gibco, Invitrogen, Carlsbad, CA, USA) and 1% penicillin/streptomycin (Gibco, Invitrogen, Carlsbad, CA, USA) and were kept at 37 °C in a humid incubator with 5% CO_2. The cells were maintained at a density between 2 x 10^5 per mL to 3 x 10^6 per mL throughout the experiments.

4.2.6 EL4 murine lymphoma tumor model

All animal experiments were carried out in accordance with guidelines of the Canadian Council on Animal Care and were approved by the Cross Cancer Institute- Alberta Health Services Animal Ethics Committee.

The tumor model is a murine lymphoma model which was previously used to evaluate apoptosis probes (Al-Ejeh et al., 2007; Guo et al., 2009; Sakurai et al., 1998; Zhao et al., 2001). EL4 cells form solid lymphoma tumors when implanted subcutaneously in C57/BL6 mice. A cell suspension of one million EL4 cells was

injected subcutaneously into the left flank of wild type female C57/BL6 mice. Seven days after implantation mice had tumors suitable for imaging or for chemotherapy treatment. The mice gained an average of 1.4 g (n=4) seven days after cell injection.

Apoptosis in these tumors was induced by intraperitoneal injection of 40 µL cyclophosphamide (50 mg/mL) and 120 µL etoposide (12.5 mg/mL) on two consecutive days. Chemotherapy dose equals 38 mg/kg tissue for etoposide and 100 mg/kg tissue for cyclophosphamide in 50% DMSO. When mice were given chemotherapy (etoposide and cyclophosphamide) for two days, they lost an average of 2.6 g (n=4). Animals were subsequently used for PET imaging and biodistribution studies.

4.2.7 In vitro cell binding studies

The method used to induce apoptosis in cells was based on the report by Burtea *et al.* (2009) where Jurkat cells are induced to undergo apoptosis by treatment with camptothecin. Approximately twenty-two million Jurkat cells were seeded to T75 flasks at a concentration of 2 million cells per mL 24 h before the binding assay and apoptosis was induced by incubation with 2 µM of camptothecin for 20-24 hours at 37 °C. The control group was seeded in the same manner without camptothecin. The level of apoptosis was assayed using annexin V-FITC and the results confirmed that Jurkat cells undergo apoptosis after treatment with 2 µM camptothecin (refer to Chapter 2). The cells were centrifuged 1 h before the binding assay and washed once with binding buffer. Binding buffer

contains 10 mM HEPES, 140 mM NaCl, and 2.5 mM $CaCl_2$. The cells were resuspended in 3 mL of binding buffer and incubated at room temperature on a shaker. The radiopeptide ([^{18}F]FBAM-CLIKKPF or [^{18}F]FBAM-CPGDLSR) was diluted in binding buffer to approximately 1 MBq/mL and 100 µL of radiopeptide was combined with 400 µL of cell suspension. The mixture was then incubated at room temperature on a shaker for 1, 15 and 30 min. To terminate the binding, cells were centrifuged at 109 x g for 3 min and the supernatant was aspirated. The cells were resuspended in 500 µL of binding buffer and the suspension was transferred to a clean Eppendorf tube. The cells were centrifuged again at 109 x g for 3 min and the supernatant was removed. The activity bound to the cell pellet was measured in a Wizard-3 1480 automatic gamma counter (Perkin Elmer Life Sciences, Woodbridge, ON, Canada).

Protein levels were quantified using the bicinchoninic acid (BCA) protein assay kit (Pierce, Rockford, IL, USA) according to the manufacturer's instructions. From the same cell suspension, 400 µL of cells were centrifuged at 109 x g for 5 min. The cell pellet was lysed with 400 µL of celLytic M reagent (Sigma-Aldrich, Oakville, ON, Canada). The cell lysate was put on ice for 10 min and then centrifuged at 10,864 x g for 8 min. The supernatant was used to determine the protein content using the BCA protein assay kit. Twenty five microliters of standards and samples were transferred to a flat bottom 96-well plate (Fisher, Nepean, ON, Canada). Solution A and solution B were mixed at 50 to 1 ratio and 200 µL of the mixture was added to each well. The plate was covered with parafilm and subsequently incubated at 37 °C for 30 min. The plate

was cooled to room temperature and the absorbance was measured at 562 nm using Multiskan spectrum spectrophotometer (ThermoScientific, Waltham, MA, USA) and SkanIt software (ThermoScientific, Waltham, MA, USA). Cell binding levels were normalized to percent of the total added amount of radioactivity corresponding to dose (%D) per milligram of protein. An unpaired t-test was performed in order to determine level of significance between treated and untreated cells.

4.2.8 Biodistribution studies in normal C3H.HeN mice

Biodistribution studies were performed in normal female C3H.HeN mice at time points of 5 min and 60 min. After intravenous injection of 1-2 MBq [^{18}F]FBAM-CLIKKPF in 80-120 µL sterile saline into the tail vein of anesthetized mice, the animals were allowed to regain consciousness until sacrifice. Animals were euthanized by cervical dislocation at 5 and 60 min post injection (p.i.) and rapidly dissected. Organs of interest were collected and weighed. The concentration of radioactivity in the urine was based on the urine voided at the time of sacrifice. Radioactivity in all tissues was measured in a Wizard-3 1480 automatic gamma counter (Perkin Elmer Life Sciences, Woodbridge, ON, Canada) and results were analyzed as percentage of injected dose per gram of tissue (%ID/g).

4.2.9 Determination of radioactive metabolites in mouse blood and urine

7-17 MBq radiopeptide ([^{18}F]FBAM-CLIKKPF or [^{18}F]FBAM-CPGDLSR) in 100 to 150 µL sterile saline was injected as a bolus through a catheter into the tail vein of isoflurane anesthetized normal CH3.HeN mice. Before radiotracer injection, mice were heparinized by subcutaneous injection of 50 µL heparin (1000 IU) and kept under anesthesia during the course of the experiment. At time points of 5 or 15 min the animal was sacrificed and a whole blood sample (approximately 500 µL) was collected. Urine samples were collected as available from the urine voided after the animal was sacrificed. Blood cells were separated by immediate centrifugation (5 min at 11,357 x g). Proteins within the sample were precipitated by adding approx 800 µL methanol to the supernatant following a second centrifugation step (5 min at 11,357 x g). Plasma and urine samples were analyzed for metabolites and original radiopeptide using radio-thin layer chromatography (radio TLC). Radio TLC was performed with silica gel aluminum plates (Fluka, Sigma-Aldrich, Oakville, ON, Canada) developed with *n*-butanol/water/acetic acid (4/1/1) and radioactive compounds were detected with an AR-2000 imaging scanner (Bioscan Inc., Washington, DC, USA). In addition, each fraction of the blood sample (blood cells, proteins and plasma) was measured for radioactivity content in the dose calibrator in order to determine radioactivity percentage distribution in the blood compartments.

4.2.10 Biodistribution studies in EL4 tumor bearing mice

Biodistribution studies were performed in C57/BL6 mice bearing EL4 tumors and C57/BL6 mice bearing EL4 tumors which were treated with

chemotherapy to induce apoptosis. Radiopeptide was administered by intravenous injection of 5-8 MBq ([^{18}F]FBAM-CLIKKPF or [^{18}F]FBAM-CPGDLSR) in 80-120 µL sterile saline into the tail vein of anesthetized mice. Animals were euthanized by cervical dislocation at 60 min p.i. (after 60 min dynamic PET scan) and rapidly dissected. Organs of interest were collected and weighed. The concentration of radioactivity in the urine was based on the urine voided at the time of sacrifice. Radioactivity in all tissues was measured in a Wizard-3 1480 automatic gamma counter (Perkin Elmer Life Sciences, Woodbridge, ON, Canada) and results were analyzed as percentage of injected dose per gram of tissue (%ID/g).

4.2.11 Dynamic PET imaging in EL4 tumor bearing mice

Positron emission tomography experiments were performed using C57/BL6 mice bearing EL4 tumors and C57/BL6 mice bearing EL4 tumors which were treated with chemotherapy to induce apoptosis. EL4 tumor uptake was evaluated with [^{18}F]FDG, and the two ^{18}F-radiolabeled peptides; [^{18}F]FBAM-CLIKKPF and [^{18}F]FBAM-CPGDLSR. The animals were anesthetized through inhalation of isoflurane in 40% oxygen/60% nitrogen (gas flow, 1 L/min), and body temperature was kept warm with a heating pad for the entire experiment. Mice were positioned and immobilized in the prone position with their medial axis parallel to the axial axis of the scanner and their thorax, abdomen and hind legs (organs of interest: heart, kidneys, bladder, tumors) in the centre of the field of view of the microPET R4 scanner (Siemens Preclinical Solutions, Knoxville,

TN, USA). The amount of radioactivity present in the injection solution in a 0.5 mL syringe was determined with a dose calibrator (Atomlab 300, Biodex Medical Systems, Shirley, NY, USA), which was cross calibrated with the scanner. The emission scan of a 60 min dynamic PET acquisition was started. After a delay of approximately 15 s, 5-8 MBq of the radiotracer of interest in 70-130 µL sterile saline solution was injected through a tail vein catheter. While [^{18}F]FDG was injected in 100% saline, the solution of [^{18}F]FBAM-CLIKKPF and [^{18}F]FBAM-CPGDLSR contained 5-10% ethanol by volume. Data acquisition continued for 60 min in 3D list mode. The list mode data were sorted into sinograms with 53 time frames (10×2, 8×5, 6×10, 6×20, 8×60, 10×120 and 5×300 s). The frames were reconstructed using maximum *a posteriori* (MAP) reconstruction mode. The pixel size was 0.085×0.085×0.12 cm, and the resolution in the centre field of view was 1.8 mm. No correction for partial volume effects was performed. The image files were further processed using the ROVER v2.0.21 software (ABX GmbH, Radeberg, Germany). Masks for defining 3D regions of interest (ROI) were set and the ROIs were defined by thresholding. ROI time-activity curves (TAC) were generated for subsequent data analysis. Standardized uptake values [SUV= (activity/mL tissue)/ (injected activity/body weight), mL/g] were calculated for each ROI.

All data are expressed as SUV means ± S.E.M. from n investigated animals. All TACs were constructed using GraphPad Prism 4.0 (GraphPad Software, San Diego, CA, USA). Where applicable, statistical differences were tested using an unpaired t-test and were considered significant for $P<0.05$.

4.2.12 Histological analysis of tumors

After imaging was complete we dissected the animals and fixed the tumor samples to produce slides for histological analysis of apoptosis. The terminal deoxynucleotidyl transferase dUTP nick end labeling (TUNEL) assay is used to detect DNA fragmentation caused during apoptosis. In this assay, terminal deoxynucleotidetransferase adds fluorescein-labeled nucleotides to the 3' termini at double stranded breaks in fragmented DNA which is indicative of apoptosis (Yagle et al., 2005). TUNEL assays were performed according to the manufacturer's instructions using the FragEL fluorescent DNA Fragmentation detection kit (EMD Biosciences, San Diego, CA, USA). Each tumor sample was preserved in formalin overnight at room temperature and then embedded in paraffin to produce slides for subsequent histological analysis of apoptosis. Slices were freed of paraffin through xylene and graded ethanol washes and then incubated with proteinase K (EMD Biosciences, San Diego, CA, USA) (100 µL of 20 µg/mL proteinase K in 10 mM Tris pH 8.0). After proteinase digestion the slides were placed in equilibration buffer and the proprietary FragEL labeling mixture (EMD Biosciences, San Diego, CA, USA) was added and the slides were incubated at 37 °C for 1.5 h in a humid chamber. Slides were prepared with mounting media containing DAPI. Slides were analyzed for apoptotic cells in tumor samples (control) and chemotherapy treated tumor samples using a Zeiss microscope (Axioplan IIM, objective PlanNeofluor 10x/0.30), Metamorph

software (Universal Imaging Corp, Molecular Devices), and a sensitive, cooled CCD camera (CoolSnapHQ, Photometrics).

4.3 Results

4.3.1 Radiolabeling of peptides with [^{18}F]FBAM

The radiosynthesis was designed to prepare ^{18}F-radiolabeled peptides of very high purity suitable for subsequent cell testing and animal studies. The radiolabeling of CLIKKPF with [^{18}F]FBAM resulted in an average radiochemical yield of [^{18}F]FBAM-CLIKKPF of 54.5 ± 15.7% decay corrected (26.5 ± 7.7% non decay corrected) (n=9) (based on starting [^{18}F]FBAM activity). [^{18}F]FBAM-CLIKKPF has a HPLC retention time of 18.0 min (System A) which is consistent with cold reference FBAM-CLIKKPF. The radiolabeling of CPGDLSR with [^{18}F]FBAM resulted in an average radiochemical yield of [^{18}F]FBAM-CPGDLSR of 50.3 ± 7.1% decay corrected (22.8 ± 2.1% non decay corrected) (n=4) (based on starting [^{18}F]FBAM activity). [^{18}F]FBAM-CPGDLSR has a retention time of 20.7 min according to HPLC analysis (System A) which is consistent with cold reference FBAM-CPGDLSR.

4.3.2 Radiolabeled peptides evaluated in cell model of apoptosis

[^{18}F]FBAM-CLIKKPF and [^{18}F]FBAM-CPGDLSR were evaluated for ability to bind to apoptotic Jurkat cells (treated with camptothecin) and healthy Jurkat cells (no camptothecin treatment). Binding of the radiolabeled peptides was measured at two time points (15 min and 30 min) and percent of dose per mg of

protein was calculated. For [^{18}F]FBAM-CLIKKPF, after 15 minutes the untreated cells had an average of 7.6 ± 2.0 %D/mg protein and the treated cells had an average of 16.7 ± 2.2 %D/mg protein (n=3) (**Figure 4-1**). The treated cells have significantly more radiolabeled peptide binding after 15 min compared to untreated cells as determined by an unpaired t-test (p value=0.006). After 30 minutes the untreated cells had an average of 5.8 ± 0.1 %D/mg protein and the treated cells had an average of 13.7 ± 4.4 %D/mg protein (n=3) (**Figure 4-1**). The treated cells have significantly more radiolabeled peptide binding after 30 min compared to untreated cells as determined by an unpaired t-test (p value=0.03). For [^{18}F]FBAM-CPGDLSR, after 15 min the untreated cells had an average of 1.6 ±0.8 %D/mg protein and the treated cells had an average of 3.3 ± 2.4 %D/mg protein (n=3) (**Figure 4-2**). Although close, there is no significant difference between the treated and untreated cells after 15 min (p value= 0.31). After 30 min the untreated cells had an average of 2.4 ± 0.6 %D/mg protein and the treated cells had an average of 4.4 ± 1.3 %D/mg protein (n=3) (**Figure 4-2**). Although close, there is no significant difference between the treated and untreated cells after 30 min (p value= 0.0662).

4.3.3 Biodistribution in normal C3H.HeN mice

The biodistribution of [^{18}F]FBAM-CLIKKPF was evaluated in healthy C3H.HeN mice at 5 min and 60 min p.i.. After 5 min there was high uptake of [^{18}F]FBAM-CLIKKPF in the gallbladder, duodenum, liver and kidneys (**Figure 4-**

3). After 60 min there was high uptake of [^{18}F]FBAM-CLIKKPF in small intestine, urine, gallbladder and liver (**Figure 4-3**).

4.3.4 Radioactive metabolites in blood and urine from healthy mice

In vivo stability of [^{18}F]FBAM-CLIKKPF and [^{18}F]FBAM-CPGDLSR were evaluated in healthy CH3.HeN mice. Blood plasma and urine samples were analyzed by radio-TLC to determine percentage of intact radiolabeled peptide. For [^{18}F]FBAM-CLIKKPF, at 5 min p.i. there was an average of 61 % intact [^{18}F]FBAM-CLIKKPF remaining in the plasma and an average of 29% intact [^{18}F]FBAM-CLIKKPF in the urine. At 15 min p.i. there was an average of 25% intact [^{18}F]FBAM-CLIKKPF remaining in the plasma and an average of 14% intact [^{18}F]FBAM-CLIKKPF in the urine. The remainder of the sample contained radio-metabolites which were not identified. For [^{18}F]FBAM-CPGDLSR, at 5 min p.i. there was an average of 42% intact [^{18}F]FBAM-CPGDLSR remaining in the plasma and an average of 18% intact [^{18}F]FBAM-CPGDLSR in the urine. The remainder of the sample contained radio-metabolites which were not identified. At 15 min p.i. there was an average of 11% intact [^{18}F]FBAM-CPGDLSR in the urine. In the plasma we were unable to detect [^{18}F]FBAM-CPGDLSR after 15 min and were only able to detect radio-metabolites.

4.3.5 Distribution of radioactivity in blood compartments from healthy mice

From blood samples obtained from healthy mice, [^{18}F]FBAM-CLIKKPF levels were measured in each blood compartment. At 5 min p.i., 28% of the total

amount of the radioactivity in the blood was found in blood cells, 10% was bound to plasma proteins and 62% was present in the plasma (n=2) (**Figure 4-4**). Only the [^{18}F]FBAM-CLIKKPF in the plasma is immediately available for delivery to the target organs. At 15 min p.i., 29% of the total amount of the radioactivity in the blood was found in blood cells, 16% was bound to plasma proteins and 55% was present in the plasma (n=2).

Similarly, from blood samples obtained from healthy mice, [^{18}F]FBAM-CPGDLSR levels were measured in each blood compartment. At 5 min p.i., 23% of the total amount of radioactivity in the blood was found in blood cells, 16% was bound to plasma proteins and 61% was present in the plasma (n=2) (**Figure 4-5**). Only the [^{18}F]FBAM-CPGDLSR in the plasma is immediately available for delivery to the target organs. At 15 min p.i., 40% of the total amount of radioactivity in the blood was found in blood cells, 17% was bound to plasma proteins and 43% was present in the plasma.

4.3.6 Biodistribution in EL4 tumor bearing mice

The biodistribution of [^{18}F]FBAM-CLIKKPF and [^{18}F]FBAM-CPGDLSR were evaluated in EL4 tumor bearing C57BL6 mice at 60 min p.i.. In the control mice (no chemotherapy) there was high uptake of both peptides in the gallbladder, small intestine, duodenum, urine and liver (**Figure 4-6 and 4-7**). In the mice treated with chemotherapy to induce apoptosis in the tumors there was high uptake of the peptides in the gallbladder, small intestine, duodenum, urine and liver (**Figure 4-6 and 4-7**).

4.3.7 Dynamic PET imaging in EL4 tumor bearing mice

EL4 tumor bearing mice were imaged with PET using three different radiotracers: [^{18}F]FDG, [^{18}F]FBAM-CLIKKPF and [^{18}F]FBAM-CPGDLSR. Images were obtained for each tracer in control mice (no chemotherapy) and mice treated with chemotherapy.

The [^{18}F]FDG PET images of an EL4 tumor bearing mouse (control with no chemotherapy) are shown in **Figure 4-8**. The tumor region is visible after 1 minute and remains visible until the end of the PET scan at 60 min. The [^{18}F]FDG PET images of an EL4 tumor bearing mouse treated with chemotherapy are shown in **Figure 4-9**. The tumor region is visible after 1 min and remains visible until the end of the PET scan at 60 min. The TACs for [^{18}F]FDG in **Figure 4-10** indicate that there is uptake of [^{18}F]FDG into the EL4 tumors. There is higher uptake of [^{18}F]FDG in the control tumors compared to the treated tumors. There is a significant difference between the SUV of the control tumors versus the treated tumors for [^{18}F]FDG at 1 hour p.i. (unpaired t-test, p value=0.002). The tumor to muscle ratio of [^{18}F]FDG over time is shown in **Figure 4-11** and is also higher in the control tumors compared to the treated tumors.

The [^{18}F]FBAM-CLIKKPF PET images of an EL4 tumor bearing mouse (control no chemotherapy) are shown in **Figure 4-12**. The [^{18}F]FBAM-CLIKKPF PET images of an EL4 tumor bearing mouse treated with chemotherapy are shown in **Figure 4-13**. The tumor region is visible in the control mouse (no chemotherapy) and the chemotherapy treated mouse from 5-15 minutes but is not

visible at 60 min. The TACs for [^{18}F]FBAM-CLIKKPF in **Figure 4-14** indicates that there is modest uptake of this radiotracer in the EL4 tumors. There was no significant difference between the standardized uptake value (SUV) of control tumors versus treated tumors for [^{18}F]FBAM-CLIKKPF peptide at time points of 5.5 min, 15 min, and 60 min (according to unpaired t-test). The kinetics of [^{18}F]FBAM-CLIKKPF in the heart, bladder and kidneys are shown in **Figure 4-15**.

The [^{18}F]FBAM-CPGDLSR PET images of an EL4 tumor bearing mouse (control no chemotherapy) are shown in **Figure 4-16**. The [^{18}F]FBAM-CPGDLSR PET images of an EL4 tumor bearing mouse treated with chemotherapy are shown in **Figure 4-17**. The tumor region is visible in the chemotherapy treated mouse from 5-10 minutes but is not visible at 60 min. The TACs for [^{18}F]FBAM-CPGDLSR in **Figure 4-18** indicates that there is modest uptake of this radiotracer in the EL4 tumors. There was no significant difference between the SUV of control tumors versus treated tumors for [^{18}F]FBAM-CPGDLSR at time points of 15 min and 60 min (according to unpaired t-test). However, at 5.5 min there was a significant difference between the SUV of the control tumors versus the treated tumors for [^{18}F]FBAM-CPGDLSR (unpaired t-test, p value= 0.01). The kinetics of [^{18}F]FBAM-CPGDLSR in the heart, bladder and kidneys are shown in **Figure 4-19**.

4.3.8 Histological analysis of tumors

To confirm apoptosis in the chemotherapy treated mice, we dissected the animals after PET analysis and prepared tumor sections for histologic examination. The TUNEL assay recognizes DNA breaks that are a characteristic feature of apoptosis. The sections from treated tumors showed increased apoptotic cells compared to sections from tumors that did not receive chemotherapy. In the control tumor (no chemotherapy) the TUNEL assay indicates very low levels of apoptotic cells in the absence of chemotherapy. The untreated tumor has a higher cell density than the treated tumor (**Figure 4-20**). In the tumor treated with chemotherapy the TUNEL assay indicates very high levels of apoptosis as indicated by the intense green staining (**Figure 4-20**).

4.4 Discussion

The goals of the present study were to 1) investigate [^{18}F]FBAM-CLIKKPF and [^{18}F]FBAM-CPGDLSR *in vitro* and *in vivo* as possible radiotracers able to bind to apoptotic cells, and 2) image chemotherapy induced apoptosis using the radiopeptides as novel PET probes. In this report we evaluate for the first time PS-specific peptide PET tracers for tumor apoptosis imaging.

The radiopeptides [^{18}F]FBAM-CLIKKPF and [^{18}F]FBAM-CPGDLSR were evaluated for *in vitro* binding to apoptotic Jurkat cells. Binding of [^{18}F]FBAM-CLIKKPF to apoptotic Jurkat cells was significantly higher than binding to untreated cells at both time points of 15 min and 30 min. This provides evidence that the addition of the [^{18}F]FBAM prosthetic group does not interfere with binding of [^{18}F]FBAM-CLIKKPF to PS. However, binding of [^{18}F]FBAM-

CPGDLSR to apoptotic Jurkat cells was not significantly higher than binding to untreated cells (at 15 min and 30 min). Thus, the addition of the [^{18}F]FBAM prosthetic group could possibly interfere with the binding of [^{18}F]FBAM-CPGDLSR to PS.

The distribution of [^{18}F]FBAM-CLIKKPF and [^{18}F]FBAM-CPGDLSR in the blood compartments indicates that the majority of the radiopeptides are found in the plasma (at 5 min and 15 min p.i.). Since the radiopeptide in the plasma is immediately available for delivery to the target organs this indicates that the majority of [^{18}F]FBAM-CLIKKPF and [^{18}F]FBAM-CPGDLSR is available for target binding and not simply bound to red blood cells or plasma proteins.

The EL4 lymphomas are inducible to undergo apoptosis and they are sensitive to treatment with radiation (Sakurai et al., 1998) and chemotherapy (Zhao et al., 2001). The EL4 tumor model has previously been used to evaluate apoptosis imaging probes (Guo et al., 2009). In this model, daily treatment with a combination of cyclophosphamide and etoposide, for 48 hours, increased the amount of apoptosis in the EL4 tumors. The distribution of apoptotic cells in treated tumors was heterogeneous which is consistent with previous reports (Zhao et al., 2001). According to Zhao *et al.* the chemotherapy treatment of etoposide and cyclophosphamide increased the amount of apoptosis from 4% (basal level) to 32% after treatment in EL4 tumors (2001). We also observed large amounts of apoptosis in treated tumors and a large reduction in tumor size after two days of chemotherapy. The histological analysis indicated “holes” in the tissue where apoptotic cells were likely already removed by macrophages. In tumors with no

treatment there are no “holes”, more cells in general, and higher cell density compared to treated tumors.

Unfortunately our results with [^{18}F]FBAM-CLIKKPF and [^{18}F]FBAM-CPGDLSR indicate that radiopeptide uptake in an *in vivo* model does not accurately measure chemotherapy induced apoptosis. In general, uptake of [^{18}F]FBAM-CLIKKPF and [^{18}F]FBAM-CPGDLSR into tumors was low and anatomical imaging such as computed tomography for localization of the tumor would have been useful to help determine the ROI. There was no significant difference between the % ID/g or SUV of control tumors versus treated tumors for [^{18}F]FBAM-CLIKKPFF (1 hour p.i.) (according to unpaired t-test). For [^{18}F]FBAM-CPGDLSR there was a significant difference between the SUV of the control tumors versus the treated tumors at 5.5 minutes. At 5 min 42% of [^{18}F]FBAM-CPGDLSR remains intact according to our *in vivo* stability studies and this indicates the peptide has increased uptake in the treated tumors. There is a significant difference between the % ID/g of control tumors versus treated tumors for [^{18}F]FBAM-CPGDLSR (1 hour p.i.) (unpaired t-test, p value= 0.04). However, the resulting SUV values at 1 hour p.i. do not indicate a significant difference between the tumor and the treated tumor. In addition, our metabolic studies indicate that only 42% of intact [^{18}F]FBAM-CPGDLSR remains after 5 minutes *in vivo* and after 1 hour there is likely very little intact [^{18}F]FBAM-CPGDLSR remaining. It is possible that a metabolite may be binding to the apoptotic treated tumors 1 hour p.i.

PET imaging was also performed with [^{18}F]FDG in EL4 tumor bearing mice. The control tumors had a significantly higher uptake of [^{18}F]FDG compared to treated tumors. We do not know the exact mechanism to cause this difference. For instance, uptake may be altered due to changes in glucose uptake and transport after chemotherapy. One factor may be the reduction in tumor volume and tumor cell density after treatment which results in fewer cells available for uptake of [^{18}F]FDG. In addition the histological analysis revealed "holes" present in the treated tumors indicating the chemotherapy is very effective and apoptotic cells have already been removed by macrophages.

Another point to consider is that the uptake of [^{18}F]FDG after chemotherapy is specific to tumor type (Young et al., 1999). [^{18}F]FDG uptake varies quite a bit depending on the type of tumor and therapy (Young et al., 1999). Apoptosis is an energy-dependent process, and it may logically be considered that successful treatment will induce apoptosis and a subsequent increase in glucose (or [^{18}F]FDG) uptake. This is known as a flare effect of tumor uptake (Wahl et al., 2009). For example, it is advised that patients with breast cancer wait after chemotherapy for a minimum of ten days before an [^{18}F]FDG PET scan (Wahl et al., 2009) to avoid this flaring effect. In our study we do not see a flaring effect when [^{18}F]FDG PET is performed 24 hours after the last chemotherapy treatment. In a clinical setting [^{18}F]FDG PET imaging is not performed 24 hours after chemotherapy, rather guidelines for lymphomas recommend waiting three weeks post therapy (Wahl et al., 2009). Another reason [^{18}F]FDG PET is delayed is to ensure that there are low levels of inflammation which is often a side effect of

various cancer therapies. Inflammatory cells have a high uptake of [^{18}F]FDG and this can make the [^{18}F]FDG PET scan difficult to interpret. Thus imaging at an early time point of 24 hours may provide a different signal than imaging three weeks post treatment. In this report we evaluate the radiotracer [^{18}F]FDG in the EL4 tumor model and we perform PET imaging 24 hours after two days of chemotherapy; however, we do not see increased [^{18}F]FDG uptake in treated tumors and therefore we do not observe a flaring effect or increased inflammation after therapy. Previous studies in patients with malignant lymphoma found that [^{18}F]FDG uptake was reduced after therapy in patients with complete remission (Hoekstra et al., 1993). This is consistent with our results in that [^{18}F]FDG uptake was reduced in tumor bearing mice after treatment with chemotherapy.

The radiopeptides [^{18}F]FBAM-CLIKKPF and [^{18}F]FBAM-CPGDLSR were both rapidly metabolized *in vivo*. After 5 min *in vivo* there was only 61% intact [^{18}F]FBAM-CLIKKPF in the plasma and after 15 min this is reduced to only 25% intact [^{18}F]FBAM-CLIKKPF in the plasma. After 5 min *in vivo* there was only 42% intact [^{18}F]FBAM-CPGDLSR in the plasma. Disadvantages of using peptides as radiotracers include catabolism by exo and endopeptidases, chelate attachment interfering with binding, and physiological effects (binding to receptors and evoking downstream response signals) (Weiner and Thakur, 2002). Rapid metabolism is somewhat expected since there are abundant endo and exo peptidases which can metabolize both of the peptides. [^{18}F]FBAM-CLIKKPF and [^{18}F]FBAM-CPGDLSR could be metabolized by endogenous peptidases such as cysteine peptidases and serine peptidases. Biodistribution analysis of [^{18}F]FBAM-

CLIKKPF and [^{18}F]FBAM-CPGDLSR indicates high uptake in the urine, small intestine, duodenum, gallbladder and liver. This indicates the radiopeptides are eliminated via both the urine and hepatobiliary excretion. Bone uptake is very low for both radiopeptides indicating low radiodefluorination of [^{18}F]FBAM-CLIKKPF and [^{18}F]FBAM-CPGDLSR.

Despite the very rapid metabolism of [^{18}F]FBAM-CLIKKPF and [^{18}F]FBAM-CPGDLSR *in vivo* there are several modifications that can be made to peptides in order to increase stability, reduce catabolism, and improve pharmacokinetics. Most peptides undergo rapid proteolysis in the plasma by endogenous peptidases (Dahms and Mentlein, 1992). We can increase resistance to exo-peptidases (which degrade peptides from the end of a polypeptide chain) by end capping which is done by acetylating the N-terminus, converting the carboxylic acid on the C-terminus into an amide, or reducing the C-terminus to an alcohol (Langer and Beck-Sickinger, 2001; Lister-James et al., 1996). We can increase resistance to endopeptidases (which cleave in the middle of peptide chains) by using D-amino acids or modified amino acids. Additional methods to inhibit proteolysis of peptides include substitution of peptide bonds, replacement of amino with imino groups, substitution of amino terminal amino acid, insertion of unusual amino acids, methylation of amide nitrogens, and cyclization of the peptide (Langer and Beck-Sickinger, 2001; McAfee and Neumann, 1996). To improve pharmacokinetics one may also add poly(ethylene glycol) (PEG) to the peptide of interest (Chen et al., 2004). Reasons for adding PEG to the peptide includes shielding receptor-mediated uptake by the reticuloendothelial systems,

preventing recognition and degradation by proteolytic enzymes, and increasing the apparent size of the peptide which reduces the renal filtration and alters biodistribution (Chen et al., 2004). In order to make [^{18}F]FBAM-CLIKKPF and [^{18}F]FBAM-CPGDLSR more stable *in vivo* we could employ some of these strategies to overcome metabolic instability.

The modifications to improve peptide stability can be very effective as demonstrated by the peptide duramycin which has been radiolabeled and evaluated as a potential radiotracer (Zhao et al., 2008). Radiolabeled duramycin is stable in solution and *in vivo* due to its structural configuration. Duramycin is a polypeptide (19 amino acids) which is stabilized by three internal thioether bridges and is cyclized (Zhao et al., 2008; Zimmermann et al., 1993). Since the peptide is cyclic there is no free peptidergic terminus which minimizes the chance of proteolyic degradation by peptidases found in the blood.

The ability to image apoptosis would have a significant impact on patient outcome. Once a new probe is validated, imaging cell death using PET could be used to evaluate the early response to treatment for individual patients and aid in the advancement of personalized medicine. This would guide physicians to select the optimal anti-cancer therapy for a patient and allow rapid identification of ineffective treatments thereby allowing reduction of side effects from ineffective treatments (Green and Steinmetz, 2002). Ongoing research is being conducted to find a novel probe to image apoptosis. Due to the variety of limitations associated with annexin V research is focused on alternatives for development into possible imaging probes (Kapty et al., 2010). Some groups are focusing on caspase

inhibitors (Chen et al., 2011; Glaser et al., 2011) however these probes are not very sensitive. We focused on developing a peptide probe for imaging apoptosis in order to capitalize on the many advantages that peptides provide as imaging agents.

In this study we evaluated two novel PET probes for imaging apoptosis: [^{18}F]FBAM-CLIKKPF and [^{18}F]FBAM-CPGDLSR. We report the first experiments evaluating PS-binding peptides radiolabeled with ^{18}F as possible radiotracers for imaging apoptosis. Due to the rapid metabolism of the peptide probes we were unable to accurately image chemotherapy induced apoptosis. In essence peptidases are widely abundant *in vivo* and they have the potential to metabolize these radiopeptides. Modifications are required in order to improve the stability of these radiopeptides as possible imaging agents for apoptosis. Future work will focus on the development of chemically modified peptides which are stable *in vivo*. Once the peptides are more metabolically stable there is opportunity for effective imaging of apoptosis.

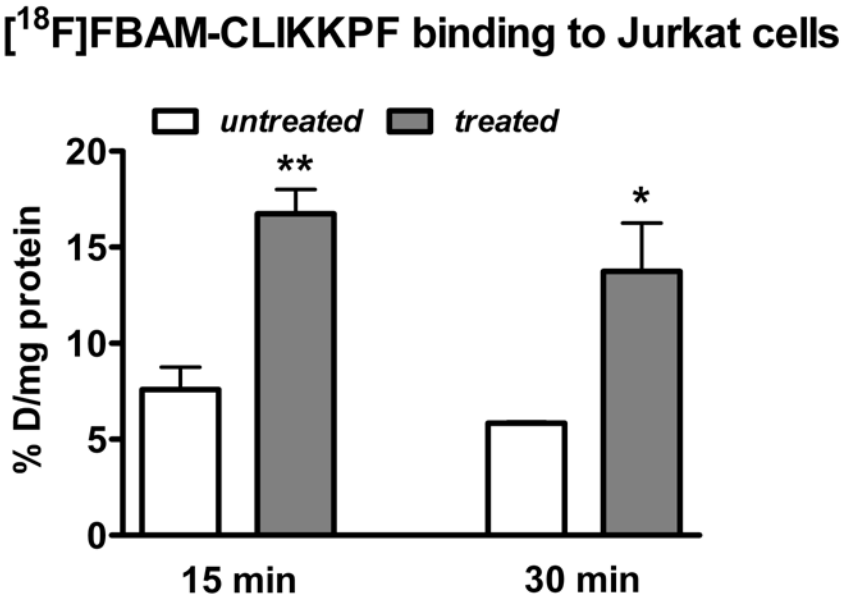

Figure 4-1. Binding of [^{18}F]FBAM-CLIKKPF to Jurkat cells treated with camptothecin and control (not treated with camptothecin). Data are shown as % D/mg protein binding. Data shown are means ± SD(n=3). ** p value= 0.006. *p value= 0.03.

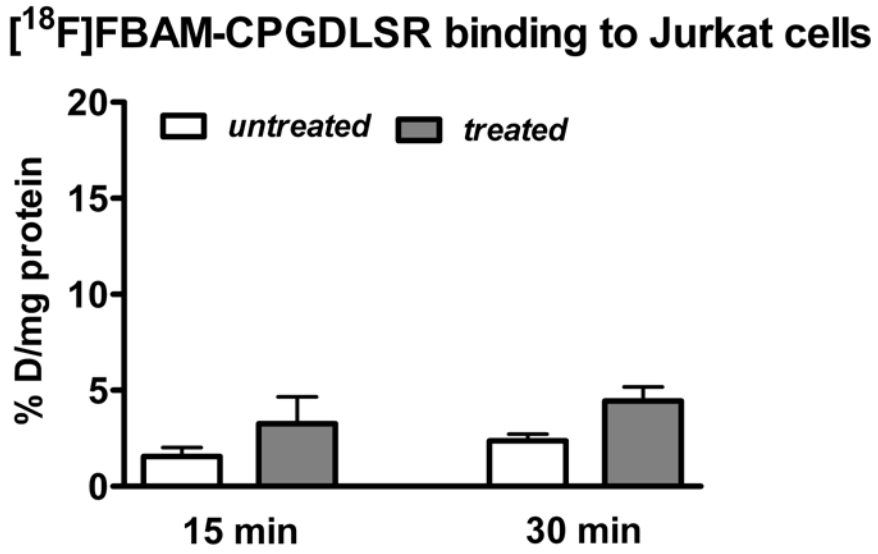

Figure 4-2. Binding to [^{18}F]FBAM-CPGDLSR to Jurkat cells treated with camptothecin and control (not treated with camptothecin). Data are shown as % D/mg protein binding. Data shown are means ± SD (n=3).

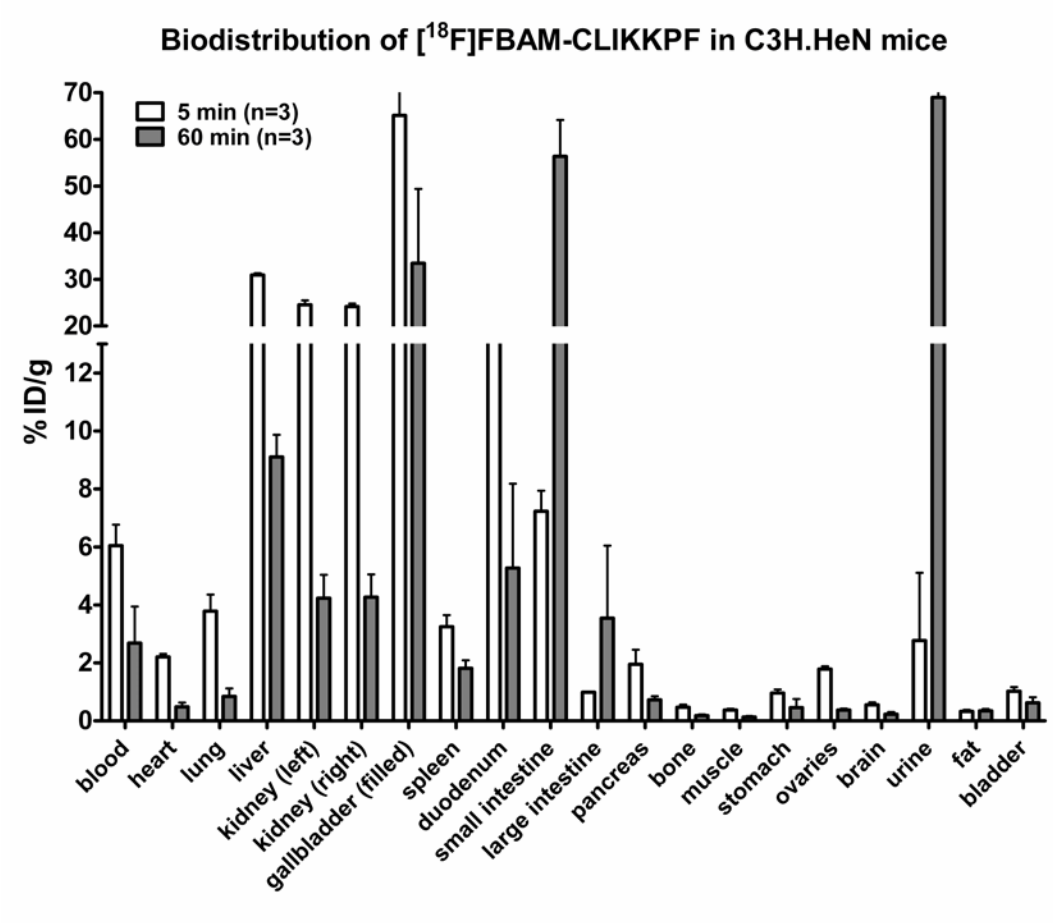

Figure 4-3. Biodistribution of [^{18}F]FBAM-CLIKKPF in C3H.HeN mice. Data are the means ± SEM of the % ID/g (n=3).

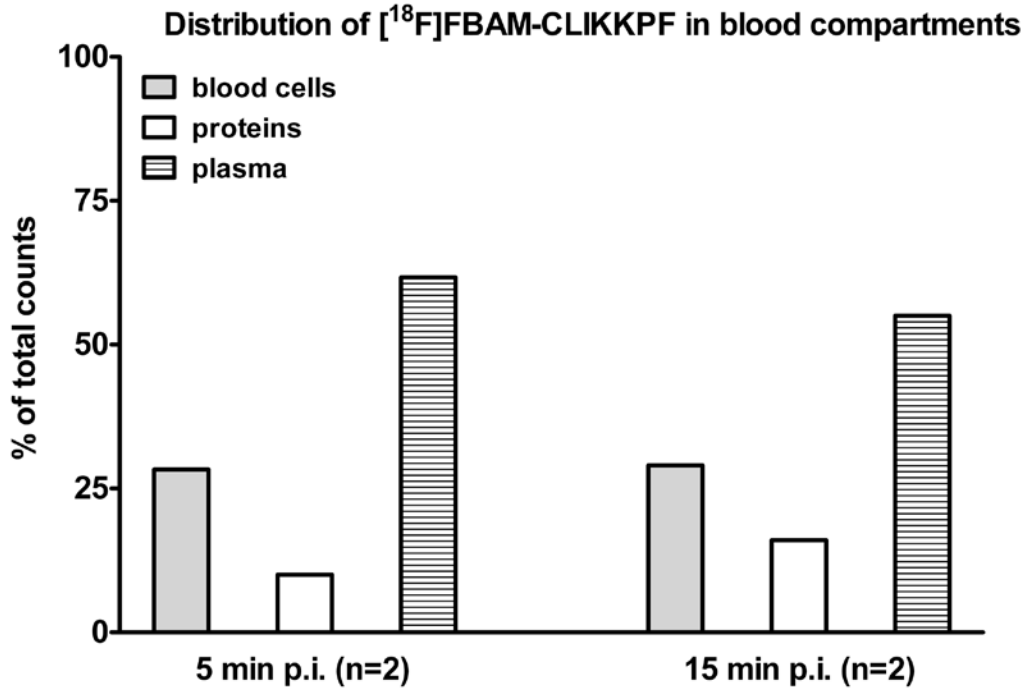

Figure 4-4. Distribution of radioactivity in blood cells, precipitated plasma protein and protein-free plasma at 5 min and 15 min p.i. of [^{18}F]FBAM-CLIKKPF. Average is presented as % of total counts from CH3.HeN mice.

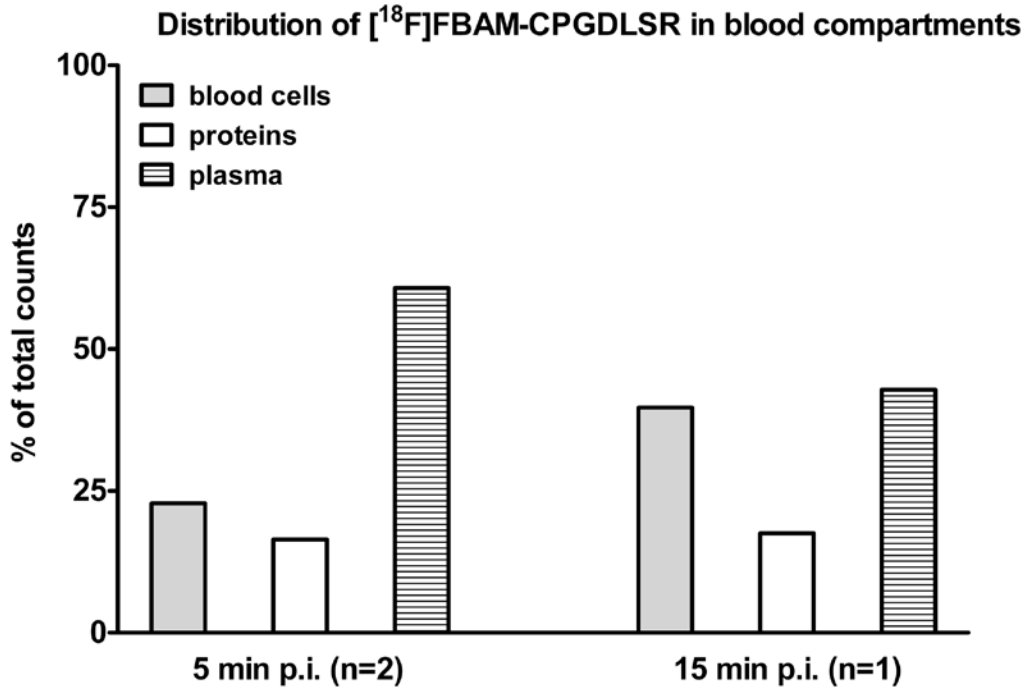

Figure 4-5. Distribution of radioactivity in blood cells, precipitated plasma protein and protein-free plasma at 5 min and 15 min p.i. of [^{18}F]FBAM-CPGDLSR. Average is presented as % of total counts from CH3.HeN mice.

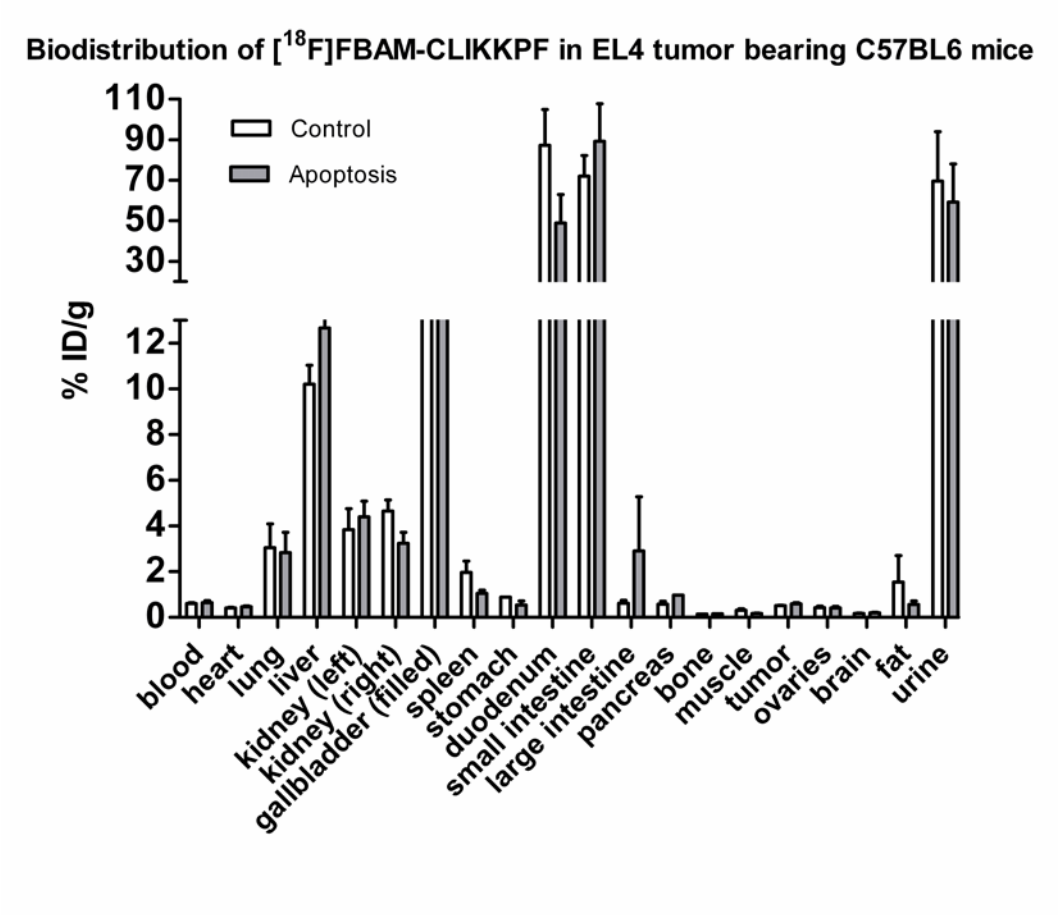

Figure 4-6. Biodistribution of [^{18}F]FBAM-CLIKKPF in EL4 tumor bearing C57BL6 mice at 60 min post injection. Data are the means ± SEM % ID/g (n=3).

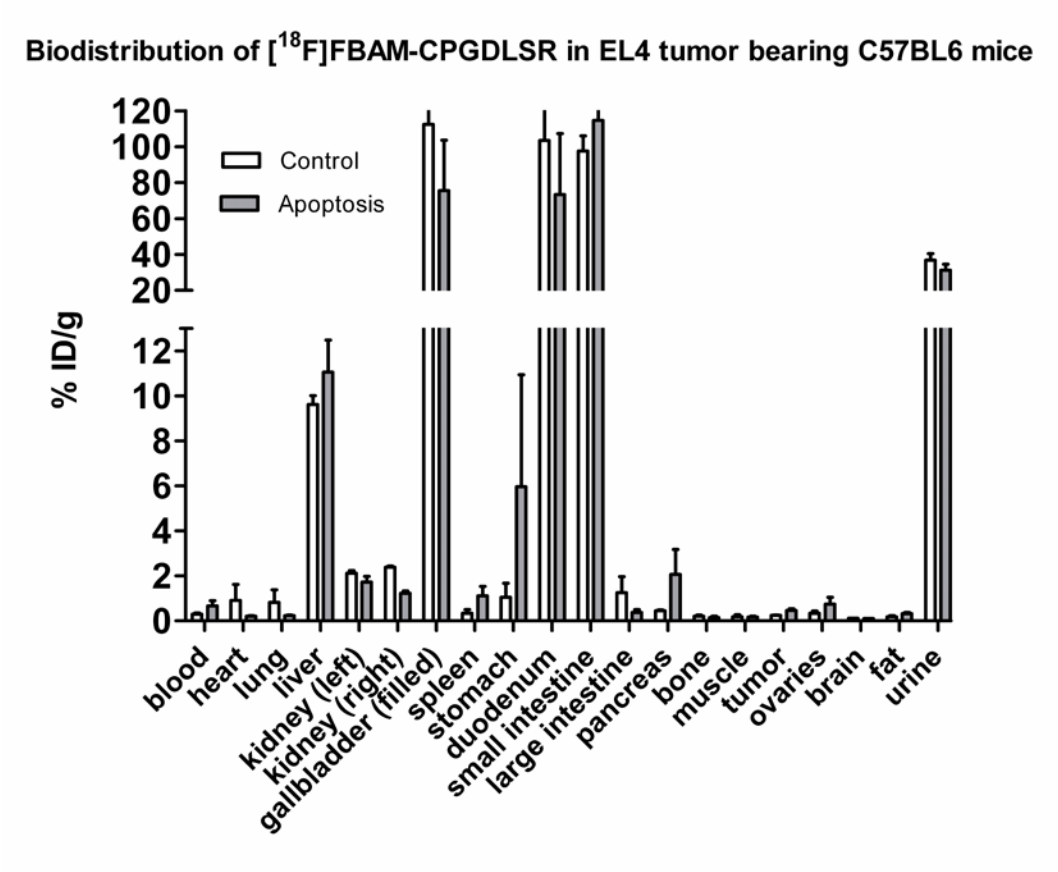

Figure 4-7. Biodistribution of [^{18}F]FBAM-CPGDLSR in EL4 tumor bearing C57BL6 mice at 60 min post injection. Data are the means ± SEM % ID/g (n=3).

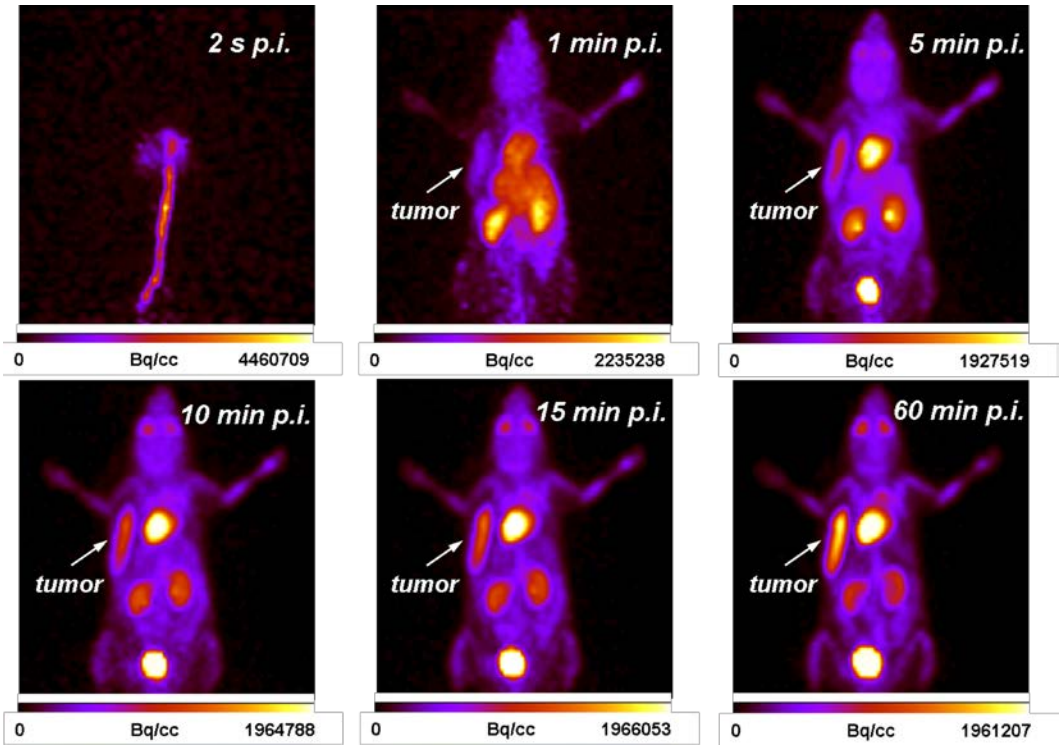

Figure 4-8. Representative dynamic small-animal PET images (up to 60 min) of [^{18}F]FDG in EL4 tumor bearing C57BL6 mouse. Bq/cc represents Becquerels per cubic centimeter.

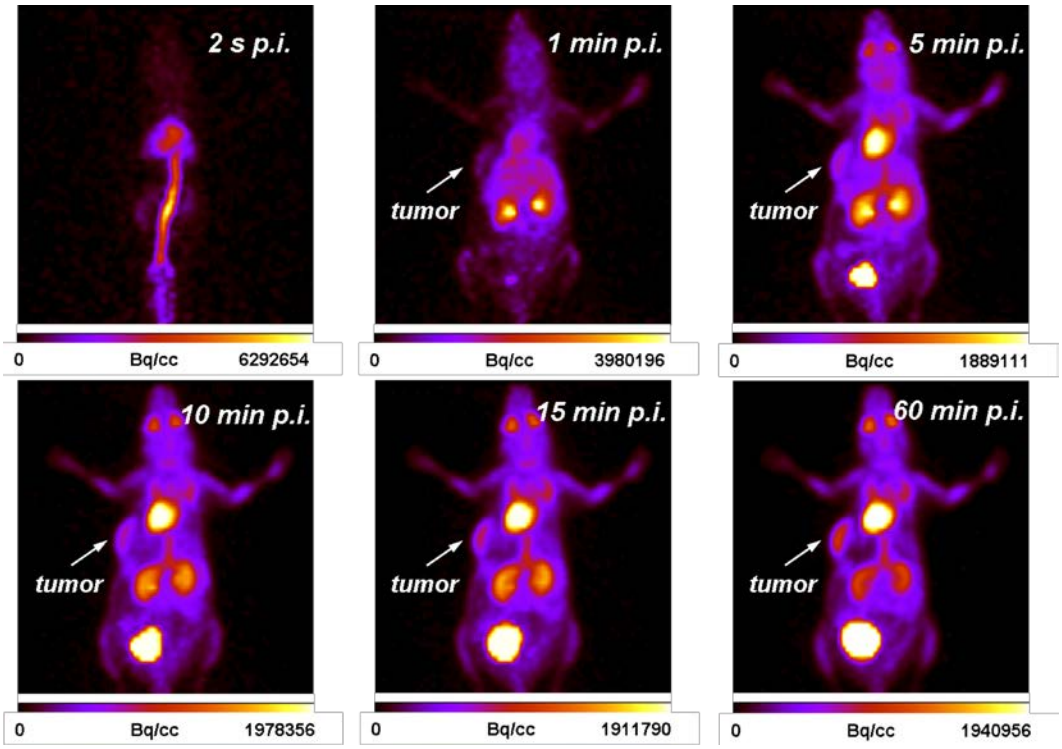

Figure 4-9. Representative dynamic small-animal PET images (up to 60 min) of [^{18}F]FDG in EL4 tumor bearing C57BL6 mouse treated with chemotherapy. Bq/cc represents Becquerels per cubic centimeter.

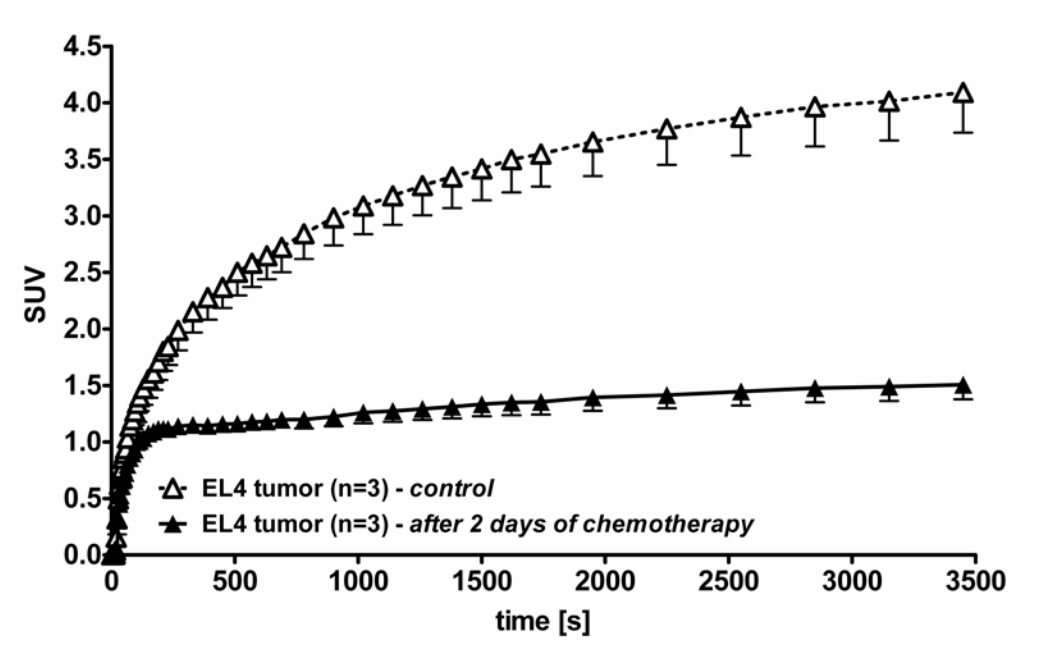

Figure 4-10. TAC of the radioactivity profile in tumor (control) and chemotherapy treated tumors after a single intravenous injection of [^{18}F]FDG. Data are shown as SUV mean ± SEM (n=3).

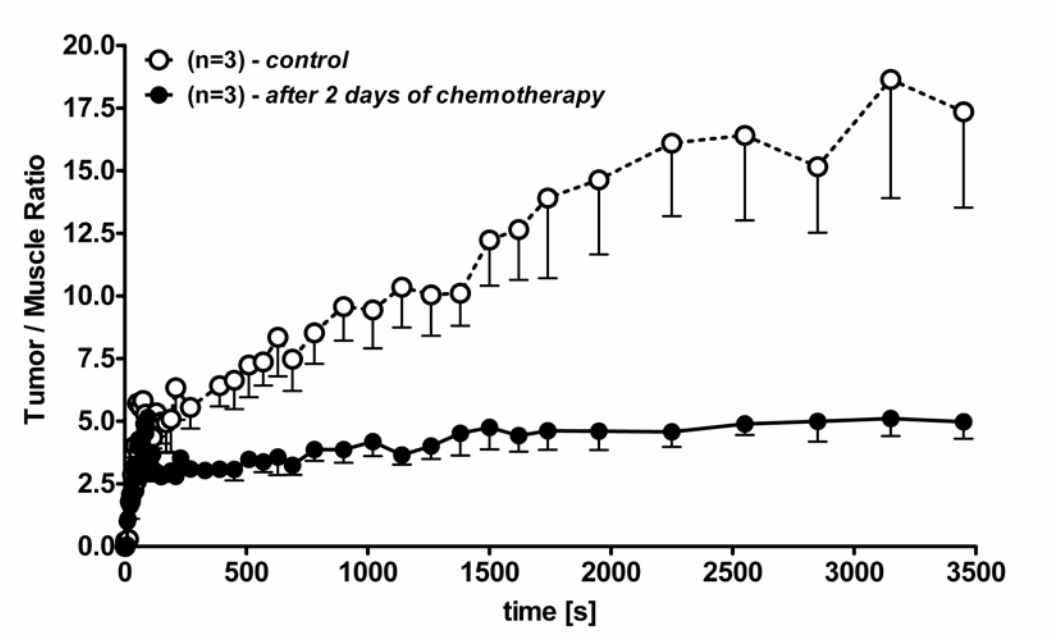

Figure 4-11. TAC of the tumor to muscle ratios in control tumors and chemotherapy treated tumors after a single intravenous injection of [^{18}F]FDG. Data are shown as SUV ratios and as mean ± SEM (n=3).

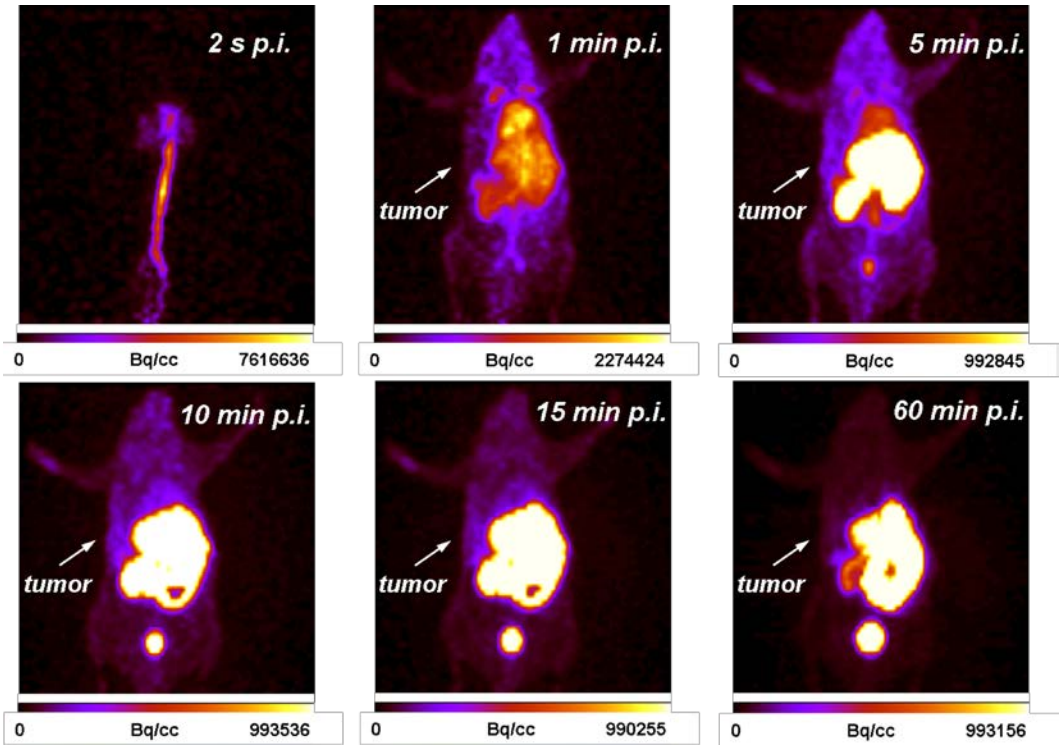

Figure 4-12. Representative dynamic small-animal PET images (up to 60 min) of [^{18}F]FBAM-CLIKKPF in EL4 tumor bearing C57BL6 mouse. Bq/cc represents Becquerels per cubic centimeter.

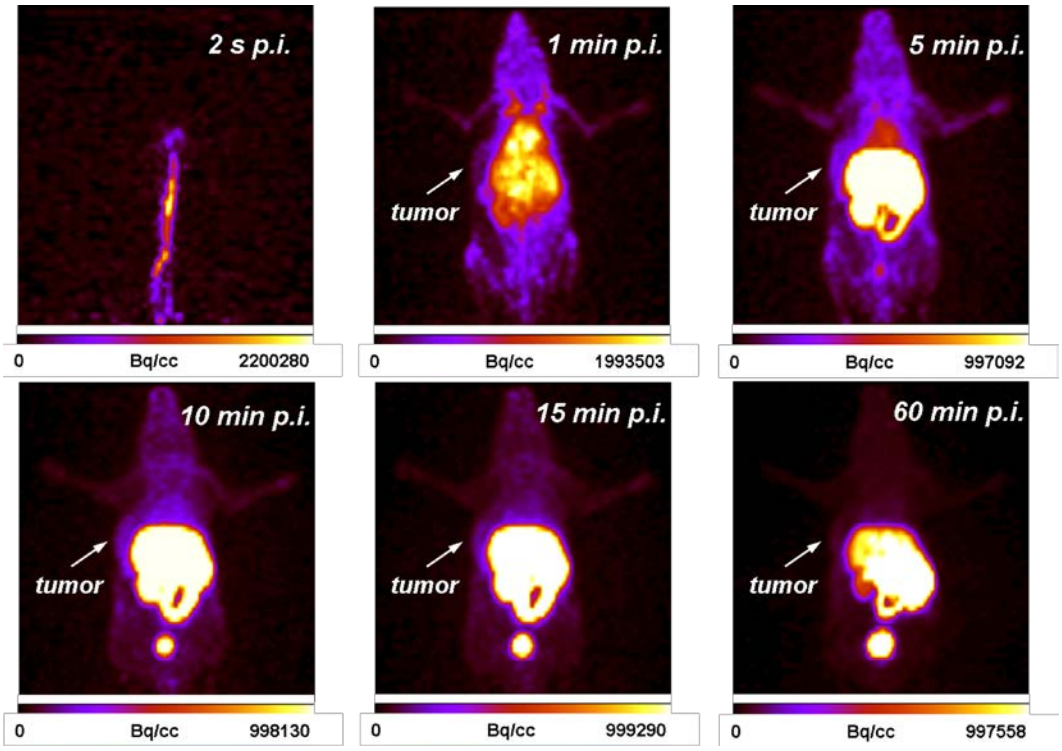

Figure 4-13. Representative dynamic small-animal PET images (up to 60 min) of [^{18}F]FBAM-CLIKKPF in EL4 tumor bearing C57BL6 mouse treated with chemotherapy. Bq/cc represents Becquerels per cubic centimeter.

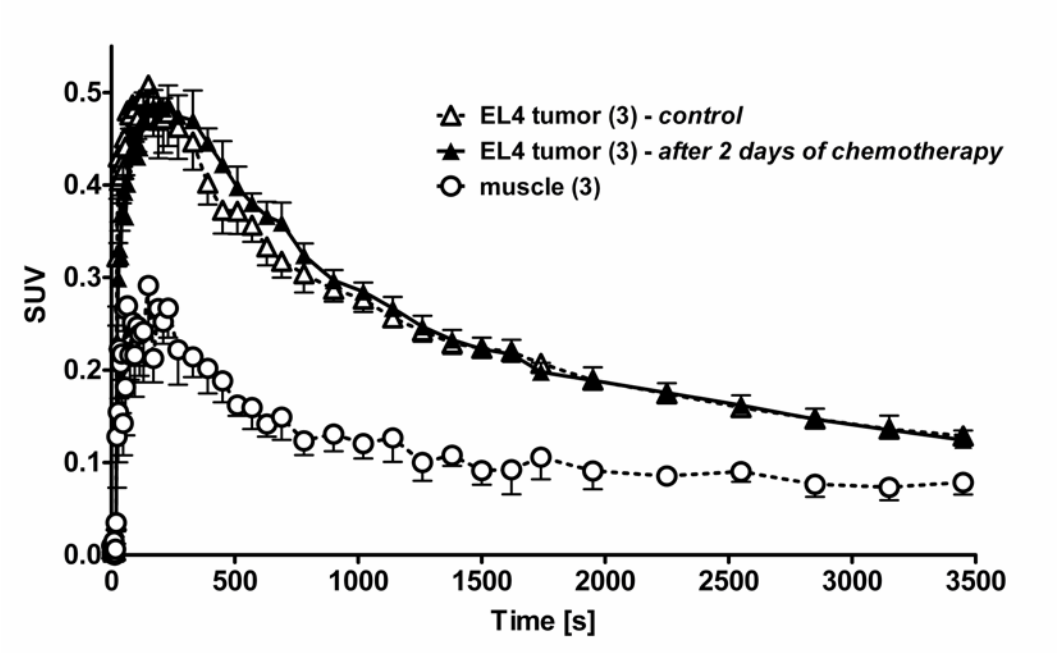

Figure 4-14. TAC of the radioactivity profile in control tumors, chemotherapy treated tumors and muscle after a single intravenous injection of [^{18}F]FBAM-CLIKKPF. Data are shown as SUV means ± SEM (n=3).

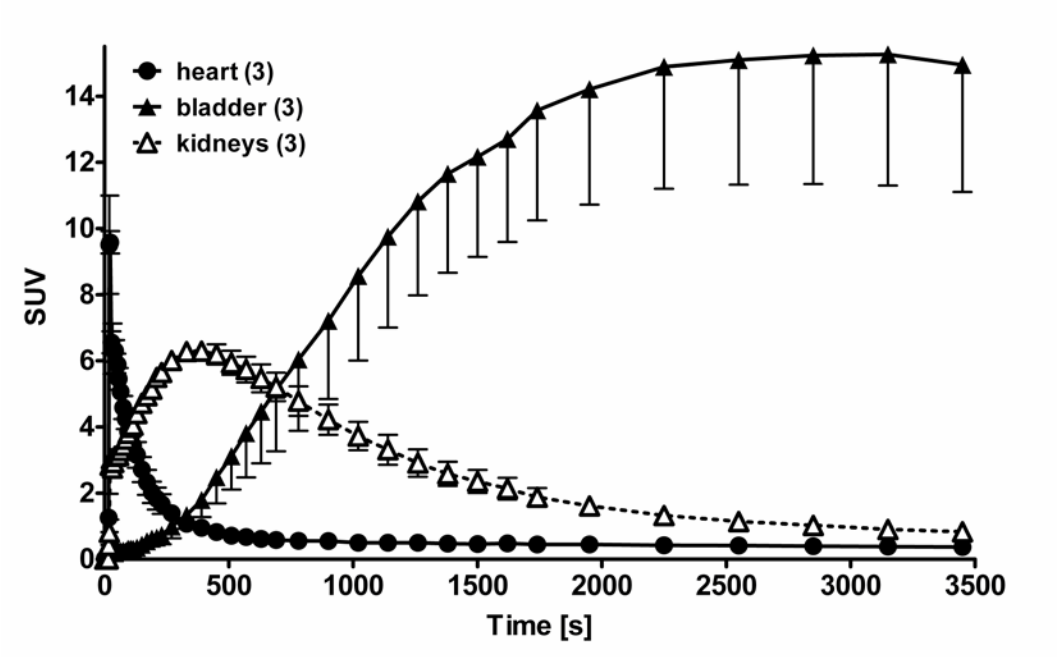

Figure 4-15. TAC of the radioactivity profile in kidneys, hearts and bladder after a single intravenous injection of [^{18}F]FBAM-CLIKKPF. Data are shown as SUV means ± SEM (n=3).

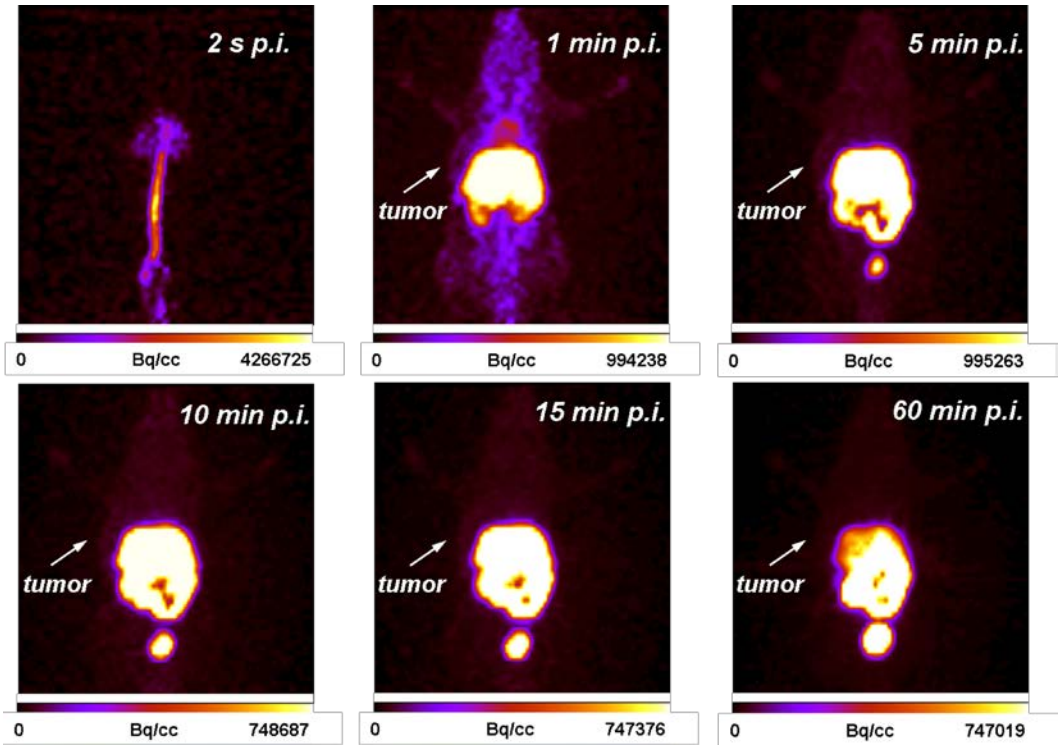

Figure 4-16. Representative dynamic small-animal PET images (up to 60 min) of [^{18}F]FBAM-CPGDLSR in EL4 tumor bearing C57BL6 mouse. Bq/cc represents Becquerels per cubic centimeter.

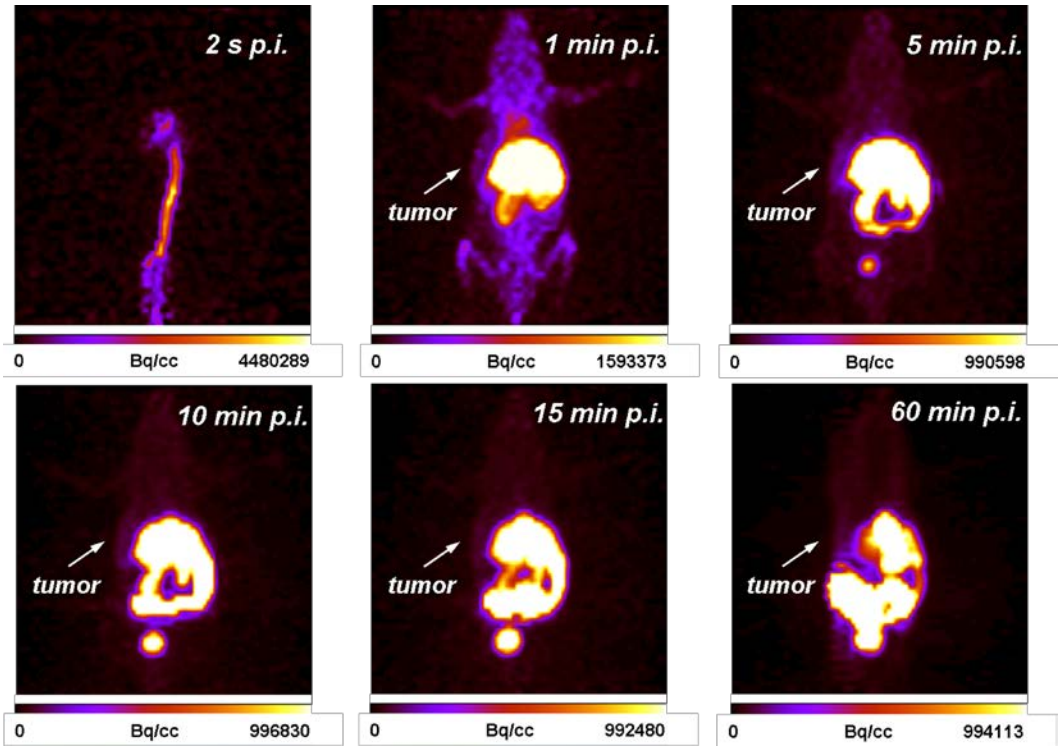

Figure 4-17. Representative dynamic small-animal PET images (up to 60 min) of [^{18}F]FBAM-CPGDLSR in EL4 tumor bearing C57BL6 mouse treated with chemotherapy. Bq/cc represents Becquerels per cubic centimeter.

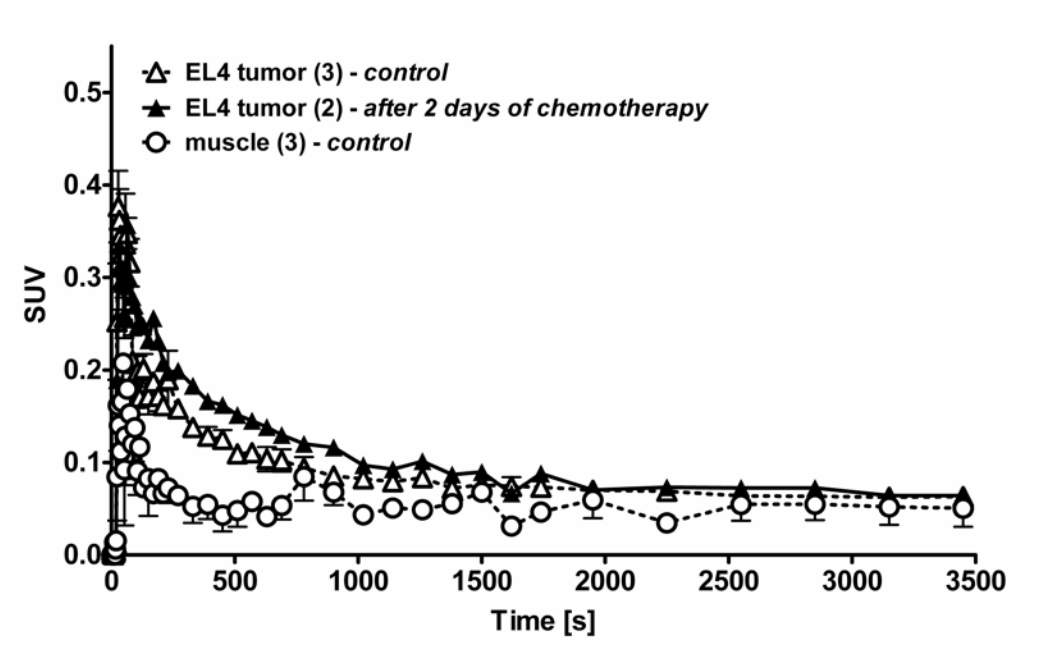

Figure 4-18. TAC of the radioactivity profile in control tumors, chemotherapy treated tumors and muscle after a single intravenous injection of [^{18}F]FBAM-CPGDLSR. Data are shown as SUV means ± SEM (n=3).

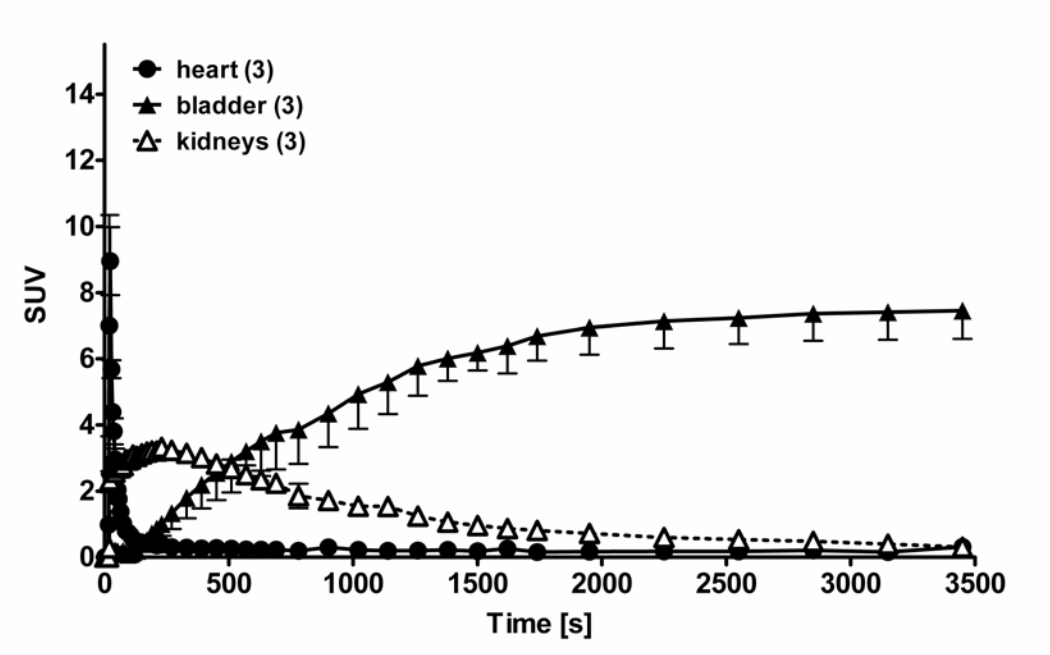

Figure 4-19. TAC of the radioactivity profile in kidneys, heart and bladder after a single intravenous injection of [^{18}F]FBAM-CPGDLSR. Data are shown as SUV means ± SEM (n=3).

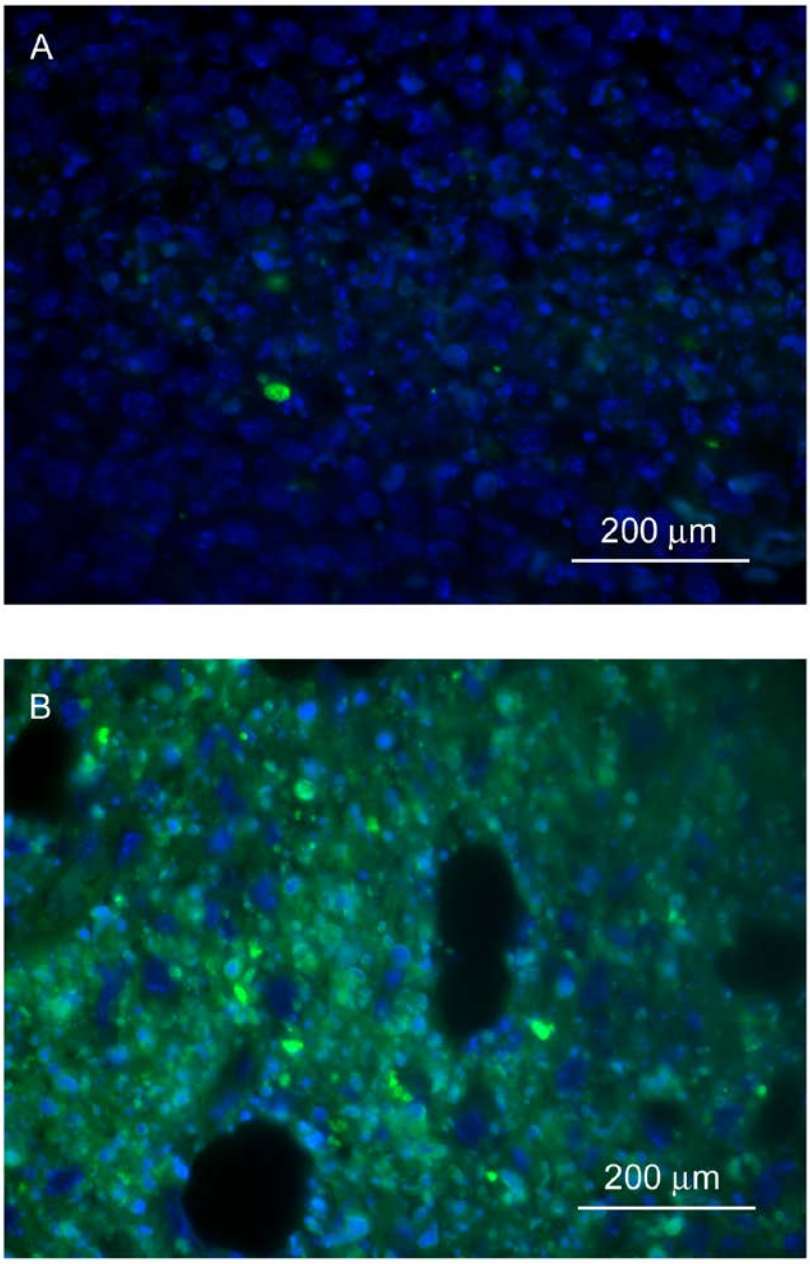

Figure 4-20. Histological analysis of a tissue section from A) EL4 tumor (control), B) EL4 tumor treated with chemotherapy. The tissue sections were analyzed for presence of apoptotic cells using the TUNEL assay. DAPI staining in blue. TUNEL staining in green.

4.5 References:

Al-Ejeh, F., Darby, J.M., Pensa, K., Diener, K.R., Hayball, J.D., Brown, M.P., 2007. In vivo targeting of dead tumor cells in a murine tumor model using a monoclonal antibody specific for the La autoantigen. Clin Cancer Res 13, 5519s-5527s.

Berndt, M., Pietzsch, J., Wuest, F., 2007. Labeling of low-density lipoproteins using the 18F-labeled thiol-reactive reagent N-[6-(4-[18F]fluorobenzylidene)aminooxyhexyl]maleimide. Nucl Med Biol 34, 5-15.

Burtea, C., Laurent, S., Lancelot, E., Ballet, S., Murariu, O., Rousseaux, O., Port, M., Vander Elst, L., Corot, C., Muller, R.N., 2009. Peptidic targeting of phosphatidylserine for the MRI detection of apoptosis in atherosclerotic plaques. Mol Pharm 6, 1903-1919.

Chen, D.L., Zhou, D., Chu, W., Herrbrich, P., Engle, J.T., Griffin, E., Jones, L.A., Rothfuss, J.M., Geraci, M., Hotchkiss, R.S., Mach, R.H., 2011. Radiolabeled isatin binding to caspase-3 activation induced by anti-Fas antibody. Nucl Med Biol.

Chen, X., Park, R., Hou, Y., Khankaldyyan, V., Gonzales-Gomez, I., Tohme, M., Bading, J.R., Laug, W.E., Conti, P.S., 2004. MicroPET imaging of brain tumor angiogenesis with 18F-labeled PEGylated RGD peptide. Eur J Nucl Med Mol Imaging 31, 1081-1089.

Dahms, P., Mentlein, R., 1992. Purification of the main somatostatin-degrading proteases from rat and pig brains, their action on other neuropeptides, and their identification as endopeptidases 24.15 and 24.16. Eur J Biochem 208, 145-154.

Devaux, P.F., 1991. Static and dynamic lipid asymmetry in cell membranes. Biochemistry 30, 1163-1173.

Glaser, M., Goggi, J., Smith, G., Morrison, M., Luthra, S.K., Robins, E., Aboagye, E.O., 2011. Improved radiosynthesis of the apoptosis marker (18)F-ICMT11 including biological evaluation. Bioorg Med Chem Lett 21, 6945-6949.

Green, A.M., Steinmetz, N.D., 2002. Monitoring apoptosis in real time. Cancer J 8, 82-92.

Guo, M.F., Zhao, Y.Q., Tian, R., Li, L., Guo, L.M., Xu, F., Liu, Y.M., He, Y.B., Bai, S., Wang, J., 2009. In vivo 99mTc-HYNIC-annexin V imaging of early tumor apoptosis in mice after single dose irradiation. J Exp Clin Cancer Res 28, 136.

Hoekstra, O.S., Ossenkoppele, G.J., Golding, R., van Lingen, A., Visser, G.W., Teule, G.J., Huijgens, P.C., 1993. Early treatment response in malignant lymphoma, as determined by planar fluorine-18-fluorodeoxyglucose scintigraphy. J Nucl Med 34, 1706-1710.

Kapty, J., Kniess, T., Wuest, F., Mercer, J.R., 2011. Radiolabeling of phosphatidylserine-binding peptides with prosthetic groups N-[6-(4-[18F]fluorobenzylidene)aminooxyhexyl]maleimide ([18F]FBAM) and N-succinimidyl-4-[18F]fluorobenzoate ([18F]SFB). Appl Radiat Isot 69, 1218-1225.

Kapty, J., Murray, D., Mercer, J., 2010. Radiotracers for noninvasive molecular imaging of tumor cell death. Cancer Biother Radiopharm 25, 615-628.

Kartachova, M., Haas, R.L., Olmos, R.A., Hoebers, F.J., van Zandwijk, N., Verheij, M., 2004. In vivo imaging of apoptosis by 99mTc-Annexin V scintigraphy: visual analysis in relation to treatment response. Radiother Oncol 72, 333-339.

Kartachova, M.S., Valdes Olmos, R.A., Haas, R.L., Hoebers, F.J., van den Brekel, M.W., van Zandwijk, N., Herk, M., Verheij, M., 2006. Mapping of treatment-induced apoptosis in normal structures: 99mTc-Hynic-rh-annexin V SPECT and CT image fusion. Eur J Nucl Med Mol Imaging 33, 893-899.

Langer, M., Beck-Sickinger, A.G., 2001. Peptides as carrier for tumor diagnosis and treatment. Curr Med Chem Anticancer Agents 1, 71-93.

Lister-James, J., Moyer, B.R., Dean, T., 1996. Small peptides radiolabeled with 99mTc. Q J Nucl Med 40, 221-233.

McAfee, J.G., Neumann, R.D., 1996. Radiolabeled peptides and other ligands for receptors overexpressed in tumor cells for imaging neoplasms. Nucl Med Biol 23, 673-676.

Reubi, J.C., Maecke, H.R., 2008. Peptide-based probes for cancer imaging. J Nucl Med 49, 1735-1738.

Sakurai, H., Mitsuhashi, N., Murata, O., Kitamoto, Y., Saito, Y., Hasegawa, M., Akimoto, T., Takahashi, T., Nasu, S., Niibe, H., 1998. Early radiation effects in highly apoptotic murine lymphoma xenografts monitored by 31P magnetic resonance spectroscopy. Int J Radiat Oncol Biol Phys 41, 1157-1162.

Vance, J.E., Steenbergen, R., 2005. Metabolism and functions of phosphatidylserine. Prog Lipid Res 44, 207-234.

Vangestel, C., Van de Wiele, C., Mees, G., Peeters, M., 2009. Forcing cancer cells to commit suicide. Cancer Biother Radiopharm 24, 395-407.

Wahl, R.L., Jacene, H., Kasamon, Y., Lodge, M.A., 2009. From RECIST to PERCIST: Evolving Considerations for PET response criteria in solid tumors. J Nucl Med 50 Suppl 1, 122S-150S.

Weiner, R.E., Thakur, M.L., 2002. Radiolabeled peptides in the diagnosis and therapy of oncological diseases. Appl Radiat Isot 57, 749-763.

Weiner, R.E., Thakur, M.L., 2005. Radiolabeled peptides in oncology: role in diagnosis and treatment. BioDrugs 19, 145-163.

Yagle, K.J., Eary, J.F., Tait, J.F., Grierson, J.R., Link, J.M., Lewellen, B., Gibson, D.F., Krohn, K.A., 2005. Evaluation of 18F-annexin V as a PET imaging agent in an animal model of apoptosis. J Nucl Med 46, 658-666.

Young, H., Baum, R., Cremerius, U., Herholz, K., Hoekstra, O., Lammertsma, A.A., Pruim, J., Price, P., 1999. Measurement of clinical and subclinical tumour response using [18F]-fluorodeoxyglucose and positron emission tomography: review and 1999 EORTC recommendations. European Organization for Research and Treatment of Cancer (EORTC) PET Study Group. Eur J Cancer 35, 1773-1782.

Zhao, M., Beauregard, D.A., Loizou, L., Davletov, B., Brindle, K.M., 2001. Non-invasive detection of apoptosis using magnetic resonance imaging and a targeted contrast agent. Nat Med 7, 1241-1244.

Zhao, M., Li, Z., Bugenhagen, S., 2008. 99mTc-labeled duramycin as a novel phosphatidylethanolamine-binding molecular probe. J Nucl Med 49, 1345-1352.

Zimmermann, N., Freund, S., Fredenhagen, A., Jung, G., 1993. Solution structures of the lantibiotics duramycin B and C. Eur J Biochem 216, 419-428.

Chapter 5

Conclusions and Future Directions

5.1 Summary of results

Currently the effectiveness of cancer treatment is ascertained by a change in tumor size which requires weeks to months. Structural imaging does an inadequate job of determining solid tumor response to therapy since it is only able to assess if a tumor has changed size and it is not able to assess whether the tumor is responding to therapy through cellular mechanisms such as apoptosis, senescence, necrosis or autophagy. If we were able to develop molecular imaging probes to image these cellular mechanisms we would have a much better understanding of tumor response to therapy and of tumor biology in general. There is ongoing research into developing an appropriate nuclear medicine technique for early assessment of tumor response particularly with PET probes which can combine high sensitivity and resolution particularly with clinical PET/CT and PET/MRI instruments. Molecular imaging approaches have a much greater potential to rapidly assess the effectiveness of therapy on a tumor compared to structural imaging approaches. Detection of apoptosis would give an almost immediate indication of effective cancer treatment before the tumor changes in size and could be evaluated 1-3 days after the patient receives treatment. However, there is no current clinical method to assess apoptosis levels *in vivo*.

Our approach is to develop a molecular imaging probe for apoptosis based on radiolabeled peptides which bind to externalized PS on apoptotic cells.

Peptides have a number of potential advantages as radiotracers including small size, good tissue diffusion, rapid targeting, low antigenicity, easy synthesis, well developed radiolabeling, fast blood clearance, and inexpensive production (Langer and Beck-Sickinger, 2001; Reubi and Maecke, 2008; Weiner and Thakur, 2002, 2005). We hypothesized that a peptide radiopharmaceutical binding to apoptotic cells could be developed and could be used to image cell death *in vivo* using PET. We have explored this possibility by addressing three objectives: 1) determining the binding characteristics of four peptides for ability to bind to phosphatidylserine, 2) radiolabeling PS-binding peptides with ^{18}F, and 3) performing *in vitro* and *in vivo* analysis of ^{18}F radiolabeled PS-binding peptides.

In the first part of this study we investigated two PS binding peptides described previously (Burtea et al., 2009) (LIKKPF and PGDLSR) and two novel peptides produced by the addition of a cysteine residue (CLIKKPF and CPGDLSR). We evaluated these peptides to determine the binding characteristics using a plate assay, liposome assay, and a cell based apoptotic assay to assess binding to PS. Using a plate assay we determined the dissociation constant for these four peptides (LIKKPF K_d= 0.69 µM, PGDLSR K_d= 0.40 µM, CLIKKPF K_d= 1.9 µM, CPGDLSR K_d= 7.9 µM) and we found that they all bind to PS in the presence of calcium buffer. The liposome construct is designed to be similar to apoptotic cells with respect to PS externalization; and in this regard can be considered a mimic of apoptotic cells with externalized PS. The results of the liposome assay indicate that all four peptides and annexin V bind to 10% PS liposomes and do not bind to PC liposomes (0% PS) according to confocal

microscopy analysis. The cell assay indicates that CLIKKPF and CPGDLSR bind specifically to apoptotic cells and do not bind to healthy cells. Our analysis indicates that CLIKKPF and CPGDLSR are able to bind at the membrane bilayer and are also present in the cytosol.

In the second part of this study, we present the scope and limitations of the two ^{18}F-labeled prosthetic groups, [^{18}F]SFB and [^{18}F]FBAM, for the ^{18}F-radiolabeling of PS binding peptides. We radiolabeled our peptides of interest and compared radiolabeling yield and chemoselectivity of each prosthetic group. Since neither of our peptides of interest contained a sulfhydryl group they were modified by the addition of a cysteine residue at the N-terminus. The radiolabeling reaction for both peptides with cartridge purified [^{18}F]FBAM was strongly dependent on peptide concentration. Radiolabeling with [^{18}F]FBAM proceeds at room temperature and only requires a short reaction time resulting in a single radiolabeled product and high radiochemical yield for both peptides. Thus using [^{18}F]FBAM, peptides CLIKKPF and CPGDLSR were chemoselectively labeled at the thiol group of the terminal cysteine. Based on the results of this study, it can be concluded that [^{18}F]FBAM has the potential to play an important role for the radiolabeling of cysteine containing peptides. While [^{18}F]SFB remains a popular prosthetic group our studies have demonstrated some of the problems which may arise depending on the nature of the peptide to be labeled. The presence of multiple reactive primary amino groups in a peptide can lead to a complex mixture of singly and multiply labeled products and thus poor chemoselectivity to labeling at the N-terminus.

The goals of the third part of the study were to 1) investigate [^{18}F]FBAM-CLIKKPF and [^{18}F]FBAM-CPGDLSR *in vitro* and *in vivo* as possible radiotracers able to bind to apoptotic cells, and 2) image chemotherapy induced apoptosis using the radiopeptides as novel PET probes. We report the first experiments evaluating PS-binding peptides radiolabeled with ^{18}F as possible radiotracers for imaging apoptosis. Results of the *in vitro* tests indicate that binding of [^{18}F]FBAM-CLIKKPF to apoptotic Jurkat cells was significantly higher than binding to untreated cells at both time points of 15 min and 30 min. Unfortunately our results with [^{18}F]FBAM-CLIKKPF and [^{18}F]FBAM-CPGDLSR indicate that radiopeptide uptake in an *in vivo* model does not accurately measure chemotherapy induced apoptosis. Due to the rapid metabolism of the peptide probes we were unable to accurately image chemotherapy induced apoptosis. The rapid metabolism of the peptides is due to the abundance of peptidases *in vivo*. Modifications are required in order to improve the stability of these radiopeptides as possible imaging agents for apoptosis.

5.2 Contributions to the field

In this report we evaluated four peptides using two novel methods to determine binding to PS. We determined the dissociation constant for four peptides and found that these four peptides are able to bind to PS and are possible probes for development into novel PET tracers. We have developed two new assays which can be employed by other researchers seeking to find novel PS-binding probes. Both of these assays (plate assay and liposome assay) can be

easily reproduced, can be used to test a wide variety of concentrations of a compound and do not require extensive laboratory material and equipment required for cell culture techniques. These assays can also be applied with other classes of compounds such as small molecules, proteins and oligonucleotides. The plate assay has been used previously by our group to screen several nucleotide sequences derived by computational modeling which were designed to bind to PS (Tseng et al., 2011). These assays have allowed us to rapidly test modifications made to our lead compounds to determine if binding affinity is improved or impaired. Both of these assays may prove to be valuable tools in the rapid *in vitro* assessment of potential apoptosis targeting probes which bind to PS and could help to accelerate discovery of compounds which can be used to imaging apoptosis.

In this study we report the use of [^{18}F]SFB, a popular prosthetic group for incorporating ^{18}F, and the use of [^{18}F]FBAM, a less widely used prosthetic group for incorporating ^{18}F. Prosthetic groups are very useful for incorporating ^{18}F into various molecules such as peptides, proteins and oligonucleotides. We found that despite the wide popularity of [^{18}F]SFB as a prosthetic group it may not be the most suitable prosthetic group when radiolabeling peptides and our studies have demonstrated some of the problems that may arise depending on the nature of the peptide to be labeled. Due to the nature of this prosthetic group a primary amine is required for labeling to occur and on the converse the presence of multiple primary amino groups in a peptide can lead to a complex mixture of singly and multiply labeled products and thus poor chemoselectivity. We also tested

[^{18}F]FBAM for radiolabeling of two peptides of interest and found the reaction produced very high radiochemical yields and the peptides CLIKKPF and CPGDLSR were chemoselectively labeled at the thiol group of the terminal cysteine. We report the effective use of the prosthetic group [^{18}F]FBAM which can easily be prepared using an automated synthesis unit in even less time than it takes to prepare [^{18}F]SFB. The contribution of this work is that we have demonstrated effective peptide labeling using an alternative prosthetic group ([^{18}F]FBAM) which may have advantages over [^{18}F]SFB in some situations and can be easily synthesized using an automated unit. We hope that this research will encourage others to try [^{18}F]FBAM as a possible prosthetic group for radiolabeling of probes and expand the choices of available and effective prosthetic groups for incorporation of ^{18}F.

In this study we evaluated two novel PET probes for imaging apoptosis: [^{18}F]FBAM-CLIKKPF and [^{18}F]FBAM-CPGDLSR. We report the first experiments evaluating PS-binding peptides radiolabeled with ^{18}F as possible radiotracers for imaging apoptosis. We focused on developing a peptide probe for imaging apoptosis in order to capitalize on the many advantages that peptides provide as imaging agents. We evaluated the radiopeptides *in vitro* which indicated that the addition of the [^{18}F]FBAM to the peptide may or may not interfere with the binding of the peptide to PS. [^{18}F]FBAM-CLIKKPF bound to apoptotic cells significantly more than to healthy cells. However, [^{18}F]FBAM-CPGDLSR did not bind to apoptotic cells more than to healthy cells. We have studied the biodistribution and the metabolic stability *in vivo* for these two

radiopeptides. We have determined that the radiopeptides are rapidly metabolized due to the abundance of peptidases present *in vivo*. We perfomed dynamic PET imaging using a tumor model of apoptosis and aimed to image apoptosis using the two radiopeptides. However, we were unable to accurately image apoptosis in the tumors despite the large amount of apoptosis induced by chemotherapy. This work indicates that it is possible to develop a radiotracer based on a specific target of interest (in this case PS) and evaluate the tracer *in vitro* and *in vivo* to determine characteristics of the radiotracer. From this knowledge base, modifications can be made to the radiopeptides to improve characteristics such as stability and biodistribution in order to optimize the ability to effectively image apoptosis *in vivo*.

5.3 Future directions

Based on the results presented in this thesis it is recommended to extend the research on the peptides evaluated in this thesis. Caution is recommended when considering the future use of [^{18}F]FBAM-CPGDLSR since the *in vitro* experiments reveal that it did not have higher binding to apoptotic cells compared to healthy cells. It is possible that the addition of [^{18}F]FBAM may have altered the binding affinity of this peptide. On the other hand, [^{18}F]FBAM-CLIKKPF had significantly higher binding to apoptotic cells compared to healthy cells indicating that this radiotracer is a good candidate for future development. In the radiopharmacological evaluation of [^{18}F]FBAM-CLIKKPF we were unable to image tumor apoptosis due to the rapid metabolism of the peptide by various peptidases. Improving the metabolic stability of [^{18}F]FBAM-CLIKKPF needs to

be the focus of future research; which could subsequently improve the stability and effectiveness of this peptide for future imaging of apoptosis. There are many possible modifications that can be made to peptides in order to increase resistance to endo- and exo-peptidases. Possible modifications to increase resistance of [^{18}F]FBAM-CLIKKPF to exopeptidases include end capping by converting the carboxylic acid on the C-terminus to an amide or reducing the C-terminus to an alcohol (Langer and Beck-Sickinger, 2001; Lister-James et al., 1996). The N-terminus residue is likely not metabolized by exopeptidases since [^{18}F]FBAM is attached at the N-terminus and it likely interferes with the function of N-terminus specific peptidases. Modifications to increase resistance of [^{18}F]FBAM-CLIKKPF to endopeptidases include incorporating D-amino acids, substitution of peptide bonds or incorporating peptidomimetic sequences and spacers (Langer and Beck-Sickinger, 2001; McAfee and Neumann, 1996). It may be possible to stabilize a peptide by only adding a few D-amino acids (Langer and Beck-Sickinger, 2001) and therefore this is a worthy approach. For [^{18}F]FBAM-CLIKKPF we could incorporate D-amino acids to replace the L-amino acids leucine, isoleucine, lysine or proline (these are all sites of possible hydrolysis by common peptidases). After modifications have been made to the peptides they would need to be radiolabeled with [^{18}F]FBAM and undergo *in vitro* testing to determine if they retain ability to bind to PS on apoptotic cells.

Future work may also evaluate the binding of peptides to PS and possible internalization in more depth. We have generally observed binding of [^{18}F]FBAM-CLIKKPF to healthy Jurkat cells. The method to evaluate binding to

Jurkat cells does not differentiate the difference between peptide binding at the cell surface and peptide uptake into the cells. There are various possibilities to account for the [^{18}F]FBAM-CLIKKPF binding to the healthy Jurkat cells including: passive uptake, cell-penetrating properties (possibly conferred by lysine residues), uptake into cells by endocytosis, or increased phospholipid binding due to increased lipophilicity imparted by addition of FBAM. Future work may want to further evaluate the mechanism of binding/uptake of [^{18}F]FBAM-CLIKKPF.

There is ongoing research to develop novel probes to image apoptosis. The report by Xiong *et al* found a peptide with high affinity for PS (K_d= 100 nM) (Xiong et al., 2011). When the peptide was radiolabeled with ^{99m}Tc and evaluated in a melanoma model of apoptosis in mice there was a significant difference between the %ID/g in chemotherapy treated versus untreated tumors(Xiong et al., 2011). This peptide could be radiolabeled with ^{18}F and evaluated as a novel PET probe. Additionally a report by Zheng *et al* found a cyclic peptide mimic of lactadherin to bind to PS with affinity in the micromolar range (Zheng et al., 2011). The novelty of this peptide is that it does not require calcium for binding to apoptotic cells (Zheng et al., 2011). The level of calcium *in vivo* is typically lower than the concentration commonly used for in vitro assays (2.5 mM); therefore, since binding of this peptide to PS is calcium independent if may provide an advantage for *in vivo* imaging of apoptosis. It would be interesting to radiolabel this peptide with ^{18}F and evaluate as a potential PET tracer. The PS-binding peptides may have limited affinity for PS and typically do not bind in the nanomolar range; however, it is possible to try using dendrimers as an approach to

increase affinity of the peptides to PS. Dendrimers are repetitively branched molecules which could potentially be used to increase affinity of the known peptide sequence to PS. Peptide dendrimers have been extensively reviewed (Niederhafner et al., 2005, 2008) and may be an interesting approach to develop a novel imaging agent. Instead of one peptide interacting with PS (as studied in this thesis), a dendrimer could have multiple copies of the peptide interacting with PS and therefore potentially increase the binding affinity to PS.

5.4 Significance

In a clinical context, imaging cell death *in vivo* has great significance in evaluating therapeutic response and has the potential to assist in the design of appropriate individualized and optimized therapy. Conventional imaging modalities (e.g., computed tomography [CT] and magnetic resonance imaging [MRI]) typically provide anatomical information that may not indicate tumor response to therapy until weeks to months after treatment initiation. With conventional imaging modalities, ineffective therapies may be used for long periods of time before these treatments' ineffectiveness becomes evident. Evaluation of tumor response to chemotherapy and external-beam radiotherapy (XRT) after the earliest cycles of therapy would allow optimization of dosing and therapies, thereby improving patient outcomes and quality of life.

Once validated, imaging cell death using PET could be used to evaluate the early response to treatment for individual patients and aid in the advancement of personalized medicine. This would guide physicians to select the optimal anti-cancer therapy for a patient and allow rapid identification of ineffective treatments

thereby reducing side effects (Green and Steinmetz, 2002). Imaging of apoptosis can be used to analyze the apoptotic effects of a new drug, quantify apoptosis before and after a new therapy, optimize drug combinations, determine optimal dosing and dosing schedules, document toxicity, and select for patients likely to respond to the treatment (Belhocine and Blankenberg, 2006; Green and Steinmetz, 2002).

Overall successful imaging of apoptosis to assess tumor response to therapy would be very useful clinically and would have a great impact on the quality of life of cancer patients. This thesis reports the first experiments of PS-binding peptides radiolabeled with ^{18}F and evaluated as imaging agents for apoptosis. We successfully evaluated peptides that bind to PS and found candidates for radiolabeling with ^{18}F. We then radiolabeled two PS-binding peptides with [^{18}F]FBAM and were able to produce a sufficient quantity of purified radiolabeled peptides for biological testing. Despite the rapid metabolism of the radiopeptides *in vivo*, this is the first report where radiolabeled PS-binding peptides were evaluated in a tumor model of apoptosis. The next step requires the development of metabolically stable PS-binding peptides which could potentially be effective imaging probes to detect apoptosis *in vivo*.

5.5 References

Burtea, C., Laurent, S., Lancelot, E., Ballet, S., Murariu, O., Rousseaux, O., Port, M., Vander Elst, L., Corot, C., Muller, R.N., 2009. Peptidic targeting of phosphatidylserine for the MRI detection of apoptosis in atherosclerotic plaques. Mol Pharm 6, 1903-1919.

Green, A.M., Steinmetz, N.D., 2002. Monitoring apoptosis in real time. Cancer J 8, 82-92.

Langer, M., Beck-Sickinger, A.G., 2001. Peptides as carrier for tumor diagnosis and treatment. Curr Med Chem Anticancer Agents 1, 71-93.

Niederhafner, P., Sebestik, J., Jezek, J., 2005. Peptide dendrimers. J Pept Sci 11, 757-788.

Niederhafner, P., Sebestik, J., Jezek, J., 2008. Glycopeptide dendrimers. Part I. J Pept Sci 14, 2-43.

Reubi, J.C., Maecke, H.R., 2008. Peptide-based probes for cancer imaging. J Nucl Med 49, 1735-1738.

Tseng, C.Y., Ashrafuzzaman, M., Mane, J.Y., Kapty, J., Mercer, J.R., Tuszynski, J.A., 2011. Entropic fragment-based approach to aptamer design. Chem Biol Drug Des 78, 1-13.

Weiner, R.E., Thakur, M.L., 2002. Radiolabeled peptides in the diagnosis and therapy of oncological diseases. Appl Radiat Isot 57, 749-763.

Weiner, R.E., Thakur, M.L., 2005. Radiolabeled peptides in oncology: role in diagnosis and treatment. BioDrugs 19, 145-163.

Xiong, C., Brewer, K., Song, S., Zhang, R., Lu, W., Wen, X., Li, C., 2011. Peptide-based imaging agents targeting phosphatidylserine for the detection of apoptosis. J Med Chem 54, 1825-1835.

Zheng, H., Wang, F., Wang, Q., Gao, J., 2011. Cofactor-free detection of phosphatidylserine with cyclic peptides mimicking lactadherin. J Am Chem Soc 133, 15280-15283.

Appendix A

Standard Amino Acid Abbreviations

Amino Acid	**3-Letter Abbreviation**	**1-Letter Abbreviation**
Alanine	Ala	A
Arginine	Arg	R
Asparagine	Asn	N
Aspartic acid	Asp	D
Cysteine	Cys	C
Glutamic acid	Glu	E
Glutamine	Gln	Q
Glycine	Gly	G
Histidine	His	H
Isoleucine	Ile	I
Leucine	Leu	L
Lysine	Lys	K
Methionine	Met	M
Phenylalanine	Phe	F
Proline	Pro	P
Serine	Ser	S
Threonine	Thr	T
Tryptophan	Trp	W
Tyrosine	Tyr	Y
Valine	Val	V